NATIONAL ADVISORY COMMITTEE FOR AERONAUTICS

WARTIME REPORT

ORIGINALLY ISSUED
January 1943 as
Memorandum Report

STABILITY AND CONTROL TESTS OF A 3/4-SCALE MODEL OF THE XP-69 AIRPLANE IN THE NACA FULL-SCALE TUNNEL

By Harold H. Sweberg

Langley Memorial Aeronautical Laboratory
Langley Field, Va.

WASHINGTON

L-642

MEMORANDUM REPORT

for the

Army Air Forces, Materiel Command

STABILITY AND CONTROL TESTS OF A 3/4-SCALE MODEL OF THE XP-69 AIRPLANE IN THE NACA FULL-SCALE TUNNEL

By Harold H. Sweberg

INTRODUCTION

At the request of the Army Air Forces, Materiel Command, tests have been made in the NACA full-scale tunnel to determine the longitudinal- and lateral-stability and control characteristics of a 3/4-scale model of the XP-69 airplane. The XP-69 airplane is a single-engine, low-wing monoplane with dual-rotating propellers. Engine cooling is obtained by means of a rear-underslung ducting system. Inasmuch as stability data on airplanes equipped with dual-rotating propellers are meager, the effects of propeller operation on the stability and control characteristics of this airplane are of particular interest.

The data include measurements of the forces and moments on the model at various angles of attack and angles of yaw. These measurements were made with the propellers removed and operating and with the landing flaps retracted and deflected. The effects of elevator, rudder, and aileron deflection on control-surface effectiveness and on hinge moments were determined. The general nature of the slipstream behind

dual-rotating propellers was investigated by surveys of the velocity and direction of the air flow in the region of the tail plane with the propellers removed and operating.

SYMBOLS

C_D drag coefficient $\left(\frac{X}{q_o S}\right)$

C_{D_R} resultant drag coefficient with propellers operating $\left(\frac{X}{q_o S}\right)$

C_Y lateral-force coefficient $\left(\frac{Y}{q_o S}\right)$

C_L lift coefficient $\left(\frac{Z}{q_o S}\right)$

C_l rolling-moment coefficient $\left(\frac{L}{q_o S_b}\right)$

C_m pitching-moment coefficient $\left(\frac{M}{q_o S_b}\right)$

C_n yawing-moment coefficient $\left(\frac{N}{q_o S_b}\right)$

C_{h_e} elevator hinge-moment coefficient $\left(\frac{H_e}{q_o S_e c_e}\right)$

C_{h_r} rudder hinge-moment coefficient $\left(\frac{H_r}{q_o S_r c_r}\right)$

C_{h_a} aileron hinge-moment coefficient $\left(\frac{H_a}{q_o S_a c_a}\right)$

where

X force along X axis, positive when directed backward

Y force along Y axis, positive when directed to right

Z force along Z axis, positive when directed upward

L rolling moment about X axis, positive when it tends to depress the right wing

M pitching moment about Y axis, positive when it tends to depress the tail

N	yawing moment about the Z axis, positive when it tends to retard the right wing
H_e	elevator hinge moment, positive downward
H_r	rudder hinge moment, positive toward left
H_a	aileron hinge moment, positive downward
q_o	free-stream dynamic pressure $\left(\frac{1}{2}\rho V_o^2\right)$
ρ	mass density of air
V_o	free-stream velocity
$\bar{c}$	mean aerodynamic chord
b	wing span
S_e	elevator area aft of hinge
S_r	rudder area aft of hinge
S_a	aileron area aft of hinge
c_e	root mean square elevator chord
c_r	root mean square rudder chord
c_a	root mean square aileron chord
T_c	effective thrust coefficient $\left(\frac{\text{effective thrust}}{\rho V_o^2 D^2}\right)$
C_P	power coefficient $\left(\frac{\text{engine power}}{\rho n^3 D^5}\right)$
C_T	effective thrust coefficient $\left(\frac{\text{effective thrust}}{\rho n^2 D^4}\right)$
η	propeller efficiency $\left(\frac{C_T}{C_P} V/nD\right)$
V/nD	propeller advance-diameter ratio
n	propeller rotational speed
β_F	blade angle of front propeller

β_R blade angle of rear propeller

D propeller diameter

cp chord of wing directly behind propeller

bi span of that part of wing immersed in the slipstream

ΔC_{L_P} increment of lift coefficient due to propeller operation

ΔC_{L_T} increment of lift coefficient due to propeller thrust force

ΔC_{L_N} increment of lift coefficient due to normal force on a propeller inclined to the air stream

ΔC_{L_s} increment of lift coefficient due to the passage of the slipstream over wing

ΔC_{m_P} increment of pitching-moment coefficient due to propeller operation

ΔC_{m_T} increment of pitching-moment coefficient due to propeller thrust force

ΔC_{m_N} increment of pitching-moment coefficient due to normal force on a propeller inclined to the air stream

ΔC_{m_s} increment of pitching-moment coefficient due to passage of slipstream over the wing

ΔC_{m_t} pitching-moment coefficient due to the horizontal tail surface

α angle of attack of thrust axis, degrees

ψ angle of yaw, degrees; positive when left wing moves forward

i_t angle of stabilizer setting with respect to the thrust axis, degrees; positive with trailing edge down

δ_e elevator deflection (with respect to stabilizer chord) degrees; positive when trailing edge of elevator is moved down

δ_r rudder deflection, degrees; positive when trailing edge of rudder is moved to left

δ_a aileron deflection, degrees; positive when trailing edge of aileron is moved down (subscript L denotes left aileron)

δ_f flap deflection, degrees

δ_{e_T} elevator tab deflection, degrees

δ_{r_T} rudder tab deflection, degrees

δ_{a_T} aileron tab deflection, degrees

$\Delta\delta_a$ total deflection of both ailerons, degrees

ϵ local downwash angle at tail measured relative to free-stream direction, degrees

ϵ_{av} average downwash angle across elevator hinge line as found from air-flow surveys, degrees

ϵ_p propeller downwash angle at wing center of pressure, degrees

q local dynamic pressure $\left(\frac{1}{2}\rho V^2\right)$

V local velocity

$(q/q_o)_{av}$ average dynamic-pressure ratio across elevator hinge line as found from air-flow surveys

s velocity increment factor back of propeller disk

a_o lift-curve slope for infinite aspect ratio

c_l section lift coefficient

p rolling velocity, radians per second

λ empirical factor used in formula for increase in lift of wing due to slipstream velocity

DESCRIPTION OF MODEL

A summary of pertinent characteristics of the full-scale version of the XP-69 airplane is given below:

Gross weight, lb	18,000
Engine - Wright Aeronautical Corp.	R-2160-3
Normal rating - 2300 bhp at 4200 rpm, sea level to 35,000 ft altitude	
Military rating - 2500 bhp at 4600 rpm, sea level to 35,000 ft altitude	
Propellers - two three-blade, dual-rotating	
Wing area, sq ft	505
Wing span, ft	52
Mean aerodynamic chord, ft	10.34
Airfoil section:	
Inboard	NACA 662-114
Outboard	NACA 662-213
Aspect ratio	5.32
Angle of incidence, relative to thrust line	1° 43.75'
Washout	2° 30'
Aileron area, aft of hinge line, sq ft (total)	35.6
Horizontal tail area, sq ft (total)	102
Stabilizer area, sq ft	61.2
Elevator area (including balance - 22 percent elevator area), sq ft	40.8
Vertical tail area, sq ft (total)	49.7
Fin area, sq ft	27.4
Rudder area (including balance - 16 percent rudder area), sq ft	22.3
Flap area, sq ft (total)	66.6

A three-view drawing showing the important dimensions of the 3/4-scale model of the XP-69 airplane is given in figure 1. The outer surfaces of the model were constructed of sheet aluminum which was covered with a plastic filler and sanded to a smooth finish before the tests were made.

Two 10-foot-diameter dual-rotating propellers of fixed-pitch construction were used to simulate the full-scale airplane propeller unit. Power was supplied to the propellers by two 25-horsepower electric motors installed in the fuselage. The front motor was directly connected to the front propeller, while the rear motor drove the rear propeller through chains and a countershaft. The motor frames were supported in a cradle so that they were free to rotate about their axes and were restrained from rotating by means of helical springs connected to the supporting frame. The angular deflection of the motor frame served as a measure of the motor torque.

Balanced, slotted flaps were used as a high-lift device. When deflected, the flaps moved to the rear and down and means were provided for several flap-angle adjustments ranging from 5° to 40°.

Both the ailerons and the elevators were of the sealed hinge-type construction. The

control surfaces were statically balanced by means of lead weights placed forward of the hinge lines. All of the control surfaces were equipped with balancing tabs which could be adjusted to give various ratios of tab deflection to control surface deflection.

METHODS AND TESTS

Figure 2 shows the 3/4-scale model of the XP-69 airplane mounted in the NACA full-scale tunnel (reference 1). The methods by which the data were corrected for jet-boundary and blocking effects are discussed in references 2 and 3.

Tests with propellers removed were made through a range of angles of attack and tunnel airspeeds to determine scale effect on the model. In order to determine the stabilizer angle for trim at the dive lift coefficient, $C_L = 0.085$, tests were made at two stabilizer settings with the propellers removed. The results of these tests are shown in figure 3. The stabilizer setting, 1.6°, determined from these tests was maintained for most of the following tests.

The aerodynamic characteristics of the dual-rotating propellers were determined previously in the NACA propeller-research tunnel (reference 4). The propellers as installed on the XP-69 model are shown in figures 2 and 4. A few calculations showed that at a propeller blade angle of about 28° very little error was introduced by operating at constant

blade angle to simulate the full-scale constant-speed propeller. In order that the rear propeller absorb the same amount of power at the peak efficiency condition as the front propeller, the blade angle of the rear propeller was set at 27.7° with a blade-angle setting of 28° for the front propeller. The necessity for this difference in blade angle can be explained by the fact that the front propeller introduces a rotational component to the slipstream which increases the angle of attack of the rear propeller. It is then necessary to reduce the blade angle of the rear propeller to offset this increased angle of attack (reference 4). The aerodynamic characteristics of the dual-rotating propellers on the XP-69 model at about zero lift coefficient are shown in figure 5. These results and the results of reference 4 are in close agreement.

The chart of T_c against C_L for the power-on tests was furnished by the Republic Aviation Corporation and is given in figure 6 for operation at sea level and at 35,000 feet altitude. For the idling-power condition, a value of $T_c = 0.045$ at $C_L = 1.7$ was furnished and this thrust coefficient was used throughout the lift range to simulate the idling-power condition.

The values of thrust coefficient used to simulate the flight attitude of the yawed model were chosen to be the

same as those of the unyawed model. Since the lift coefficient decreases with increasing yaw angle, this procedure does not reproduce exactly the airplane-propeller conditions at large angles of yaw. For the yaw angle range tested ($\psi = \pm 15^{\circ}$), however, this method probably does not introduce any serious errors.

Tests were made with the horizontal tail removed and attached, in each case with the propellers removed and operating. Each condition included tests with the landing flaps retracted and deflected. The landing gear was removed for all of the tests. Measurements were also taken of the elevator control effectiveness and hinge moments at several angles of attack. The effects of elevator tab position on the hinge moments and on the pitching moments were determined. The elevator hinge moments were measured by means of a calibrated torque rod, the deflection of which was indicated by Selsyn motors located in the fuselage and in the test house.

All the tests with the model yawed were made with the horizontal and the vertical tail surfaces attached to the model and with the propellers operating. The model attitudes for each angle of yaw included high speed, climbing, and landing. With the model in the high-speed and climbing attitudes, the measurements were made at thrust coefficients approximately simulating the full- and half-rated power

conditions at sea level. With the model in the landing attitude, the measurements were made with the landing flaps deflected 40° at thrust coefficients approximately simulating the idling and half-rated power (approach attitude) conditions at sea level. For each power condition and model attitude, measurements were made of the rudder control effectiveness and hinge moments.

The method for measuring the rudder hinge moments was similar to that used for measuring the elevator hinge moments. Some tests were made to determine the effect of tab position on the rudder hinge moments and yawing moments. The effects of yaw angle on the elevator control effectiveness and hinge moments have also been determined. The model is shown yawed 15.1° in the full-scale tunnel in figure 7.

The tests to determine the aileron control effectiveness and hinge moments were made with only the left aileron deflected. All these tests were made with the propellers removed. The aileron hinge moments were measured by means of a cantilever beam equipped with a strain gage for indicating its deflection. The aileron angles were measured by recording the change in resistance of a rheostat which varied according to the movement of the aileron controls. The tests were made with the model in the yawed and unyawed conditions at several angles of attack. The effects on

aileron control effectiveness and hinge moments of installing cannons (fig. 8) and gasoline tanks (fig. 9) on the wing of the model have been determined. Tests were also made to determine the effect of tab position on the aileron hinge moments and rolling moments.

Surveys were made of the velocity and direction of the air flow in the region of the tail plane. For these tests, the horizontal and the vertical tail surfaces were removed from the model (fig. 10). The surveys were made with propellers removed and operating and for both cases included the conditions for flaps retracted and flaps deflected 40°. A complete description of the apparatus used for the surveys is given in reference 5.

RESULTS AND DISCUSSION

The results of the tests have been analyzed and are presented in three parts. The first part deals with the results of the tests to determine the longitudinal-stability characteristics of the model and includes measurements with the tail surfaces removed and attached and with the propellers removed and operating. The contributions of the horizontal tail surface, the wing-fuselage combination, and the propellers to longitudinal stability are discussed in this section. The second part deals with the lateral characteristics of the model and includes both the yawing- and

rolling-stability data. The results of the air-flow surveys are discussed in the third part.

The results of the tests are presented by means of the standard NACA coefficients of forces and moments. All of the moments have been taken about the center-of-gravity position indicated in figure 1. The data are referred to the stability axes. The X axis is the intersection of the plane of symmetry of the airplane with a plane perpendicular to the plane of symmetry and parallel with the relative wind direction; the Y axis is perpendicular to the plane of symmetry; and the Z axis is in the plane of symmetry and perpendicular to the X axis.

Longitudinal Stability, Control, and Trim

Tail-removed tests. - The results of the tests with the propellers and the horizontal and vertical tail surfaces removed are shown in figure 11. The slopes of the curves of C_m against C_L (fig. 11) indicate only a slight degree of longitudinal instability for the tail-removed condition. This is explained by the fact that the center of gravity is located fairly well forward on this model (25 percent M.A.C.). With flaps retracted, the location of the neutral point of the model without the tail was measured to be about $0.025\bar{c}$ ahead of the center of gravity. A slight decrease of longitudinal instability, resulting from the rearward shift of the center of pressure with flap deflection, was obtained

when the flaps were deflected 40° (fig. 11). The location of the neutral point of the model without the tail for the flaps-deflected condition was about $0.003\bar{c}$ ahead of the center of gravity.

The effects of propeller operation on the aerodynamic characteristics of the model without the tail are shown in figures 12 and 13 for the model with flaps retracted and with flaps deflected 40°, respectively. For the model with flaps retracted (fig. 12), propeller operation was destabilizing, although the decrease in stability was not a direct function of the amount of power applied. The destabilizing effect of propeller operation on the model without the tail, flaps retracted, may be attributed to the direct effect of the propeller forces which are destabilizing for all positive angles of attack. With flaps deflected 40°, propeller operation was destabilizing when idling power was applied; with half-rated power applied, however, propeller operation was stabilizing. This condition results from the fact that the large negative pitching moment resulting from flap deflection is increased with increased slipstream velocity over the wing. Since, for constant power operation, the thrust and therefore the slipstream velocity increases with lift coefficient, the increase in negative pitching moment will be greatest in the high-lift range.

The change in pitching moment due to propeller operation for the model without the tail may be determined from considerations of the direct effect of the propeller forces and of the slipstream effect on the wing pitching moments. It is of interest to compare the effects of propeller operation on pitching moments as calculated from these considerations with the experimental values. The total change of pitching-moment coefficient of the model without the tail may be calculated from the following equation:

$$\Delta C_{m_P} = \Delta C_{m_N} + \Delta C_{m_T} + \Delta C_{m_s}$$

The term ΔC_{m_P} is the total change in pitching-moment coefficient due to propeller operation, ΔC_{m_T} and ΔC_{m_N} represent the change due to the direct effect of the propeller forces, and ΔC_{m_s} is the change of wing pitching-moment coefficient due to the slipstream. For single-engine airplanes with flaps retracted, ΔC_{m_s} is usually very small and may be neglected (reference 6). Using the methods of references 6 and 7, the total change in pitching-moment coefficient due to propeller operation, ΔC_{m_P}, has been calculated for the flaps-retracted condition with full-rated power applied and for the flaps-deflected condition with half-rated power applied. A comparison is given between the experimental and calculated ΔC_{m_P} in figure 14. The agreement shown is good.

Propeller operation increased the slope of the lift curve of the model without the tail, the increase being approximately proportional to the amount of power applied. The increase in $dC_L/d\alpha$ with power results from the direct effect of the propeller forces and from the slipstream effects. Inasmuch as the lift coefficients of the sections immersed in the slipstream are greatest when flaps are deflected, the increase in lift due to propeller operation will be greatest for the flaps-deflected conditions. The increase in lift coefficient due to propeller operation may be calculated by means of the expression

$$\Delta C_{L_P} = \Delta C_{L_T} + \Delta C_{L_N} + \Delta C_{L_S}$$

where ΔC_{L_P} is the total change in lift coefficient due to propeller operation, ΔC_{L_T} and ΔC_{L_N} are the increments due to the direct effect of the propeller forces, and ΔC_{L_S} is the change in wing lift coefficient due to the slipstream. For the increment of lift resulting from the passage of the slipstream over a part of the wing, the semiempirical formula of reference 8 has been found to give satisfactory agreement with experimental data; thus,

$$\Delta C_{L_S} = \frac{b_i C_P}{S} s \left[\lambda c_l - 0.6 a_o \epsilon_P\right]$$

The factor λ, introduced because of the change in circulation over the wing, may be taken as 1.0 for the flaps-retracted

condition. With flaps deflected, however, owing to the marked effect of the slipstream on the flapped-wing vortex system, the value of λ is taken as 1.6 according to reference 7. The change in lift due to the direct effect of the propeller forces may be calculated by the methods given in reference 6. The agreement between the experimental and calculated values of ΔC_{L_p} that are given in figure 15 is good.

Tail-on tests. - The results of the tests with the horizontal and vertical tail surfaces on and with the propellers removed are shown in figure 16. The location of the neutral point for the tail-on condition with propellers removed was about $0.19\bar{c}$ behind the center of gravity with flaps retracted and about $0.21\bar{c}$ behind the center gravity with flaps deflected 40°.

The effects of propeller operation on the aerodynamic characteristics of the complete model for various flap conditions are shown in figures 17 to 21. Figure 17 gives the results for the model with flaps retracted and with propellers operating at full- and half-rated power. The results for full- and half-rated power for the model with flaps deflected 10.5° and 20.9° are shown in figures 18 and 19, respectively. Figure 20 gives the results of the tests with flaps deflected 40° and with the propellers operating

at full-rated, half-rated, and idling power. The effects of propeller operation on longitudinal stability, as determined by the slopes of the curves of C_m against C_L at fixed elevator for constant power operation, were destabilizing in all cases. The destabilizing effect of power was most pronounced for the condition with the flaps deflected 40°, causing instability at high lift coefficients when full-rated power was applied (fig. 20).

By comparing the results of the tests of the model with the horizontal tail on and with the propellers removed and operating, the increments of pitching-moment coefficient at the wing and tail due only to the effects of propeller operation have been determined and are shown in figure 21. The increments of tail pitching-moment coefficient due to propeller operation were small with flaps retracted; however, with flaps deflected 40° the change of tail moment was very large when high power was applied, causing the instability shown in figure 20.

The total contribution of the horizontal tail to longitudinal stability is shown in figure 22 for the model with flaps retracted, and in figure 23 for the model with flaps deflected 40°. For both conditions, propeller operation provided an increment of positive pitching-moment coefficient from the tail. With flaps retracted, the normal force on

the horizontal tail surface was positive for lift coefficients above 0.3, regardless of the power condition. With flaps deflected 40°, the normal force on the horizontal tail was negative for lift coefficients below 1.6, regardless of the power condition.

The effects of applying full- and half-rated power at 35,000 feet altitude on the aerodynamic characteristics of the model with flaps retracted have been determined and are given in figure 24. Since the thrust coefficient for any particular power condition decreases with altitude, the destabilizing effect of power on longitudinal stability and the increase in the slope of the lift curve with power are less at altitude than at sea level.

Elevator effectiveness and hinge moments. - The variations of C_m, C_L, and C_{h_e} with elevator deflection (elevator tab locked) for the propellers-removed condition are shown in figure 25. The elevator effectiveness, $dC_m/d\delta_e$, and the rate of change of elevator hinge-moment coefficient with elevator deflection, $dC_{h_e}/d\delta_e$, decreased slightly with angle of attack. For any particular elevator angle setting, the elevator hinge moments increased negatively with angle of attack.

The elevator was equipped with a balancing tab which could be adjusted to give several ratios of tab angle to

elevator deflection. The variations of tab angle with elevator deflection are given in figure 26. Figure 27 shows the variation of elevator hinge-moment coefficient with elevator deflection for the conditions of elevator tab locked and of elevator tab adjusted to give minimum and maximum deflections. With the tab locked, the measurements were made at a stabilizer angle of 1.9°; however, with the tab operating, the measurements were made at a stabilizer angle of 3.1°. Examination of the data reveals that the change of hinge-moment coefficient due to a difference in stabilizer angle of 1.2° is small, so that a comparison can be made of the hinge moments for the various tab conditions. The slope, $dC_{h_e}/d\delta_e$, for the tab-locked condition was reduced somewhat with the elevator tab adjusted to give maximum ratio deflections; little change was measured, however, with the tab adjusted to give minimum ratio deflections. The effect of the tab on pitching moments is given in figure 28 for various angles of attack. A small decrease in the slope $dC_m/d\delta_e$ was measured, the decrease being most pronounced at the lowest and the highest angles of attack.

The variations of C_m, C_L, and C_{h_e} with elevator deflection for various power conditions and with the model in the high-speed, climbing, and landing attitudes are given in figures 29 and 30. A curve is presented (fig. 31) showing

the elevator angles required to trim the airplane throughout the speed range for the condition of flaps retracted and full-rated power applied. The values of δ_e at high values of indicated airspeed were obtained from the experimental values of figure 29, and the values of δ_e at low values of indicated airspeed were obtained by extrapolating the results of figure 29 to higher lift coefficients.

The effects of the slipstream on $dC_m/d\delta_e$ and $dC_{h_e}/d\delta_e$ are illustrated in figure 32. With propellers removed, the values of $dC_m/d\delta_e$ and $dC_{h_e}/d\delta_e$ decreased with angle of attack; however, with propellers operating, the values of $dC_m/d\delta_e$ and $dC_{h_e}/d\delta_e$ increased with angle of attack. Since for constant power operation T_c increases with angle of attack, the dynamic pressure at the tail and therefore $dC_m/d\delta_e$ and $dC_{h_e}/d\delta_e$ should increase with the angle of attack. The increase appears to be approximately proportional to the amount of power applied.

The effect of tab position on the elevator hinge moments of the model with propellers operating is shown in figure 33. With the tab locked, the values of $dC_{h_e}/d\delta_e$ at $C_{h_e} = 0$ were -0.0101 and -0.0113 per degree elevator deflection for the airplane in the high-speed and climbing attitudes, respectively. With the tab adjusted to give maximum ratio deflections, the corresponding values of $dC_{h_e}/d\delta_e$ were -0.0084 and -0.0089.

In order to determine the effects of yaw on the elevator effectiveness, some tests were made with the model yawed at 5.75° and 15.1°. The results of the tests with the model in the high-speed and climbing attitudes are shown in figures 34 and 35, and the results for the model in the landing attitude (flaps deflected 40°) are shown in figures 36 and 37. A comparison is given in table I of the values of $\left(\frac{dC_m}{d\delta_e}\right)_{C_m=0}$ and $\left(\frac{dC_{h_e}}{d\delta_e}\right)_{C_{h_e}=0}$ for the model in the yawed and unyawed conditions. It is seen that, in the high-speed attitude, the elevator effectiveness decreases about 10 percent when the model is yawed 15.1°. The change of elevator effectiveness with yaw in the climbing and the landing attitudes was less than in the high-speed attitude.

Lateral Stability, Control, and Trim

Aerodynamic characteristics in yaw. - The changes of the aerodynamic characteristics with yaw angle have been determined by cross-plotting the results of rudder-effectiveness tests (similar to those shown in figs. 54 to 57) at several angles of yaw. The variations of C_L and C_m with Ψ for the model in the high-speed, climbing, and landing attitudes are shown in figures 38 to 40. It should be noted that in the landing attitude with flaps deflected the changes in C_m and C_L due to yaw were large and somewhat inconsistent for both power conditions. The effect of yaw angle

on C_m and C_L for the model in the high-speed and climbing attitudes was considerably less than for the model in the landing attitude.

The changes of C_n, C_l, and C_Y with ψ for the model in the high-speed, climbing, and landing attitudes at various power conditions are shown in figures 41 to 46. The effects of propeller operation on the effective dihedral, $dC_l/d\psi$, and on the directional stability, $dC_n/d\psi$, were most pronounced for the flaps-deflected condition. With the model in the landing attitude and idling power applied, the slope of the curve of yawing-moment coefficient against angle of yaw shows approximately neutral stability at small positive angles of yaw and instability from -2° to -8° angle of yaw (fig. 45). Inasmuch as the value of $dC_l/d\psi$ for this condition is relatively high, about 0.0018, a condition of lateral oscillatory instability will probably exist. The danger of this condition is accentuated because it occurs at the landing attitude where recovery becomes very difficult. A large decrease in effective dihedral was measured when half-rated power was applied to the model in the landing attitude; however, the directional stability was increased (fig. 46). This combination should result in a condition of spiral instability. Spiral instability is not a severe condition, however, inasmuch as little difficulty

is encountered in flying airplanes which are spirally unstable. Since it has been proposed that the model be returned to the full-scale tunnel for further engine-cooling tests, some additional tests to check the stability of the airplane in the landing attitude are contemplated.

The slope of the curve of lateral-force coefficient against angle of yaw for the model with flaps deflected 40° was increased from 0.0055 to 0.0124 when the thrust coefficient was increased from 0.045 to 0.490.

The effects of propeller operation on the directional stability, on the effective dihedral, and on the rate of change of lateral-force coefficient with yaw angle for the model in the high-speed and climbing attitudes are illustrated in figure 47. The directional stability decreased with angle of attack, but at any particular angle of attack the directional stability was higher for the full-power condition than for the half-power condition. No variation of $dC_Y/d\Psi$ with angle of attack or power was measured for the high-speed or climb conditions.

The changes in the lateral characteristics due to power result from the direct effect of the propeller forces and from the effects due to the propeller slipstream. Since the thrust axis and the center of gravity lie in the plane of symmetry, the thrust forces have no effect on the rolling

and yawing moments about the stability axes. The propeller normal force, however, lies in the plane of the propeller and causes a yawing moment which is always destabilizing. The effect of the propeller torque, which usually causes a large rolling moment for airplanes with single-rotating propellers, is probably very small and may be neglected when dual-rotating propellers are used.

When the airplane is yawed, a greater part of the slipstream is deflected over the trailing-wing panel. The result is that the increased dynamic pressure increases the lift of the trailing-wing panel and causes a decrease in effective dihedral. The decrease would be most pronounced with the flaps deflected, since the inboard sections of the wing are operating at high section lift coefficients. By the same reasoning, the drag of the trailing-wing panel is increased which results in a destabilizing yawing moment.

The adverse effects of wing-fuselage interference on the effective dihedral and the favorable effects on the directional stability of low-wing monoplanes are probably changed somewhat by the passage of the slipstream over the wing-fuselage juncture. The increase in dyanmic pressure over the vertical tail increases the control effectiveness and probably increases the directional stability depending on the angle of sidewash and the direction of the load at

the vertical tail. As the angle of yaw is increased, a point will be reached where the vertical tail passes out of the slipstream and, consequently, the control effectiveness will be decreased to the propellers-removed value. The sidewash angle at the tail results from the various components of the air flow due to the wing, the fuselage, and the slipstream and is determined as a vector addition of these components. Some changes in the pitching moments due to yaw are caused by the changes in velocity and direction of flow at the horizontal tail surface due to the slipstream.

Rudder effectiveness and hinge moments. - The variations of C_n, C_Y, and C_{h_r} with rudder deflection for the model with propellers removed are shown in figure 48. The values of $dC_n/d\delta_r$, $dC_Y/d\delta_r$, and $dC_{h_r}/d\delta_r$ changed very little with angle of attack. For the propellers-removed condition, the respective values of $dC_n/d\delta_r$ and $dC_Y/d\delta_r$ were -0.0013 and 0.0022 per degree. The value of $dC_{h_r}/d\delta_r$ at $\delta_r = 0$ was -0.0045 per degree.

The effect of various ratios of tab angle to rudder deflection on the rate of change of rudder hinge-moment coefficient with rudder deflection, $dC_{h_r}/d\delta_r$, is shown in figure 49. Figure 50 shows the variation of tab angle with rudder deflection for the different tab adjustments. A large decrease in the value of $dC_{h_r}/d\delta_r$ at $\delta_r = 0$ for no

tab was measured when the tab was adjusted to give either tab-rudder deflection ratio 1 or 2; however, there was little change of rudder hinge moments measured between tab-rudder deflection ratios 1 and 2. The effect of tab setting on the yawing-moment coefficients at several angles of attack is shown in figure 51. The tab caused a very small decrease in rudder effectiveness, $dC_n/d\delta_r$.

The effects of propeller operation on the variations of C_n, C_Y, and C_{h_r} with δ_r for the model in the high-speed, climbing, and landing attitudes are shown in figures 52 and 53. In the high-speed attitude, where the lift coefficient and thrust are low, there was little change of $dC_n/d\delta_r$ and $dC_Y/d\delta_r$ due to propeller operation. A slight increase of $dC_n/d\delta_r$ and no increase of $dC_Y/d\delta_r$ was measured with the model in the climbing attitude and full-rated power applied. With the model in the landing attitude, however, the values of $dC_n/d\delta_r$ and $dC_Y/d\delta_r$ were increased to -0.0018 and 0.0029, respectively, when half-rated power was applied. The rate of change of rudder hinge-moment coefficient with rudder deflection increased with power; a value of $dC_{h_r}/d\delta_r$ of -0.0088 was measured for the model in the landing attitude with half-rated power applied as compared with a value of -0.0045 for the model with propellers removed.

Several tests were made to determine the effects of rudder deflection on the aerodynamic characteristics of the model in yaw. The results of some of the tests with the model in the high-speed, climbing, and landing attitudes are given in figures 54 and 55 for $\psi = 15.1^\circ$ and in figures 56 and 57 for $\psi = -15.2^\circ$. The variations of $dC_n/d\delta_r$ at $C_n = 0$ and $dC_{h_r}/d\delta_r$ at $C_{h_r} = 0$ with ψ are given in figure 58 for the model in the high-speed attitude with full- and half-rated power applied, in figure 59 for the model in the climbing attitude with full- and half-rated power applied, and in figure 60 for the model in the landing attitude with idling and half-rated power applied. The effect of yaw angle on $dC_n/d\delta_r$ was small for all of the test conditions; however, an appreciable increase in $dC_{h_r}/d\delta_r$ with yaw was measured.

The rate of change of rudder hinge-moment coefficient at zero rudder deflection with yaw angle for the various model attitudes is shown in figure 61. For the high-speed and climbing attitudes, the values of $dC_{h_r}/d\psi$ was zero at small angles of yaw. For the model in the landing attitude with half-rated power applied, some variations of $C_{h_r(\delta_r=0)}$ with ψ was measured, but these were small at small angles of yaw.

The rudder angles necessary to hold a given angle of yaw for the model in the high-speed and climbing attitudes are given in figures 62 and 63 for the full- and half-rated power conditions, respectively. In the high-speed attitude, a value of $d\psi/d\delta_{r(C_n=0)}$ of about 1.1 was measured. The value of $d\psi/d\delta_{r(C_n=0)}$ for the model in the climbing attitude with full-rated power applied was about 1.2, which was increased to about 1.3 when half-rated power was applied. The rudder angles to hold a given angle of yaw for the model in the landing attitude with idling and half-rated power applied are shown in figure 64. The instability shown by the curve of figure 64 at small angles of yaw for the idling-power condition corresponds to the same instability noted in the curve of C_n against ψ (fig. 45) at small angles. The value of $d\psi/d\delta_{r(C_n=0)}$ for the model in the landing attitude with half-rated power applied was about 1.5.

Aileron effectiveness and hinge moments. - Since the ailerons on this model are well out of the region covered by the slipstream, all of the tests to determine the effects of aileron deflection were made with the propellers removed. The measurements were made for deflections of the left aileron only. Figures 65 and 66 show the variations of C_l, C_n, and C_{h_a} with aileron deflection (tab locked) for the model with flaps retracted and with flaps deflected

40°, respectively. The results with the model yawed at -10.1° and with the flaps retracted and flaps deflected 40° are shown in figures 67 and 68, respectively.

Tuft surveys had previously shown that the installation of cannons at the leading edge of the wing caused an early separation of the flow, especially in the region of the ailerons. As a result, aileron-effectiveness tests were made with the cannons installed on the wing in their maximum up position (fig. 8). The results of the tests with the cannons installed on the wing are given in figure 69.

Inasmuch as it has been proposed that the Republic Aviation Corporation install gasoline tanks on the lower surface of the wings (fig. 9) for ferrying purposes, some tests were made to determine the effects of the wing tanks on the aileron effectiveness. The results of the tests for the unyawed model are shown in figure 70. Figures 71 and 72 show the results of the tests with the wing tanks on and $\psi = -10.1^\circ$ for the flaps-retracted and flaps-deflected conditions, respectively.

The variations of C_L, C_D, and C_m with α for the model with the wing tanks on and for the model with cannons installed in their maximum up position are shown in figure 73. It will be noticed from figure 73 that the cannon installation caused a reduction of maximum lift coefficient of about

0.3. Studies made with various cannon installations showed that the reduction of maximum lift coefficient due to the cannons can be minimized by (1) lowering the cannons, (2) using a longer cannon extension from the leading edge of the wing, and (3) using a suitable fairing at the wing-cannon juncture. The gasoline tanks caused no appreciable reduction of maximum lift coefficient.

The variations of C_{h_a} with δ_a for the tab-locked and tab-operating conditions are shown in figure 74 for various angles of attack. Figure 75 shows the variation of tab angle with aileron deflection. With the aileron tab installed, some decrease in $dC_{h_a}/d\delta_a$ was measured. Figure 76 shows the variations of C_l, C_n, and C_{h_a} with aileron deflection for the case of aileron tab installed at ratio 1. The tab had very little effect on either the yawing or the rolling moments.

A few calculations have indicated that the stick forces required to obtain maximum aileron deflections with the airplane in the high-speed or cruising attitude will be excessive. This was true for the conditions of tab locked and tab operating.

A table has been prepared (table II) giving values of aileron effectiveness and helix angle, $pb/2V$, for all of the test conditions. The values of $dC_l/d\delta_a$ and $pb/2V$

have been computed for a total angular difference between up and down ailerons of 30° with an aileron differential ratio of 1:1. The term $pb/2V$, which expresses the lateral displacement of the wing tip in a given forward travel of the airplane, is a measure of satisfactory aileron control (reference 9). A value of $pb/2V$ of 0.07 represents a criterion of minimum satisfactory aileron effectiveness. The values of $pb/2V$ for all the conditions tested varied from 0.082 to 0.117.

The criteria for satisfactory aileron control presented in reference 9 should be used with caution. Flight measurements have indicated that the values of $pb/2V$ obtained in wind-tunnel tests are about 0.02 higher than those obtained in flight as a result of wing twist and sideslip angle. Furthermore, although a value of $pb/2V$ of 0.07 implies a condition of satisfactory aileron-control effectiveness, it does not imply that the rolling velocities attainable will be satisfactory. Thus, a pursuit airplane having a large wing span will require larger values of $pb/2V$ to attain rolling velocities equal to those of a pursuit airplane having a small wing span. On this basis, the rolling velocities attainable with the present XP-69 aileron installation may be inadequate.

Air-Flow Surveys

The results of the air-flow surveys are presented in figures 77 through 80. The figures show contours of q/q_o and downwash and sidewash vectors in a vertical plane through the elevator hinge line for various angles of attack and thrust coefficients. The results of the propellers-removed surveys are given in figures 77 and 78 for the flaps-retracted and flaps-deflected conditions, respectively. The effects of propeller operation on the air flow in the region of the tail plane are shown in figures 79 and 80. A table (table III) is presented, giving values of the dynamic-pressure ratios and the downwash angles averaged across each semispan of the horizontal tail surface at the elevator hinge line.

The velocity and direction of the air flow at the tail may be considered as the resultant of the various fields of flow from the wing, the fuselage, the ducting system, and the propeller slipstream. The wing wake (or region of low dynamic pressure) and the combined wakes of the wing, the fuselage, and the ducting system (or region characterized by the erratic flow just below the fuselage) are clearly evident in the surveys made with the propellers removed. (See figs. 77 and 78.) Owing to the relatively high position of the horizontal tail surface with respect to the wing, the center line of the wing wake passed below the

horizontal tail surface for all of the conditions tested. The center line of the wing wake rose relative to the tail with increasing angle of attack (figs. 77(a) to 77(c)), which resulted in a small decrease in the average dynamic-pressure ratio measured across the horizontal tail surface as the angle of attack was increased. The change in dynamic pressure at the tail due to flap deflection was small since the flap wake always passed below the horizontal tail surface.

The downwash angle at the tail, which is directly proportional to the lift coefficient, increased with angle of attack and flap deflection. The increase of downwash angle at the tail due to flap deflection was about 7° for the propellers-removed condition.

The effects of propeller operation on the dynamic pressure and the downwash angles at the tail are illustrated in table III. The values of $(q/q_o)_{av}$ and ϵ_{av} were computed separately across each semispan of the horizontal tail in order to ascertain whether the use of dual-rotating propellers eliminated the effects due to slipstream rotation. Propeller operation increased the dynamic pressure at the tail. The increase in dynamic pressure at the tail, however, was not directly proportional to the amount of power applied since the location of the slipstream center line with respect to the horizontal tail varied with angle of attack and thrust

coefficient. For all positive angles of attack the downwash at the tail increased with propeller operation; whereas, at the negative angle of attack, propeller operation resulted in a small decrease in the downwash at the tail.

When the power absorbed by the front propeller was approximately equal to the power absorbed by the rear propeller, there was little evidence of slipstream rotation in the surveys. Since the propeller blade angles were adjusted so as to absorb approximately equal power at the V/nD for peak efficiency (V/nD = 1.25), the powers absorbed by the two propellers were not equal at other values of V/nD (fig. 5). At low thrust coefficients, where the difference in power absorbed by the front and rear propellers was small, the values of $(q/q_o)_{av}$ and ϵ_{av} measured across each semispan of the horizontal tail surface were approximately equal. At the higher thrust coefficients, however, some difference in $(q/q_o)_{av}$ and ϵ_{av} was measured, although the difference was considerably less than that usually observed behind airplanes with single-rotating propellers.

SUMMARY OF RESULTS

1. Propeller operation resulted in an appreciable decrease in static longitudinal stability. With flaps retracted and full-rated power applied, the neutral point was

shifted about 7 percent of the mean aerodynamic chord forward of its position for the propellers-removed condition. With flaps deflected 40° and full-rated power applied, the neutral point was shifted about 20 percent of the mean aerodynamic chord forward of its position for the propellers-removed condition.

2. The application of power increased the slope of the lift curve, the increase being approximately proportional to the amount of power applied.

3. The elevator provided satisfactory longitudinal control throughout the lift range.

4. The elevator effectiveness and the slope of the hinge-moment curve against elevator deflection increased with power.

5. The effect of yaw angle on elevator effectiveness was small for the range of yaw angles tested.

6. A decrease in $dC_{h_e}/d\delta_e$ at zero tab of from 10 to 20 percent, depending on the power condition, was measured when the tab was adjusted to give the maximum tab angle to elevator deflection ratio.

7. The ratio of effective dihedral, $dC_l/d\Psi$, to directional stability, $dC_n/d\Psi$, varied from about 1.0 to 1.3 for the model in the high-speed and climbing attitudes with flaps retracted and with full- and half-rated power applied.

8. A large decrease in directional stability was measured when flaps were deflected and idling power applied. For the model in the landing attitude with idling power applied, the slope of the curve of C_n against Ψ showed approximately neutral stability at small positive angles of yaw and instability from -2° to -8° angle of yaw. The effective dihedral, as indicated by $dC_l/d\Psi$, was high. A condition of lateral oscillatory instability may therefore exist for landings made with idling power.

9. A large decrease in effective dihedral was measured when half-rated power was applied to the model in the landing attitude with flaps deflected; the directional stability, however, was greater than that measured for the idling-power condition.

10. The slope of the curve of yaw angle against rudder deflection at trim $d\Psi/d\delta_{r(C_n=0)}$ varied from about 1.0 to 1.3 for the model in the high-speed and climbing attitudes with full- and half-rated power applied. A large increase in $d\Psi/d\delta_{r(C_n=0)}$ was measured when flaps were deflected and idling power applied.

11. The rudder effectiveness and the rate of change of hinge-moment coefficient with rudder deflection increased with power.

12. The negative value of $dC_{h_r}/d\delta_r$ at $C_{h_r} = 0$ was reduced about 0.0025 by the use of a balancing tab.

13. The magnitude of the maximum rolling velocities attainable with a total aileron deflection of 30° may be low when compared with that attained by some present-day pursuit-type airplanes.

14. The stick forces required to obtain maximum aileron deflections with the airplane in the high-speed or cruising attitudes will be excessive.

15. A small reduction of aileron hinge moments was obtained by the use of a balancing tab.

16. The addition of cannons and gasoline tanks on the wing of the model caused very little change of aileron effectiveness.

17. The test results indicate that little or no application of the ailerons or rudder will be necessary to fly in an unyawed attitude with propellers operating.

18. With the cannons installed on the leading edge of the wing in their maximum up position, a reduction in maximum lift coefficient of about 0.3 was measured.

19. The center line of the wing wake was below the horizontal tail surface for all of the conditions tested.

20. Propeller operation increased the dynamic pressure at the tail. The downwash angles at the tail were increased for positive angles of attack and decreased for negative angles of attack when power was applied.

21. When the power absorbed by the front propeller was approximately equal to the power absorbed by the rear propeller, there was little evidence of rotation in the slipstream.

Langley Memorial Aeronautical Laboratory,
National Advisory Committee for Aeronautics,
Langley Field, Va. January 7, 1943.

REFERENCES

1. DeFrance, Smith J.: The N.A.C.A. Full-Scale Wind Tunnel. Rep. No. 459, NACA, 1933.

2. Silverstein, Abe, and Katzoff, S.: Experimental Investigation of Wind-Tunnel Interference on the Downwash behind an Airfoil. Rep. No. 609, NACA, 1937.

3. Theodorsen, Theodore, and Silverstein, Abe: Experimental Verification of the Theory of Wind-Tunnel Boundary Interference. Rep. No. 478, NACA, 1934.

4. Biermann, David, and Hartman, Edwin P.: Wind-Tunnel Tests of 4- and 6-blade Single- and Dual-Rotating Propellers. Rep. No. 747, NACA, 1942.

5. Sweberg, Harold H.: The Effect of Propeller Operation on the Air Flow in the Region of the Tail Plane for a Twin-Engine Tractor Monoplane. NACA A.R.R., Aug. 1942.

6. Goett, Harry J., and Pass, H. R.: Effect of Propeller Operation on the Pitching Moments of Single-Engine Monoplanes. NACA A.C.R., May 1941.

7. Pass, H. R.: Wind-Tunnel Study of the Effects of Propeller Operation and Flap Deflection on the Pitching Moments and Elevator Hinge Moments of a Single-Engine Pursuit-Type Airplane. NACA A.R.R., July 1942.

8. Smelt, R., and Davies, H.: Estimation of Increase in Lift due to the Slipstream. R. & M. No. 1788, British A.R.C., 1937.

9. Gilruth, R.R., and Turner, W. N.: Lateral Control Required for Satisfactory Flying Qualities Based on Flight Tests of Numerous Airplanes. Rep. No. 715, NACA, 1941.

TABLE I

Effect on Angle of Yaw on $\left(\frac{dC_m}{d\delta_e}\right)_{C_m=0}$ and $\left(\frac{dC_{h_e}}{d\delta_e}\right)_{C_{h_e}=0}$

Elevator Tab Locked; i_t, 1.6°

Flaps retracted											
ψ = 0°				ψ = 5.75°				ψ = 15.1°			
α (deg)	T_c	$\left(\frac{dC_m}{d\delta_e}\right)_{C_m=0}$	$\left(\frac{dC_{h_e}}{d\delta_e}\right)_{C_{h_e}=0}$	α (deg)	T_c	$\left(\frac{dC_m}{d\delta_e}\right)_{C_m=0}$	$\left(\frac{dC_{h_e}}{d\delta_e}\right)_{C_{h_e}=0}$	α (deg)	T_c	$\left(\frac{dC_m}{d\delta_e}\right)_{C_m=0}$	$\left(\frac{dC_{h_e}}{d\delta_e}\right)_{C_{h_e}=0}$
-0.3	0.020	-0.0223	-0.0101	-0.2	-0.023	-0.0231	-0.0086	-0.2	0.018	-0.0203	-0.0084
-.3	.012	-.0223	-.0094	-.2	.012	-.0226	-.0081	.2	-.007	-.0206	-.0084
3.9	.072	-.0230	-.0107	3.9	.072	-.0233	-.0087	3.9	.058	-.0244	-.0093
3.9	.160	-.0241	-.0113	3.9	.140	-.0266	-.0090	3.9	.124	-.0247	-.0103
Flaps deflected 40°											
12.5	0.055	-0.0236	-0.0107	12.6	0.047	-0.0208	-0.0111	12.6	0.047	-0.0217	-0.0086
8.9	.530	-.0297	-.0166	8.9	.510	.0279	-.0180	8.9	.510	-.0286	-.0167

TABLE II

Aileron Effectiveness and Values of $\frac{pb}{2V}$ Calculated for Full Deflection ($\Delta\delta_a = 30^\circ$) of Both Ailerons. Aileron Differential Ratio, 1:1

Test condition	α (deg)	$dC_l/d\delta_a$	pb/2V	Test condition	α (deg)	$dC_l/d\delta_a$	pb/2V
1. Model with bare wing; δ_f, 0°; ψ, 0°; aileron tab locked	-0.7	0.0025	0.086	5. Wing cannons installed δ_f, 0°; ψ, 0°; aileron tab locked	-0.7	0.0029	0.100
	3.8	.0032	.110		3.8	.0032	.110
	8.1	.0032	.110		8.1	.0033	.113
	12.6	.0029	.100		12.6	.0032	.110
2. Model with bare wing; δ_f, 40°; ψ, 0°; aileron tab locked	7.2	.0034	.117	6. Wing tanks installed δ_f, 0°; ψ, -10.1°; aileron tab locked	-0.6	.0025	.086
	11.6	.0033	.113		3.8	.0028	.096
	16.5	.0027	.093		8.2	.0032	.110
					12.6	.0030	.103
3. Model with bare wing; δ_f, 0°; ψ, -10.1°; aileron tab locked	-0.7	.0027	.093	7. Wing tanks installed δ_f, 0°; ψ, -10.1°; aileron tab locked	-0.6	.0028	.096
	3.8	.0030	.103		3.9	.0030	.103
	8.2	.0031	.106		8.3	.0034	.117
	12.7	.0030	.103		12.7	.0029	.100
4. Model with bare wing; δ_f, 40°; ψ, -10.1°; aileron tab locked	7.3	.0029	.100	8. Wing tanks installed δ_f, 40°; ψ, -10.1°; aileron tab locked	7.4	.0033	.113
	11.8	.0025	.086		11.8	.0030	.103
	15.3	.0024	.082		15.3	.0029	.100

L-642

TABLE III

Average Dynamic-Pressure Ratios and

Downwash Angles at Tail

α (deg)	C_L	δ_f (deg)	T_c (a)	$(q/q_o)_{av}$		ϵ_{av} (deg)	
				Right semispan of tail	Left semispan of tail	Right semispan of tail	Left semispan of tail
-0.7	0.130	0	-	0.99	0.97	1.7	1.9
3.7	.407	0	-	.98	.97	2.5	2.7
8.1	.723	0	-	.94	.95	5.8	5.8
7.1	1.275	40	-	.95	.95	11.9	12.3
11.5	1.565	40	-	.93	.93	13.9	13.5
-.7	.102	0	0.025	1.02	1.00	1.4	1.7
-.7	.125	0	.250	1.24	1.21	1.3	1.5
3.7	.435	0	.025	1.00	1.00	2.9	3.3
3.7	.450	0	.250	1.19	1.19	3.2	3.6
7.0	1.396	40	.300	1.07	1.31	14.7	13.2
6.8	1.532	40	.600	1.17	1.43	17.4	14.4
11.3	1.772	40	.300	1.24	1.25	18.7	17.2
11.3	1.815	40	.600	1.33	1.44	21.7	19.2

(a) Missing values indicate propellers removed.

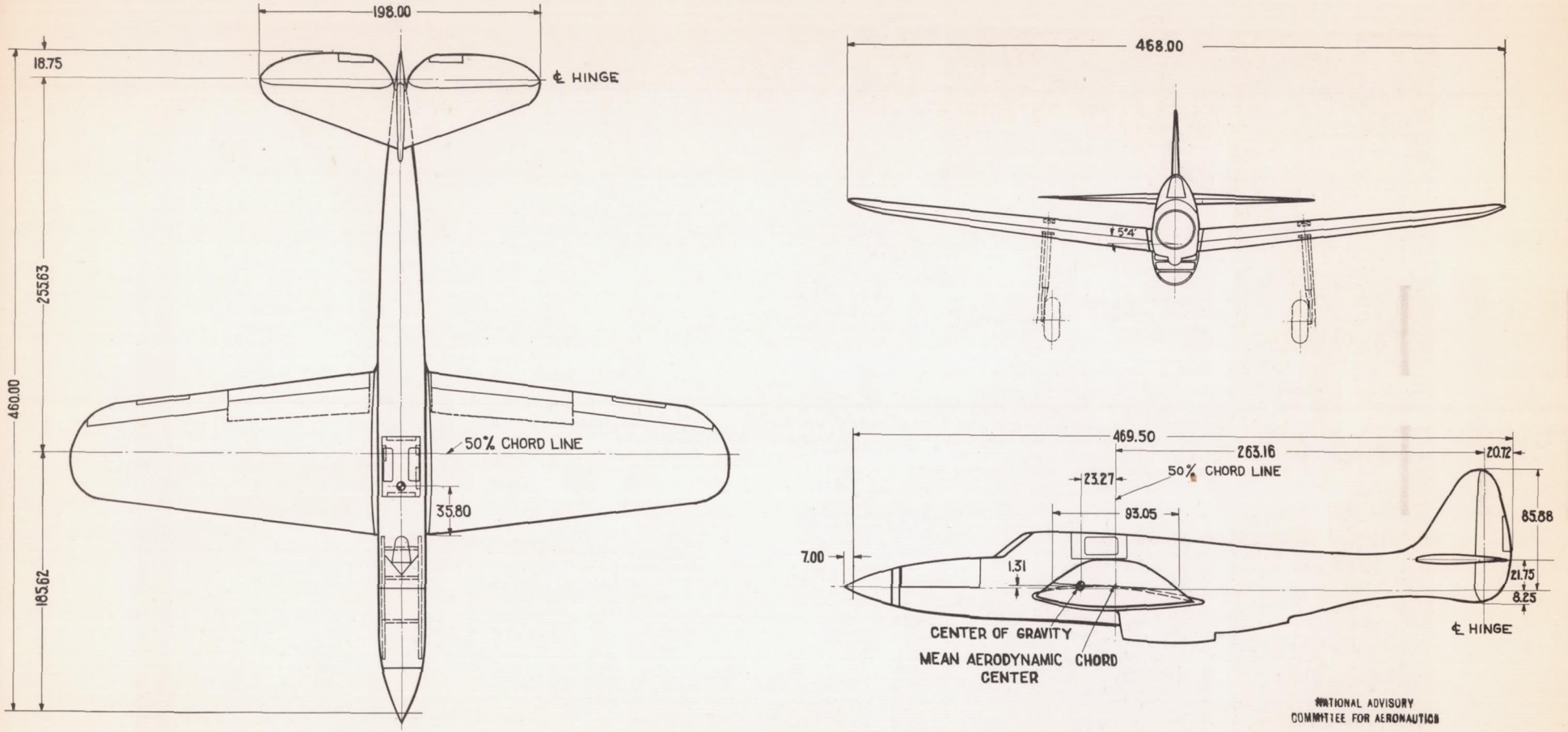

FIGURE 1. - THREE-VIEW DRAWING OF 3/4-SCALE MODEL OF THE XP-69 AIRPLANE. ALL DIMENSIONS IN INCHES.

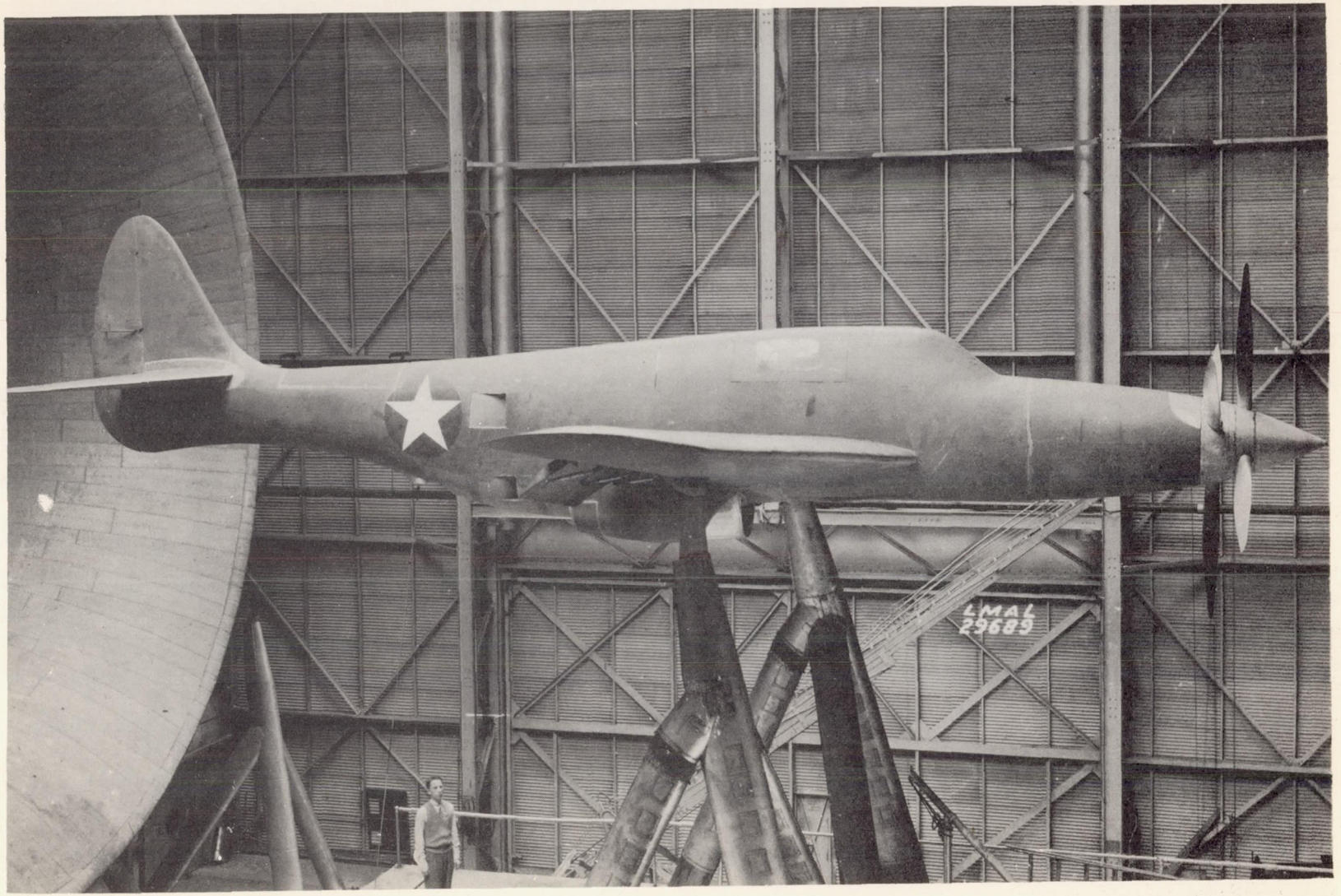

Figure 2.- The 3/4-scale model of the XP-69 airplane mounted in the NACA full-scale tunnel.

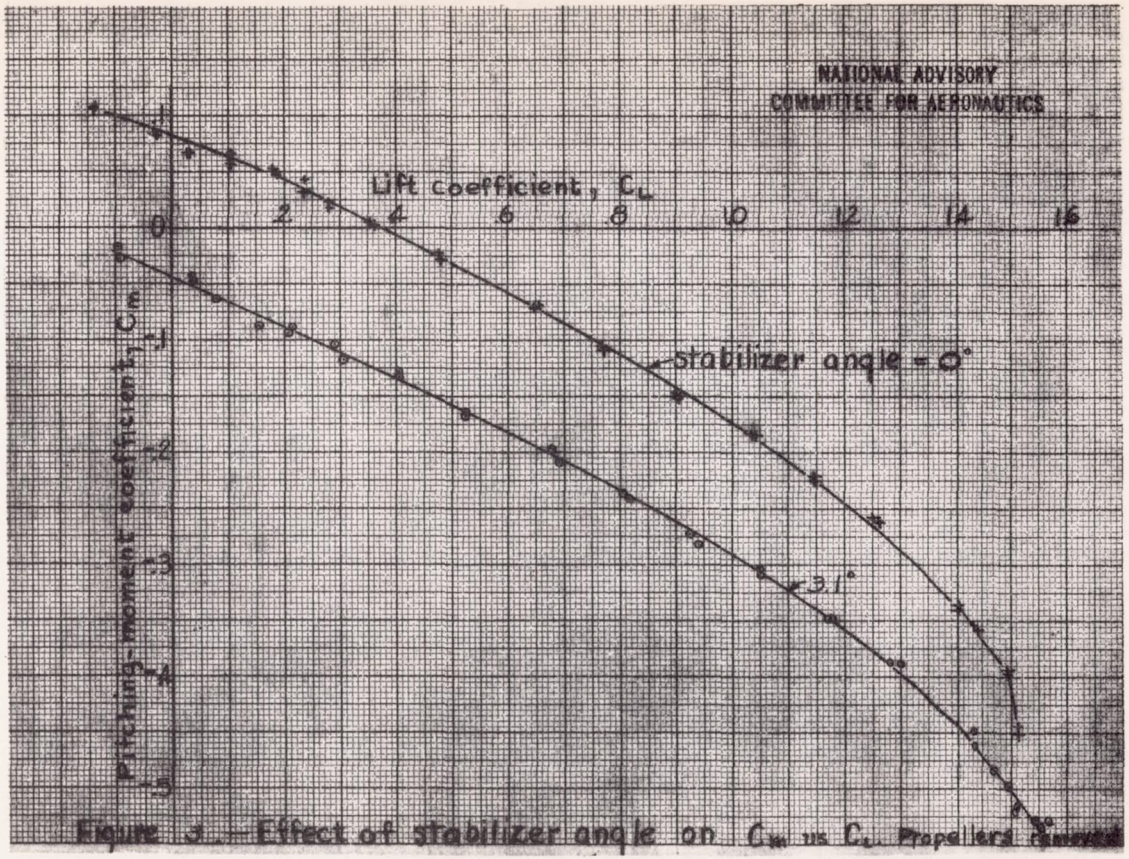

Figure 3.—Effect of stabilizer angle on C_m vs C_L. Propellers removed

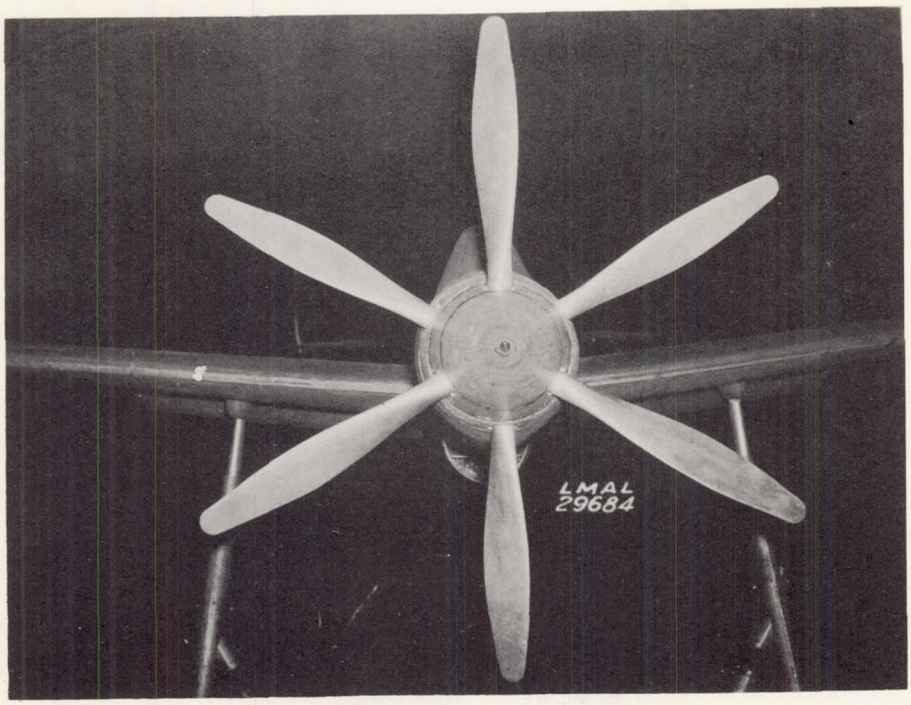

Figure 4.- Propeller installation on the 3/4-scale model of the XP-69 airplane.

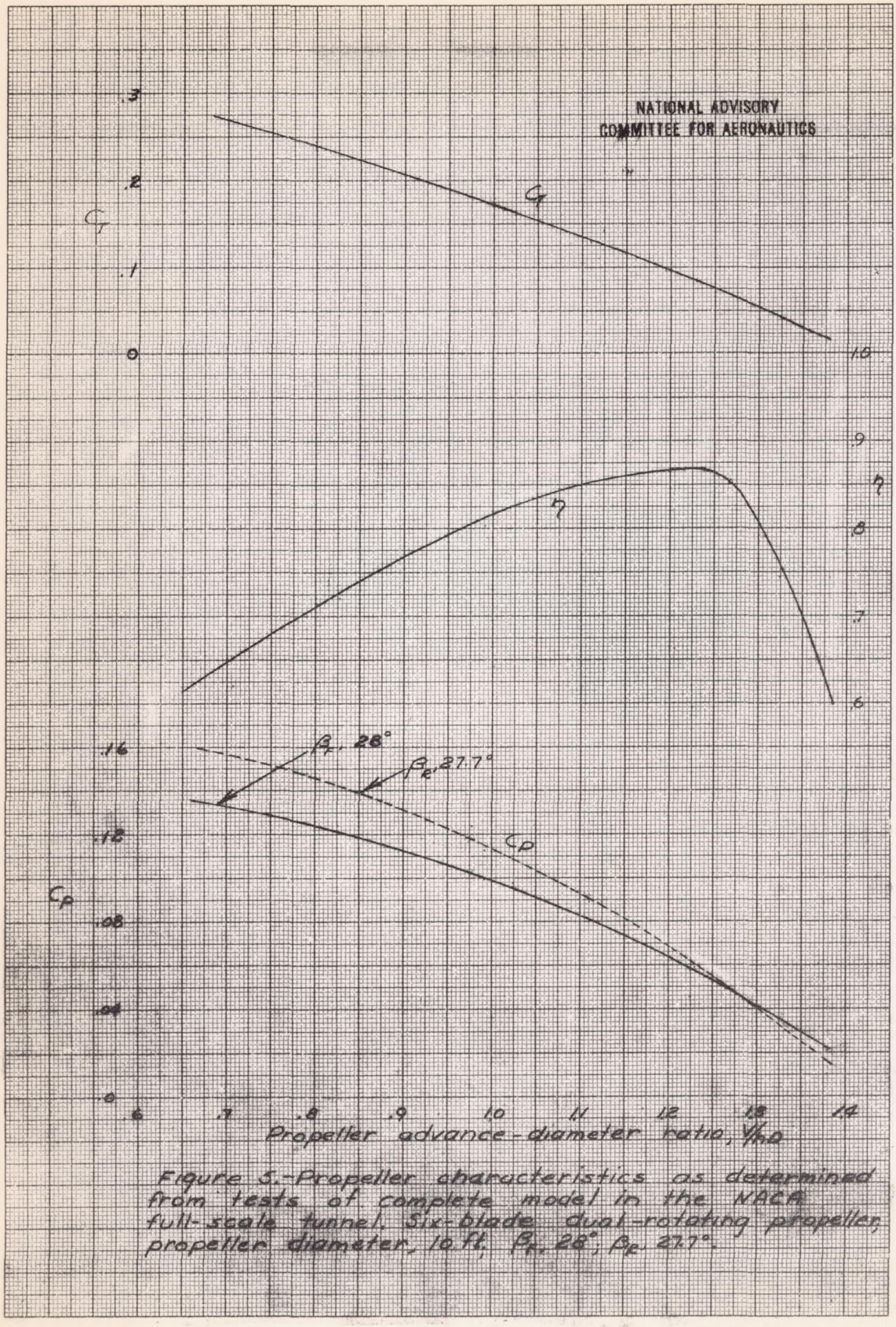

Figure 5.-Propeller characteristics as determined from tests of complete model in the NACA full-scale tunnel. Six-blade dual-rotating propeller, propeller diameter, 10 ft; β_r, 28°; β_t, 27.7°.

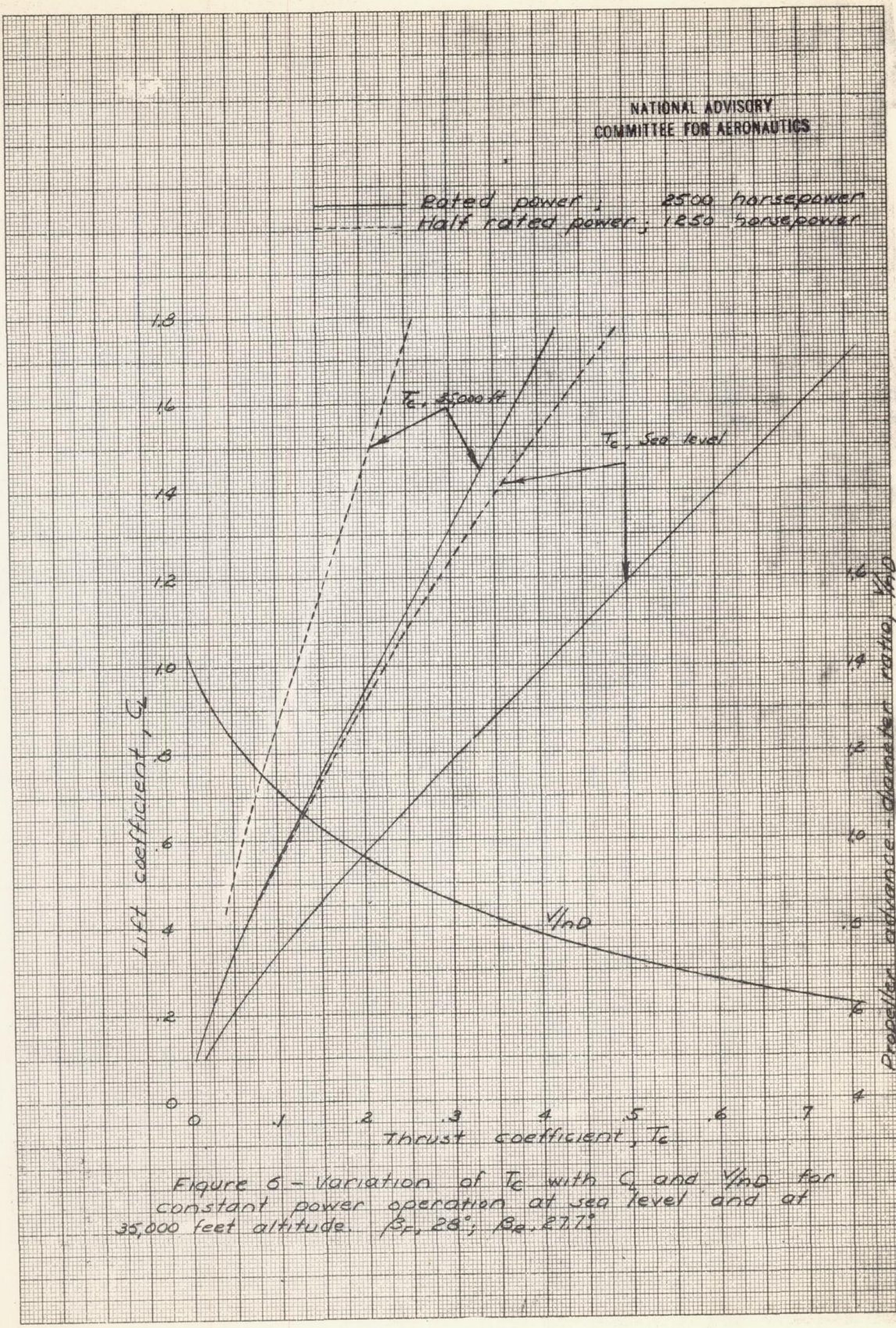

Figure 6 - Variation of T_c with C_L and V/nD for constant power operation at sea level and at 35,000 feet altitude. β_F, 28°; β_e, 27.7°

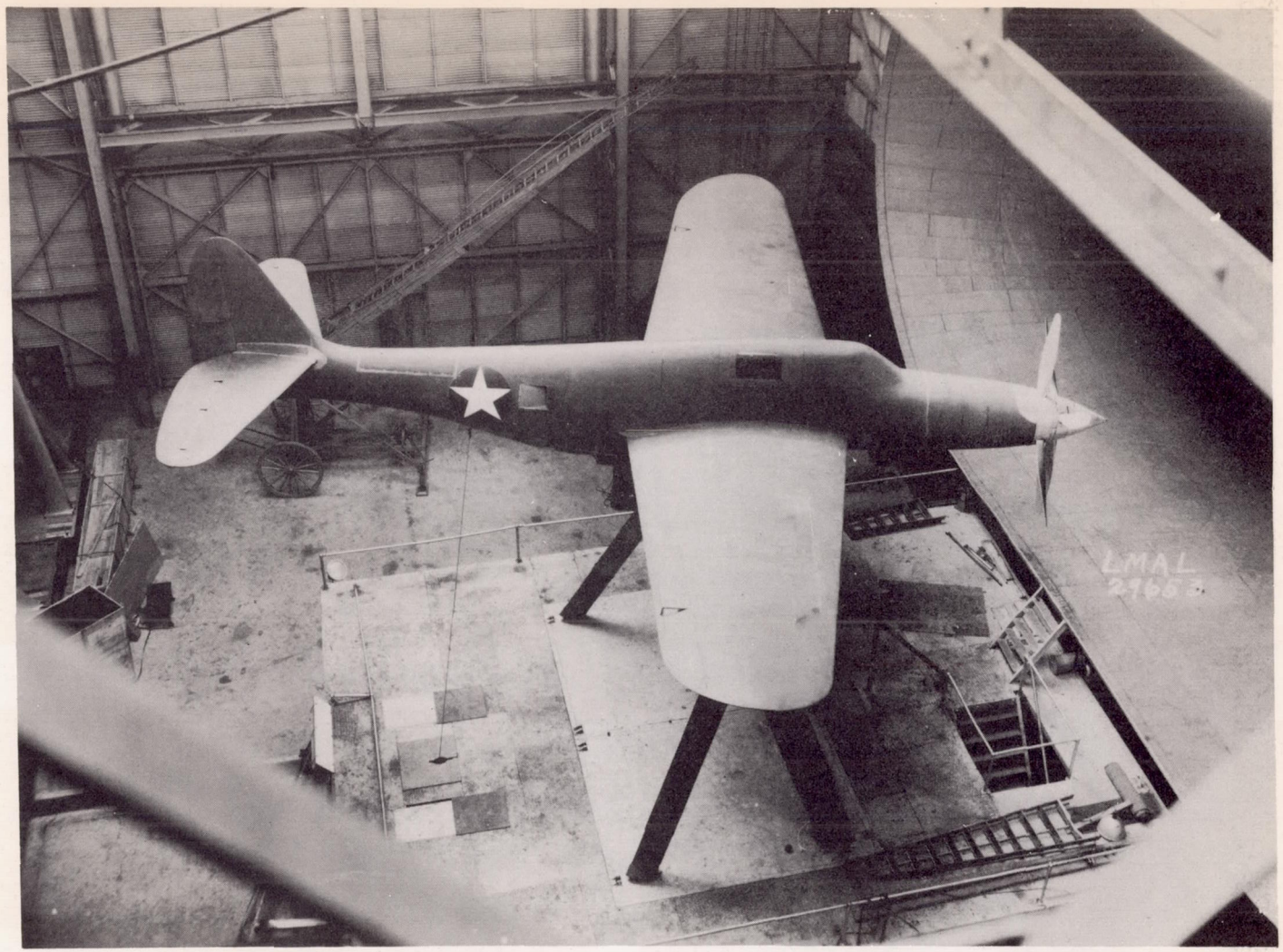

Figure 7.- The XP-69 model in yawed condition. $\Psi = 15.1^{\circ}$.

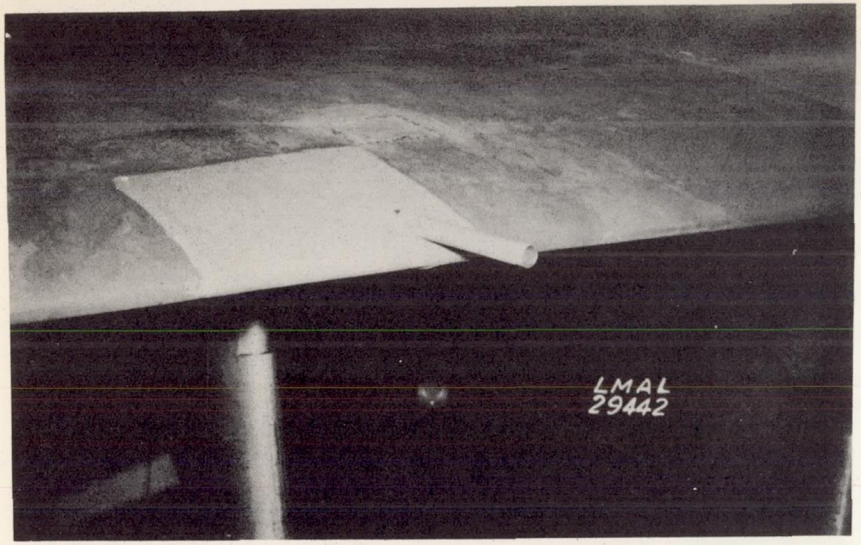

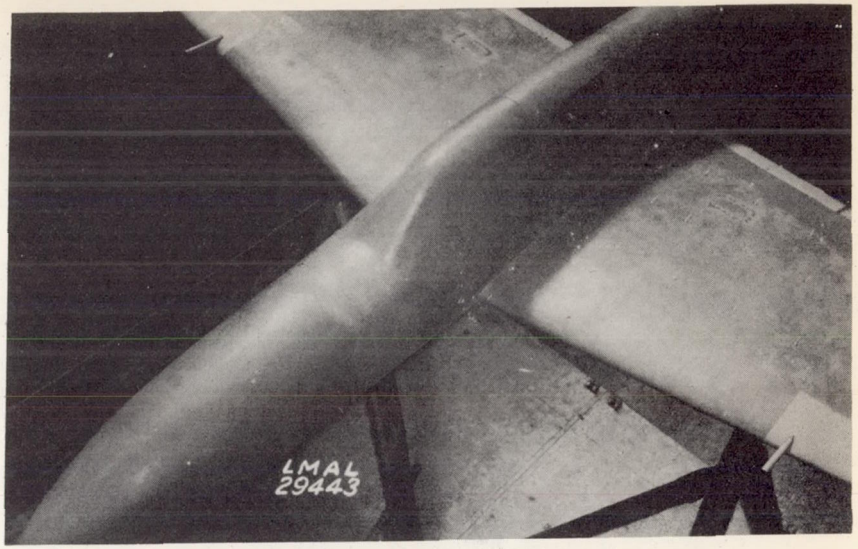

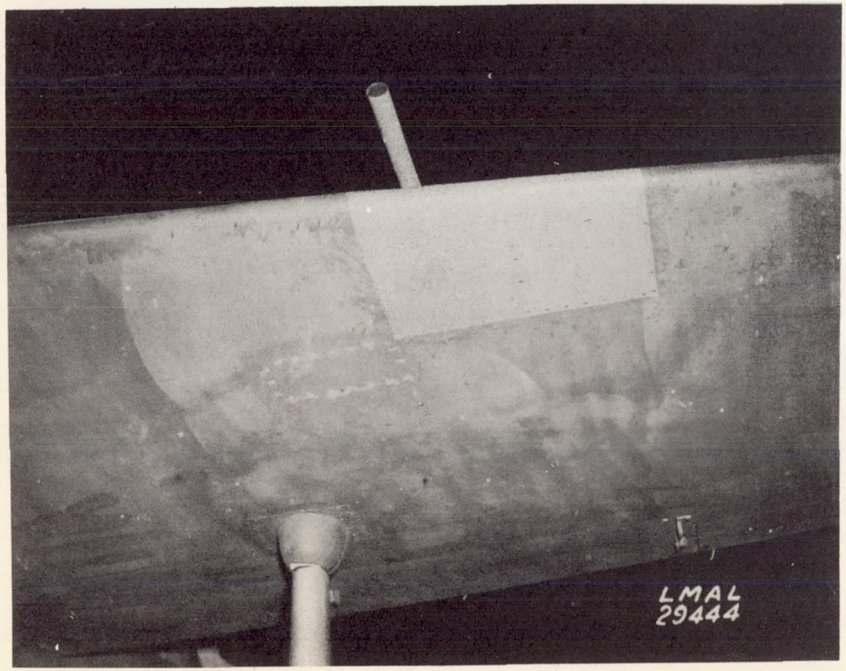

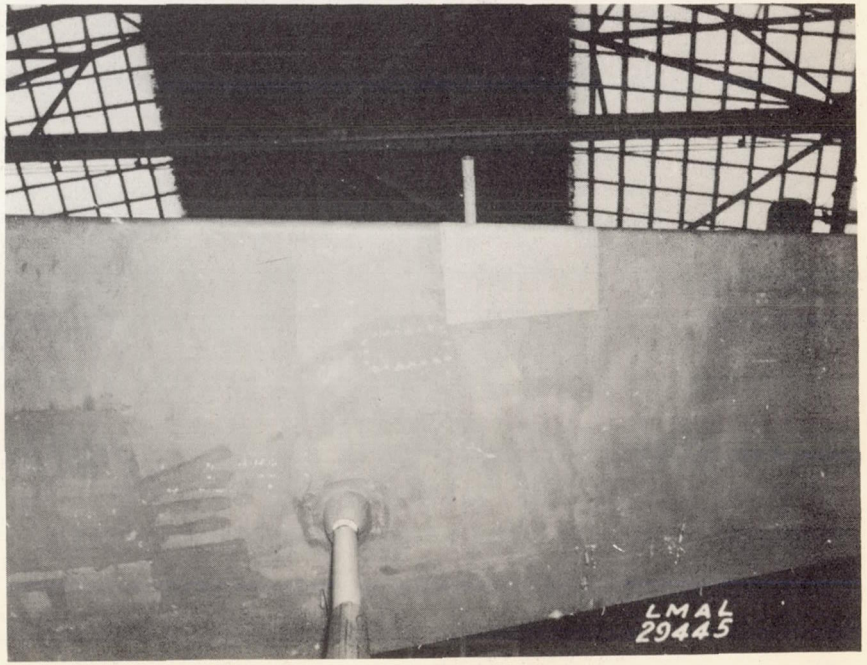

Figure 8.- Cannon installation on XP-69 model. Cannon in maximum-up position.

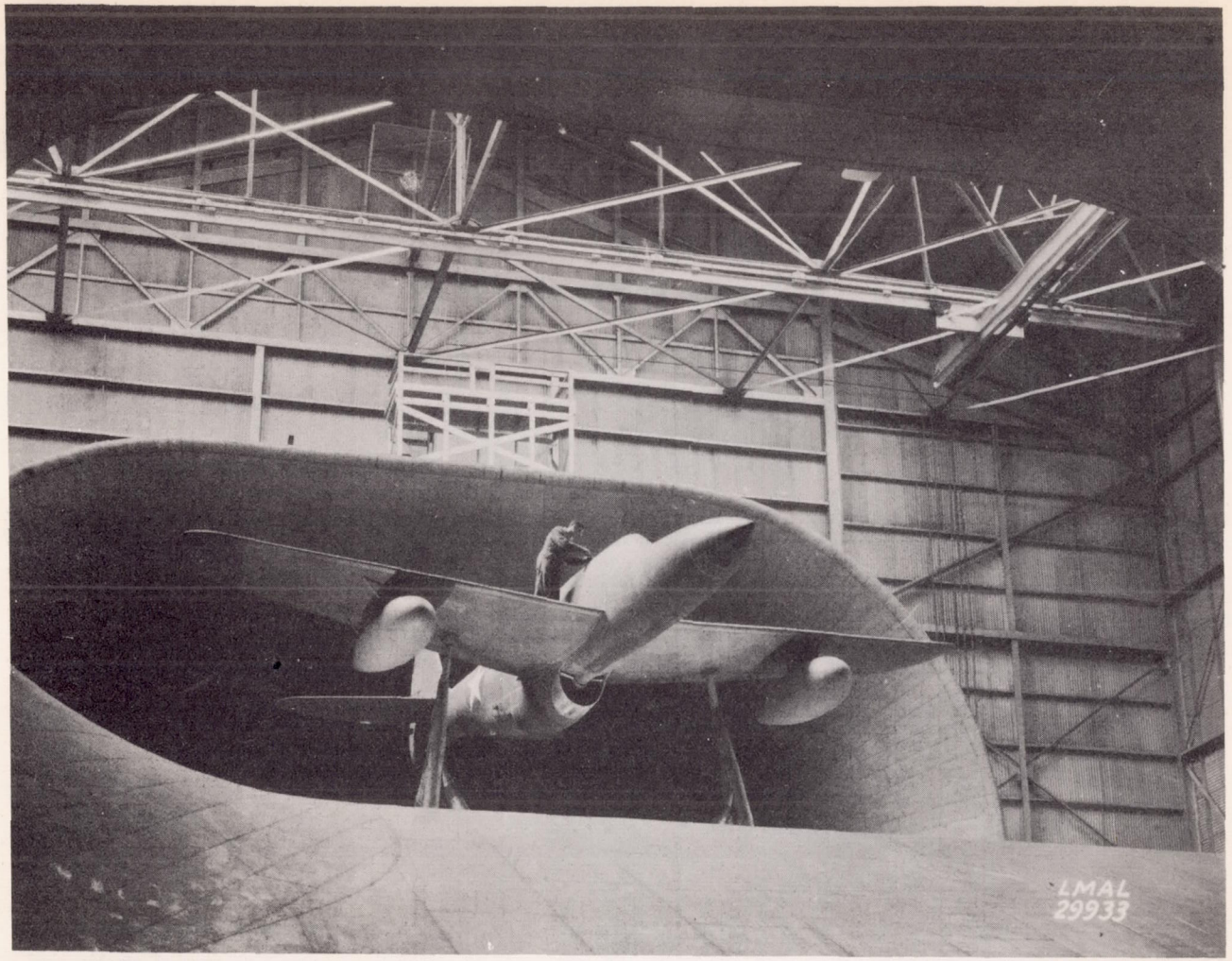

Figure 9.- The XP-69 model with wing gasoline tanks installed.

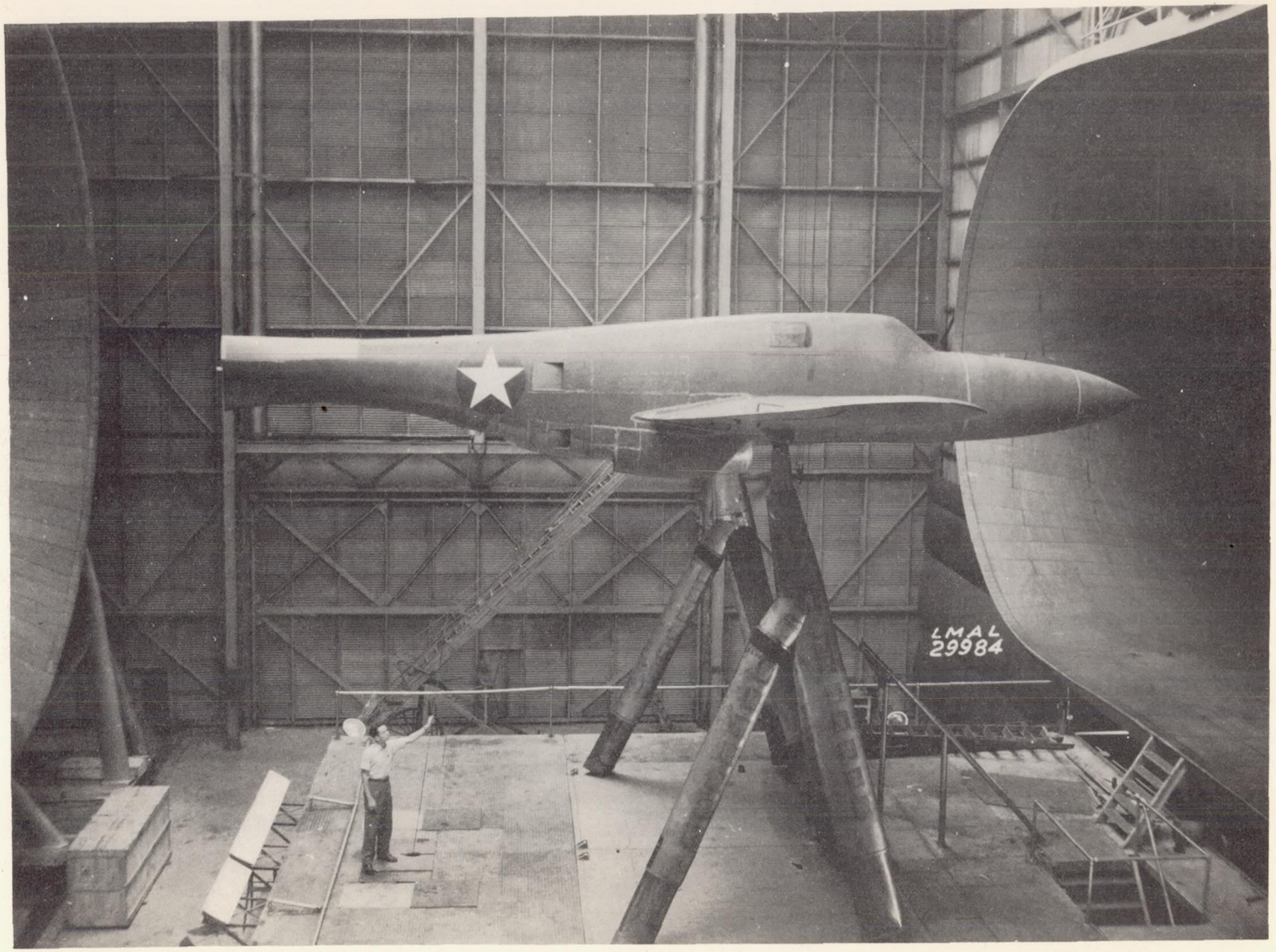

Figure 10.- The XP-69 model with horizontal and vertical tail surfaces removed.

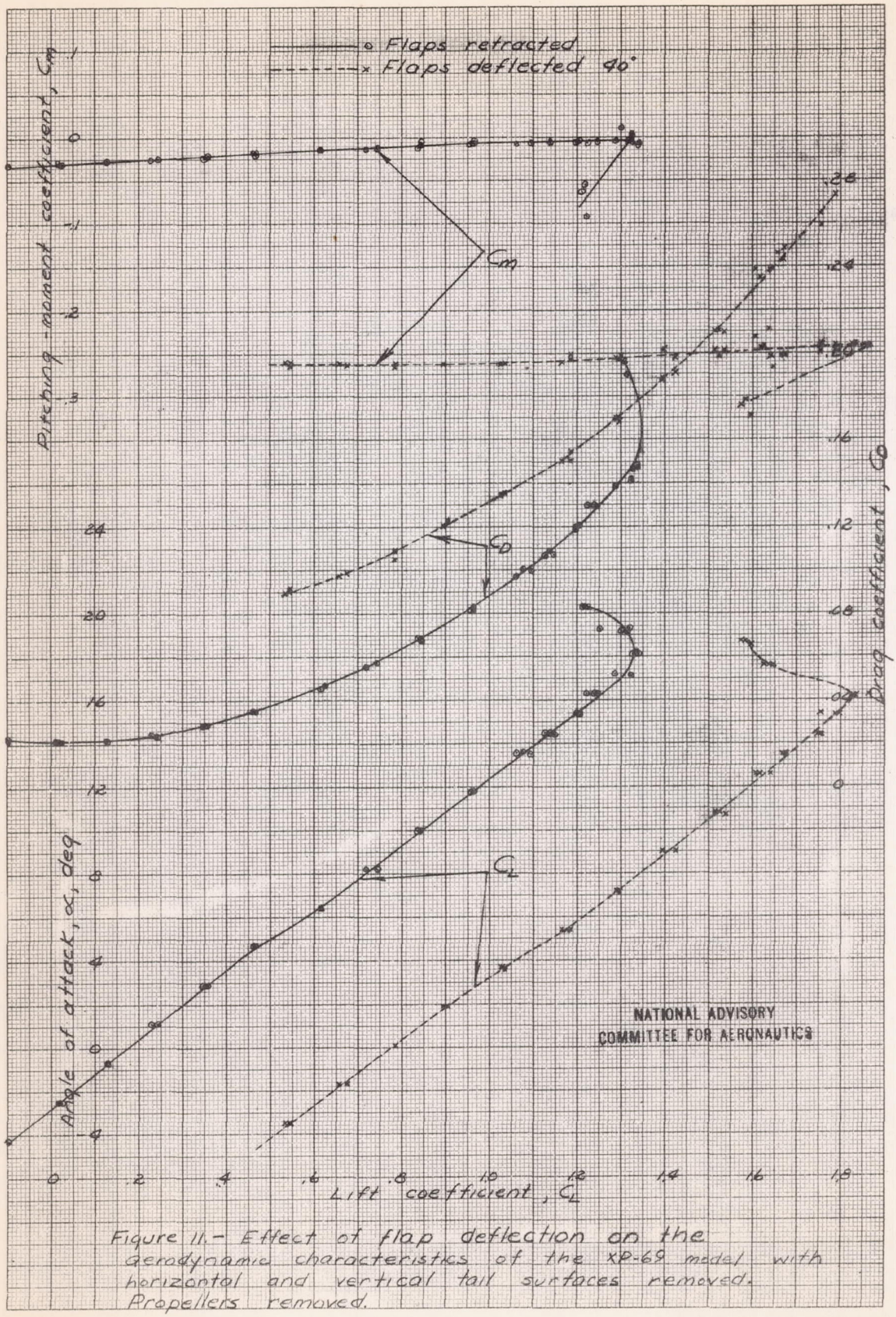

Figure 11.- Effect of flap deflection on the aerodynamic characteristics of the XP-69 model with horizontal and vertical tail surfaces removed. Propellers removed.

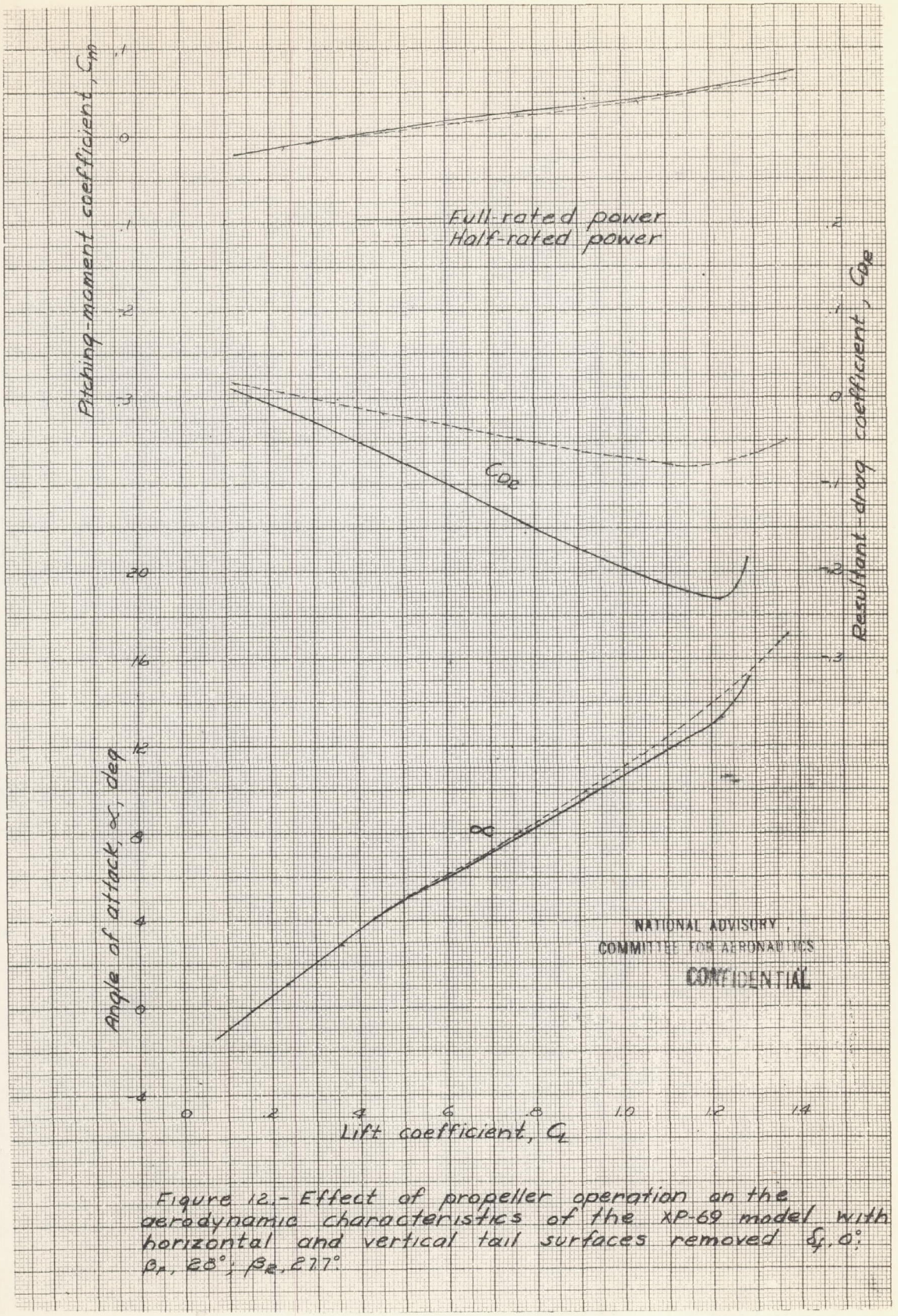

Figure 12.- Effect of propeller operation on the aerodynamic characteristics of the XP-69 model with horizontal and vertical tail surfaces removed δ_f, 0°; β_1, 28°; β_2, 27.7°.

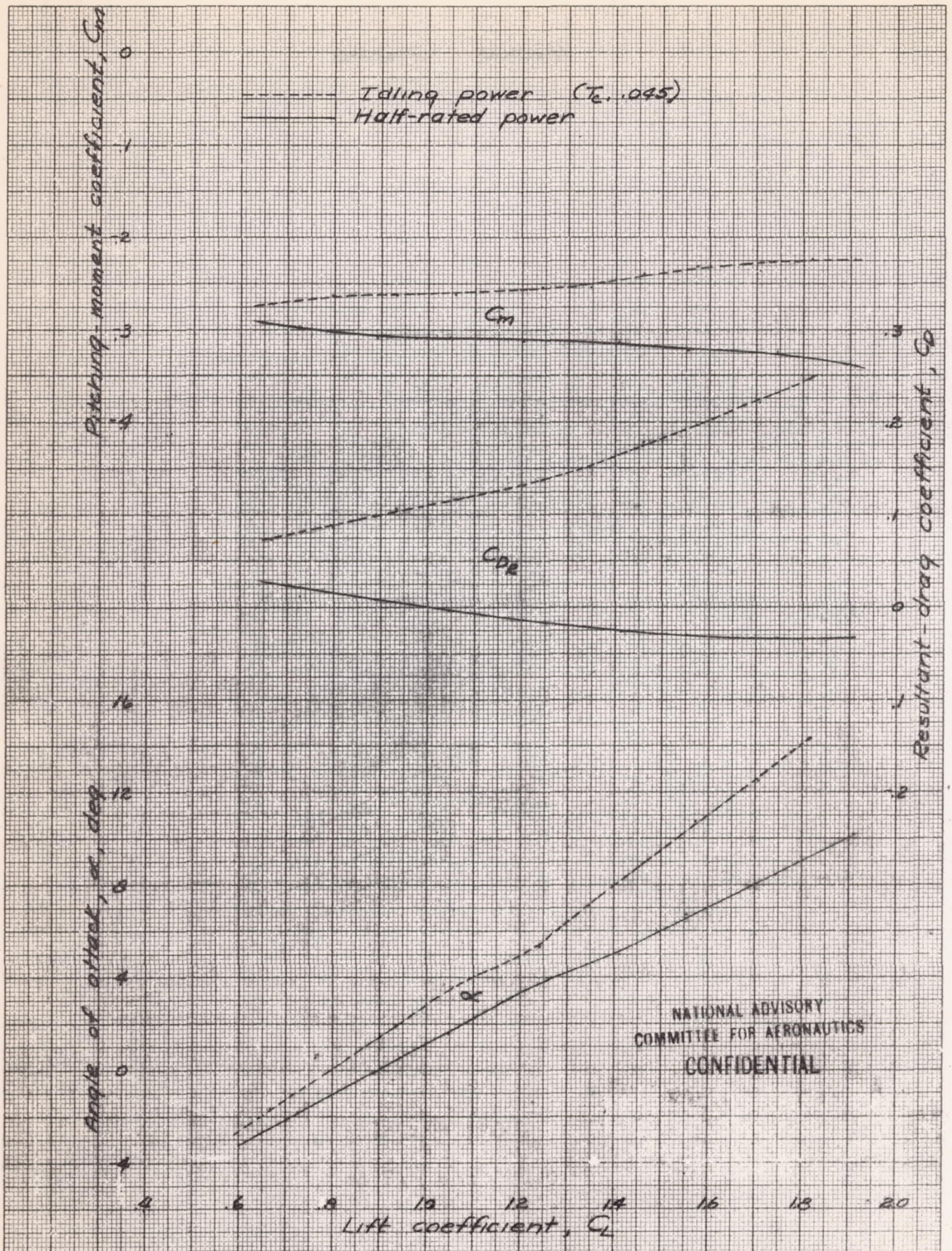

Figure 13.- Effect of propeller operation on the aerodynamic characteristics of the XP-69 model with horizontal and vertical tail surfaces removed. δ_f, 40°; β_F, 28°; β_R, 27.7°.

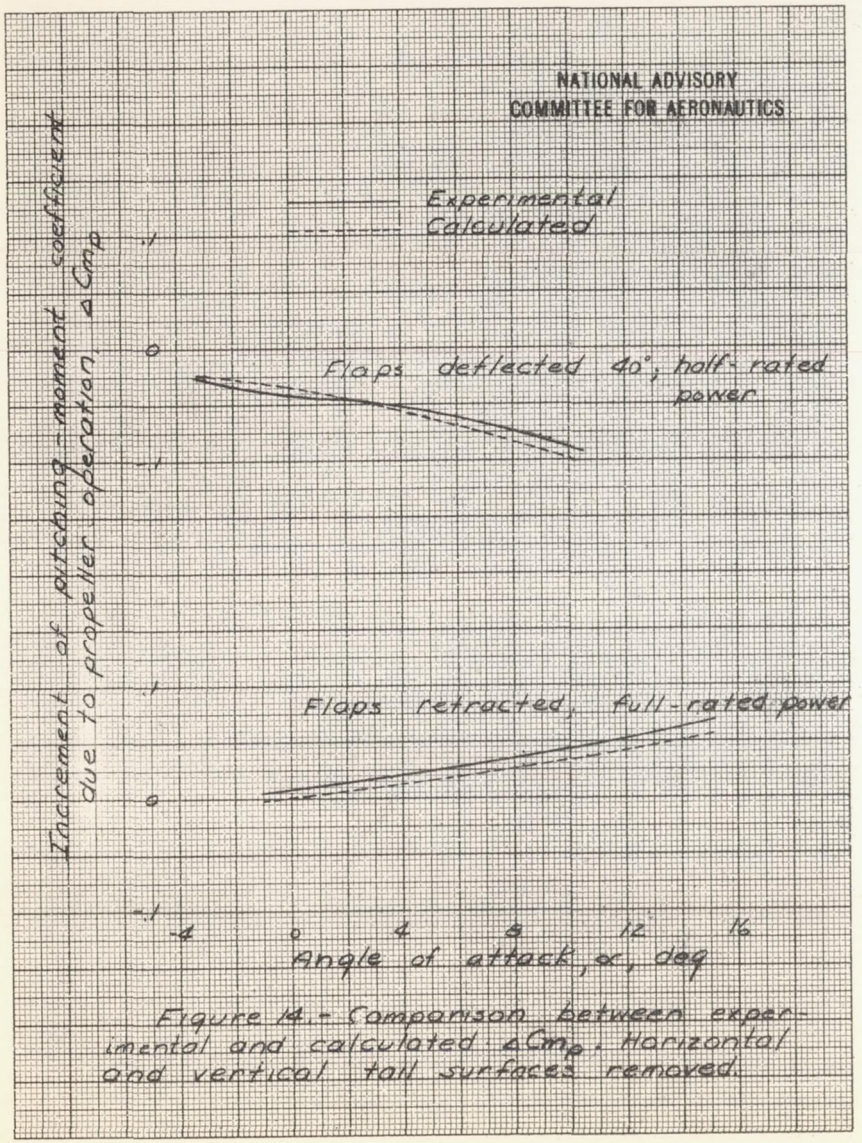

Figure 14.- Comparison between experimental and calculated ΔC_{m_p} - Horizontal and vertical tail surfaces removed.

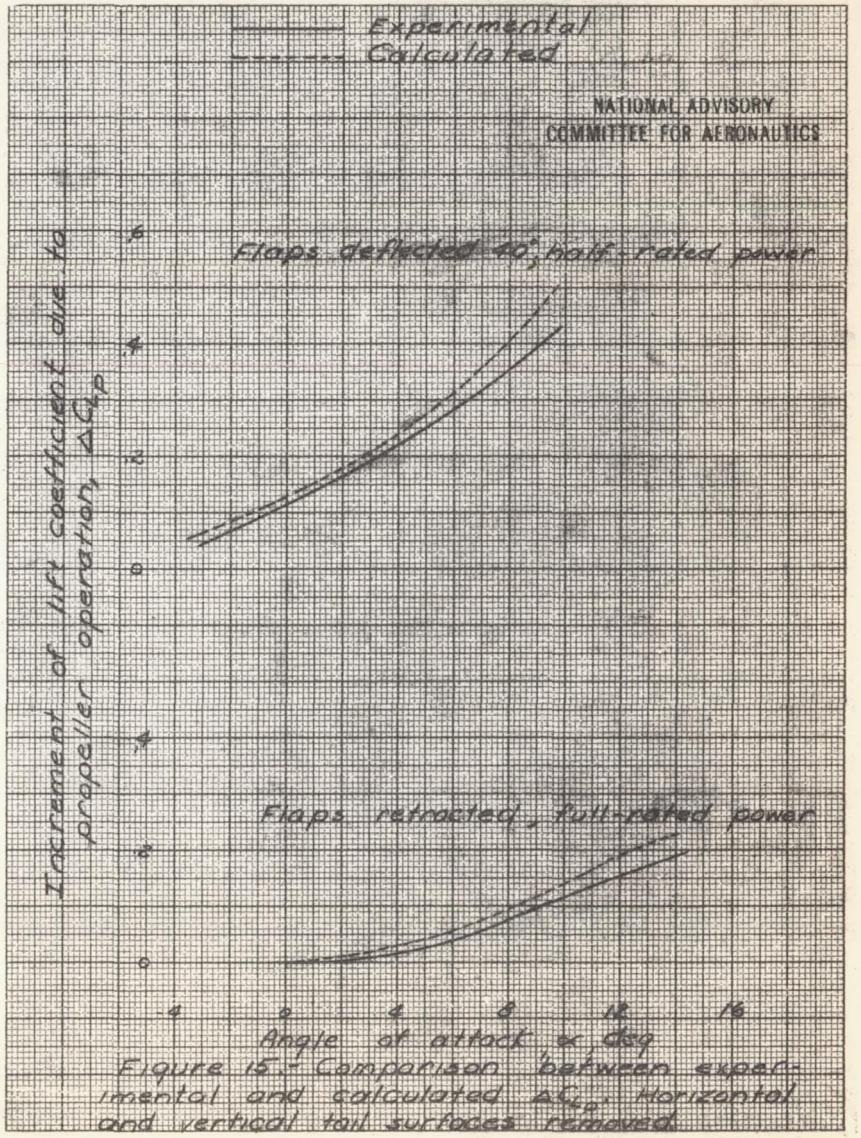

Figure 15.- Comparison between experimental and calculated ΔC_{L_p} - Horizontal and vertical tail surfaces removed.

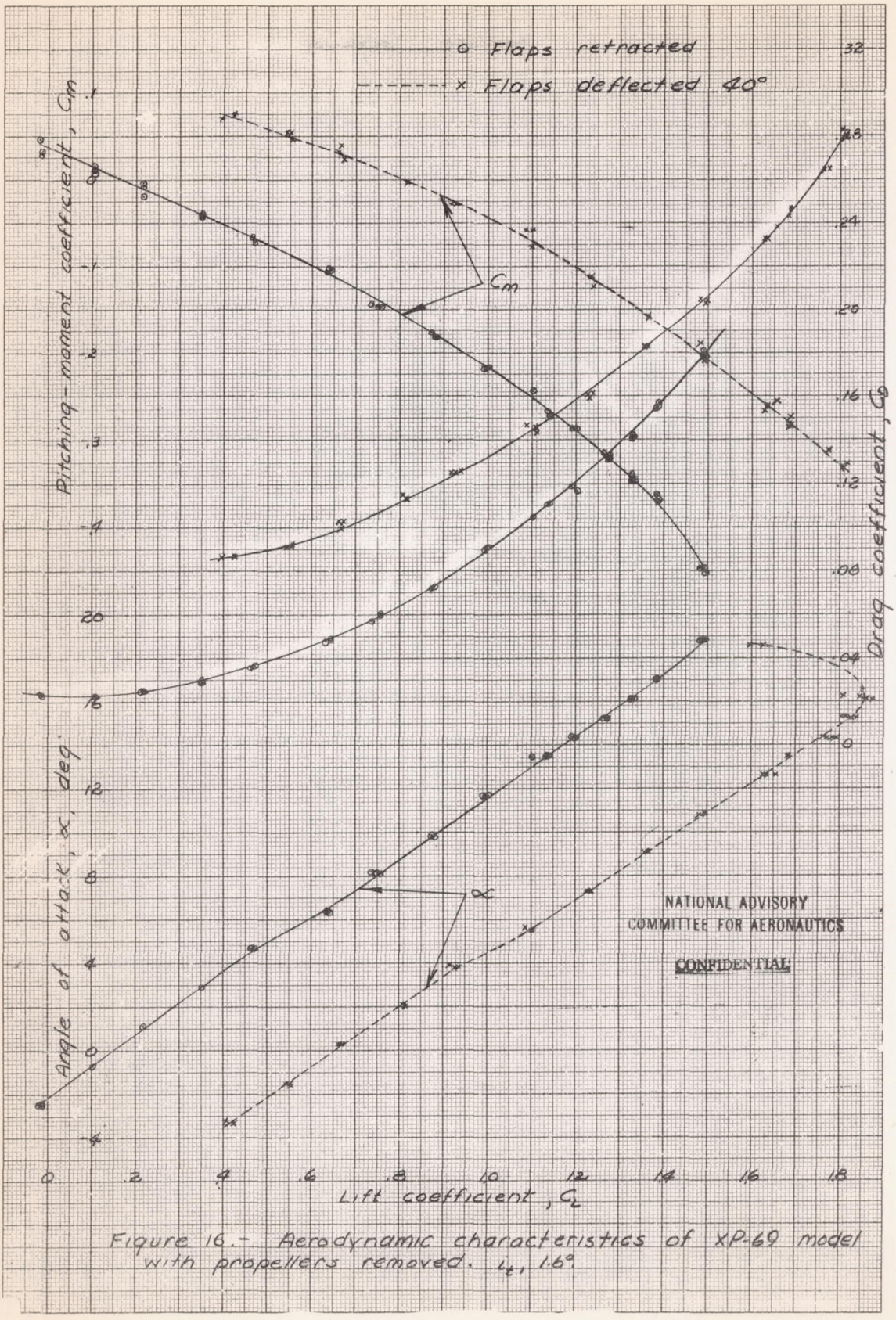

Figure 16.- Aerodynamic characteristics of XP-69 model with propellers removed. i_t, 1.6°

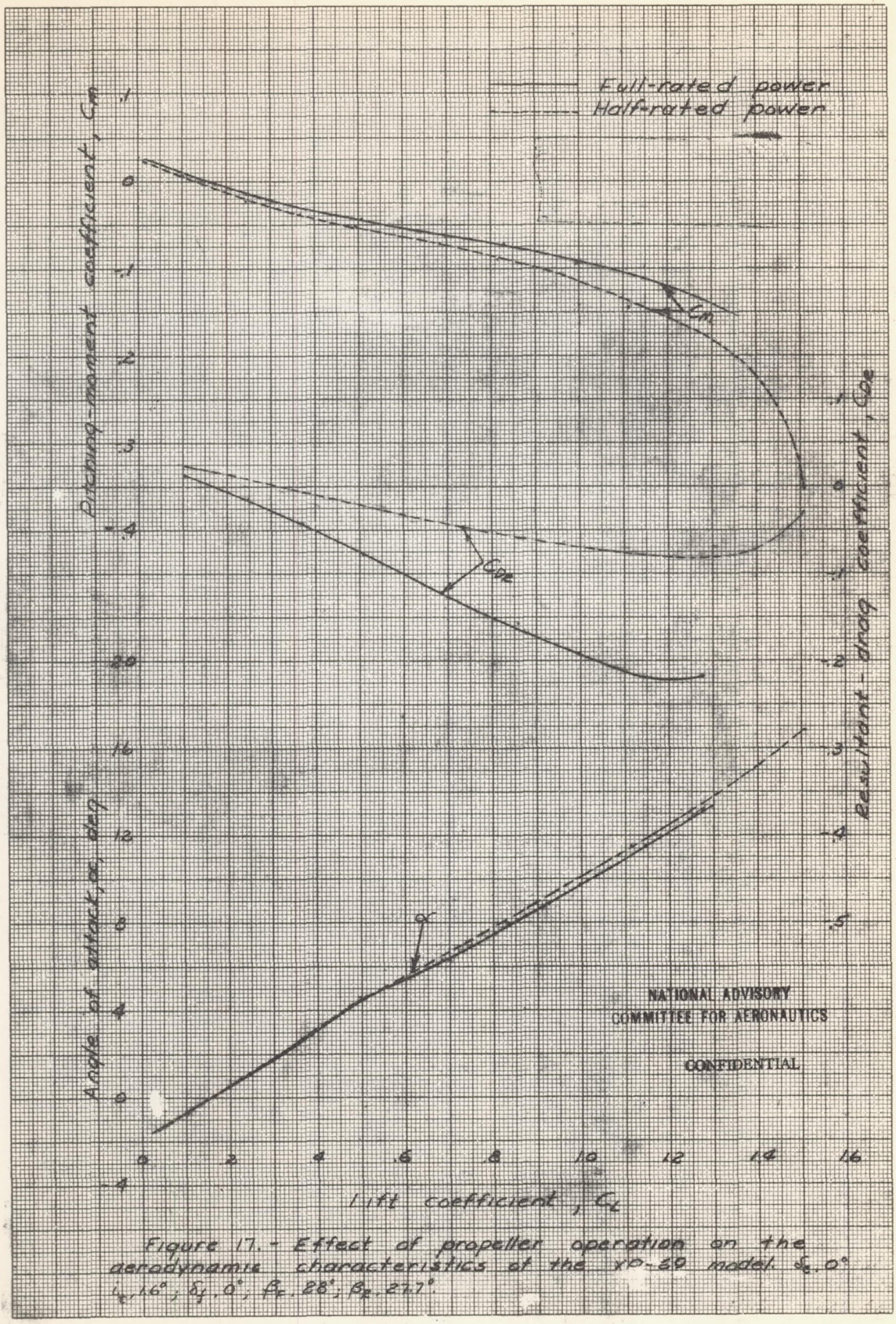

Figure 17. - Effect of propeller operation on the aerodynamic characteristics of the XP-39 model. δ_e, 0°; i_t, 1.6°; δ_f, 0°; $\beta_{.8}$, 28°; $\beta_{.8}$, 27.7°.

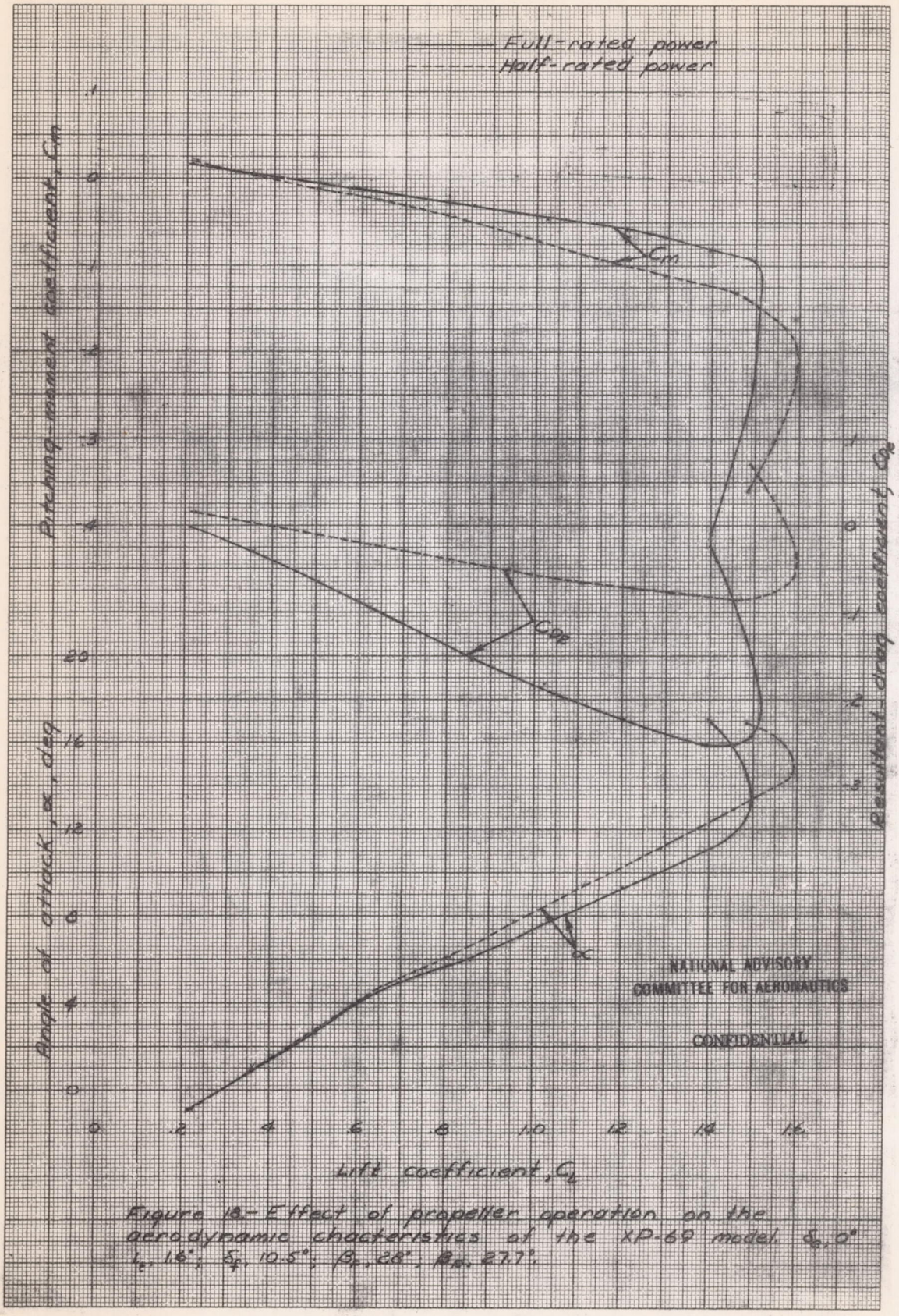

Figure 18.- Effect of propeller operation on the aerodynamic characteristics of the XP-69 model. δ_e, 0°; i_t, 1.6°; δ_f, 10.5°; $\beta_{p_{0.8}}$, 28°; β_{p_R}, 27.7°.

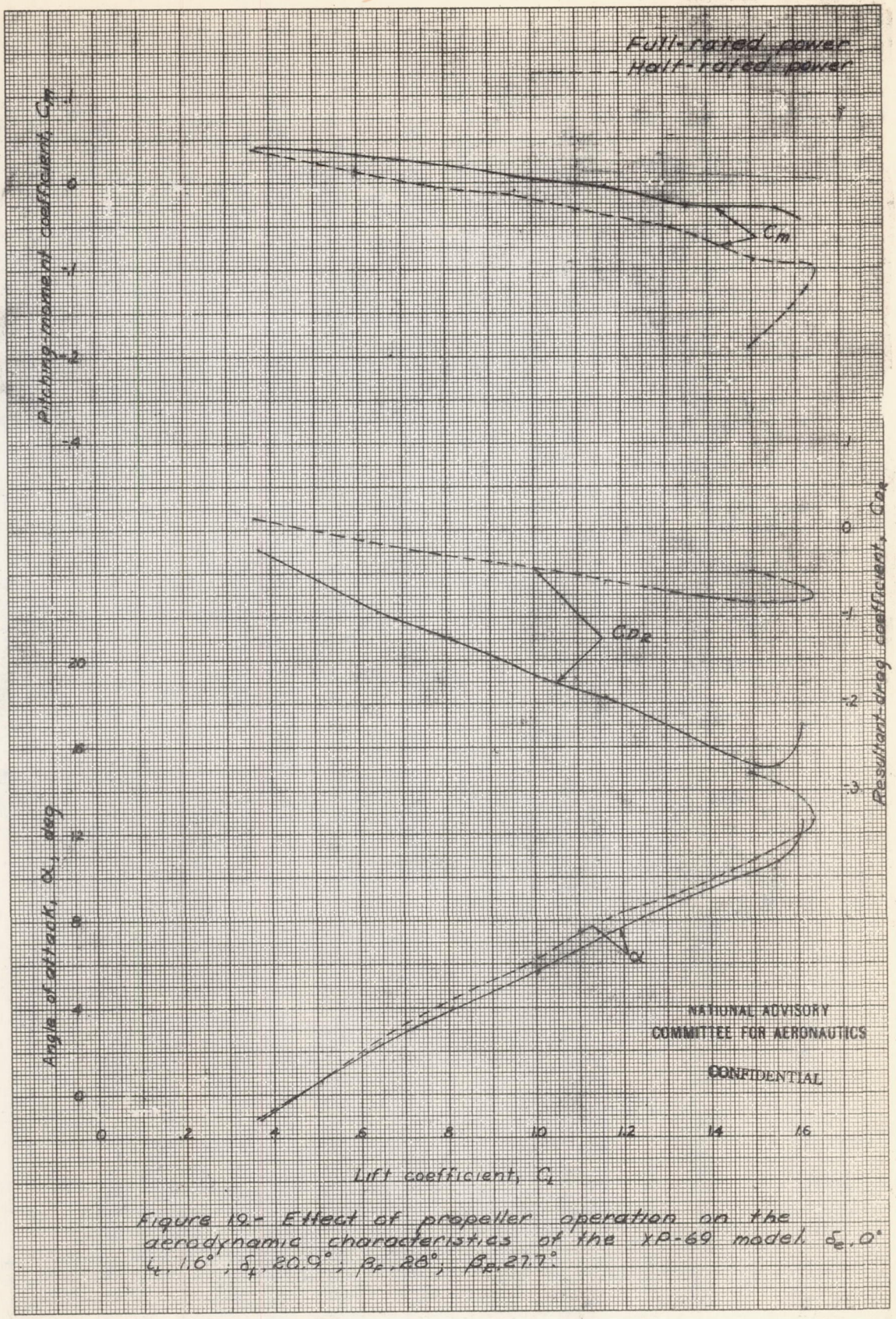

Figure 19.- Effect of propeller operation on the aerodynamic characteristics of the XP-69 model. δ_e, 0°; i_t, 1.6°; δ_f, 20.9°; $\beta_{P_{.75R}}$, 28°; $\beta_{P_{.75R}}$, 27.7°.

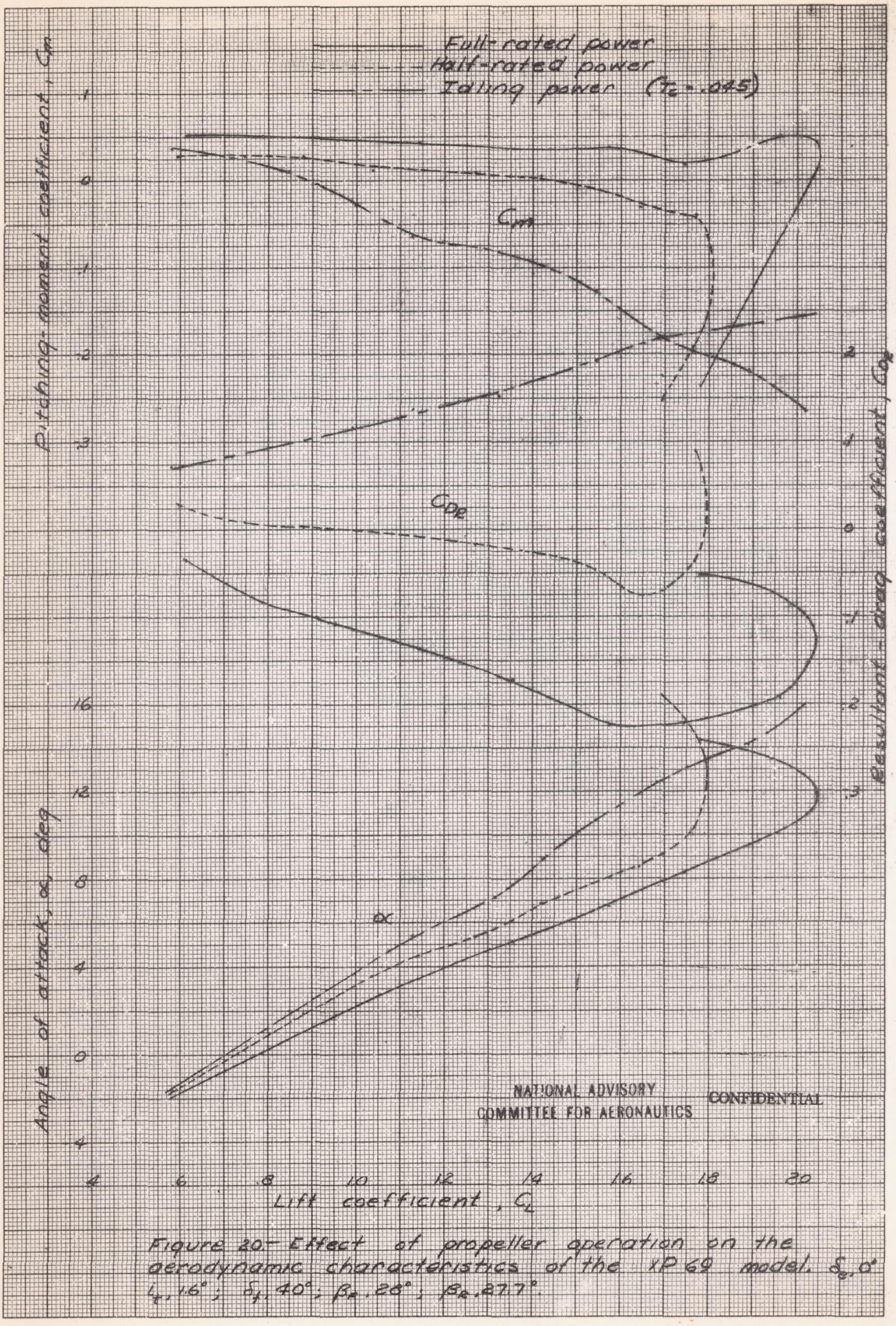

Figure 20.- Effect of propeller operation on the aerodynamic characteristics of the XP-69 model. δ_e, 0°; i_t, 1.6°; δ_f, 40°; $\beta_{.8}$, 28°; $\beta_{.8}$, 27.7°.

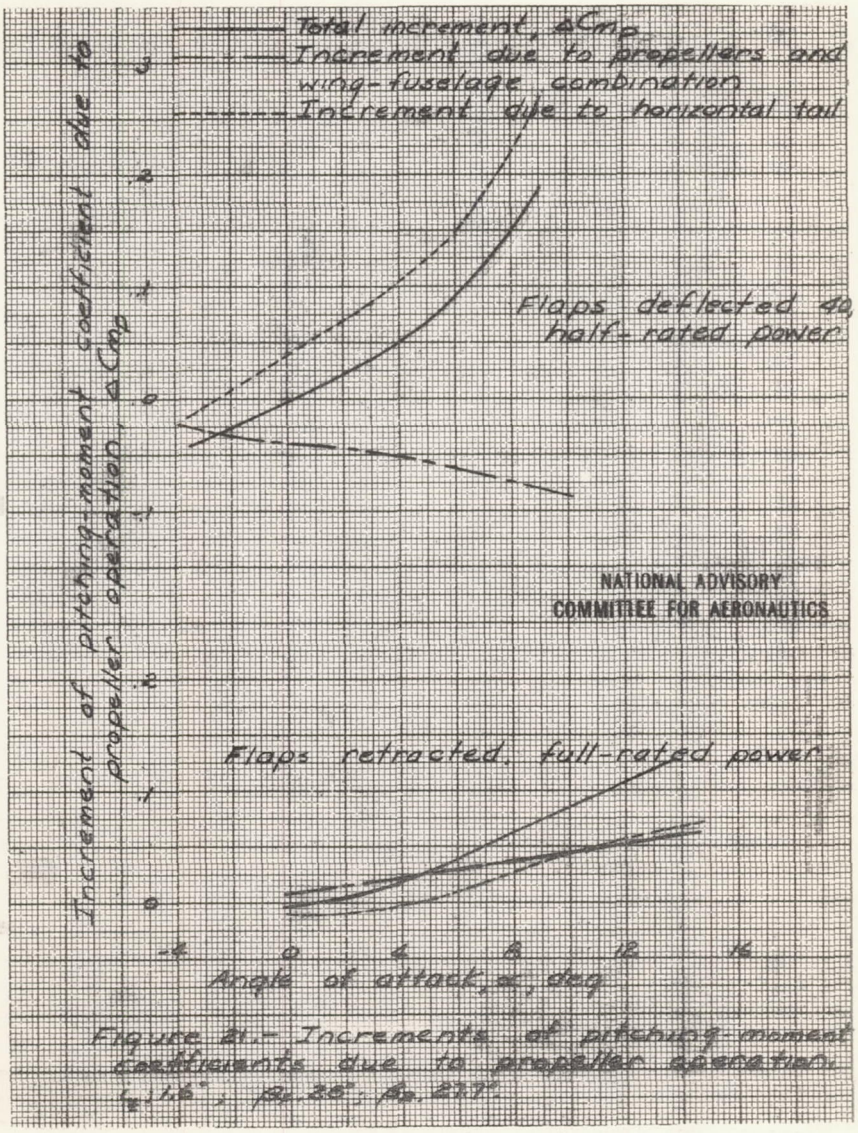

Figure 21.- Increments of pitching-moment coefficients due to propeller operation. i_w, 1.5°; $\beta_{0.8}$, 30°; $\beta_{0.8}$, 27.7°.

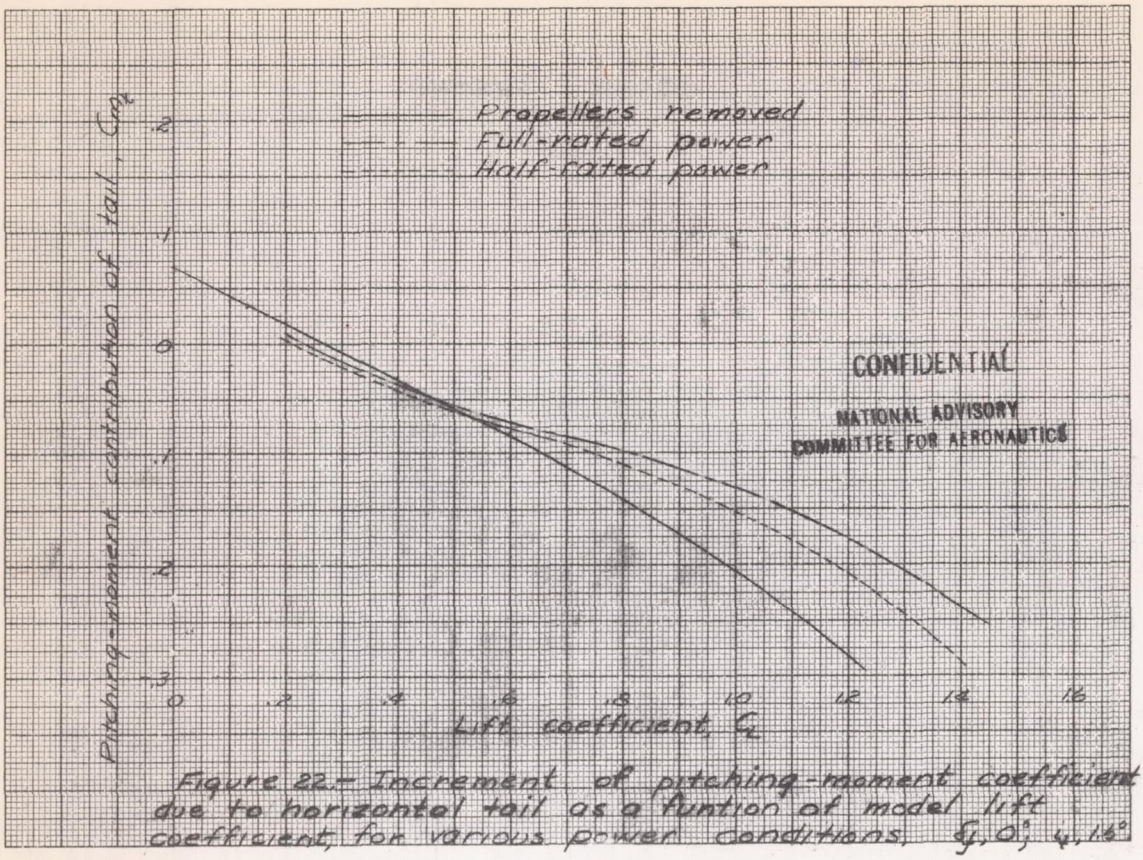

Figure 22.- Increment of pitching-moment coefficient due to horizontal tail as a function of model lift coefficient, for various power conditions. δ_f, 0°; i_t, 1.6°

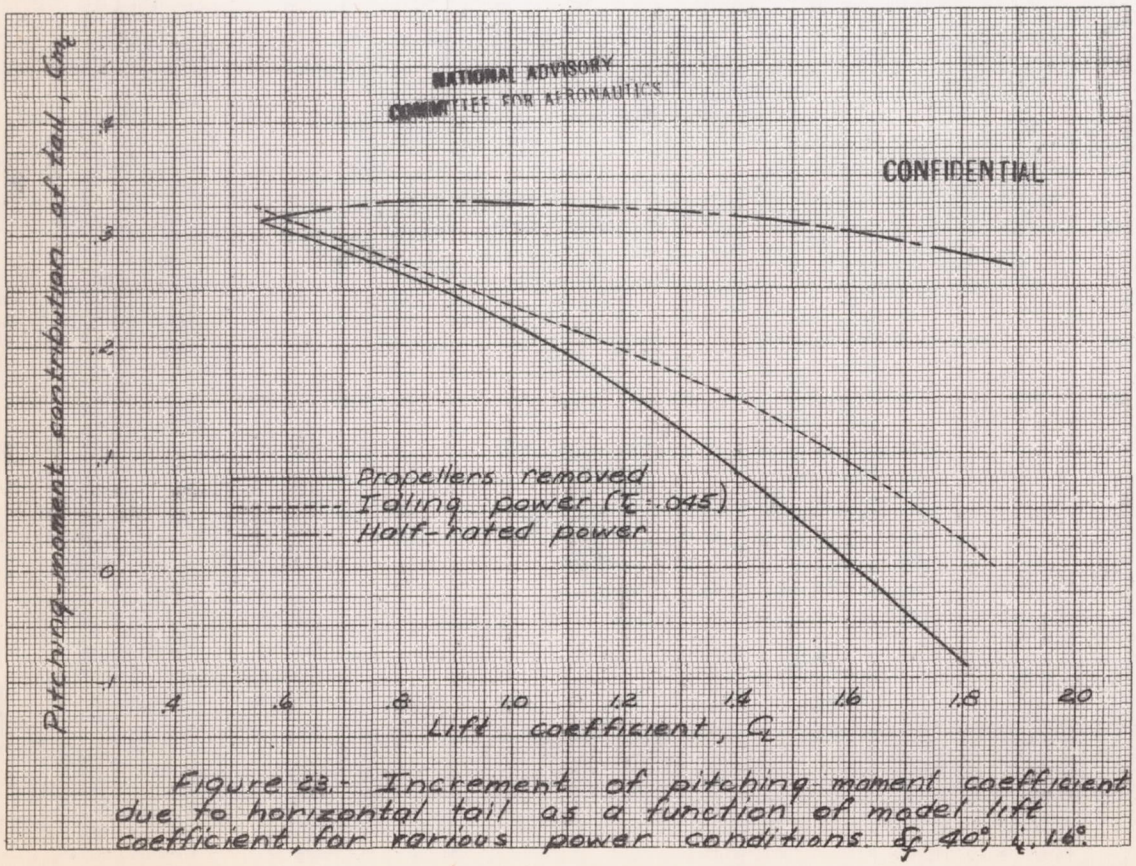

Figure 23.- Increment of pitching-moment coefficient due to horizontal tail as a function of model lift coefficient, for various power conditions. δ_f, 40°; i_t, 1.6°

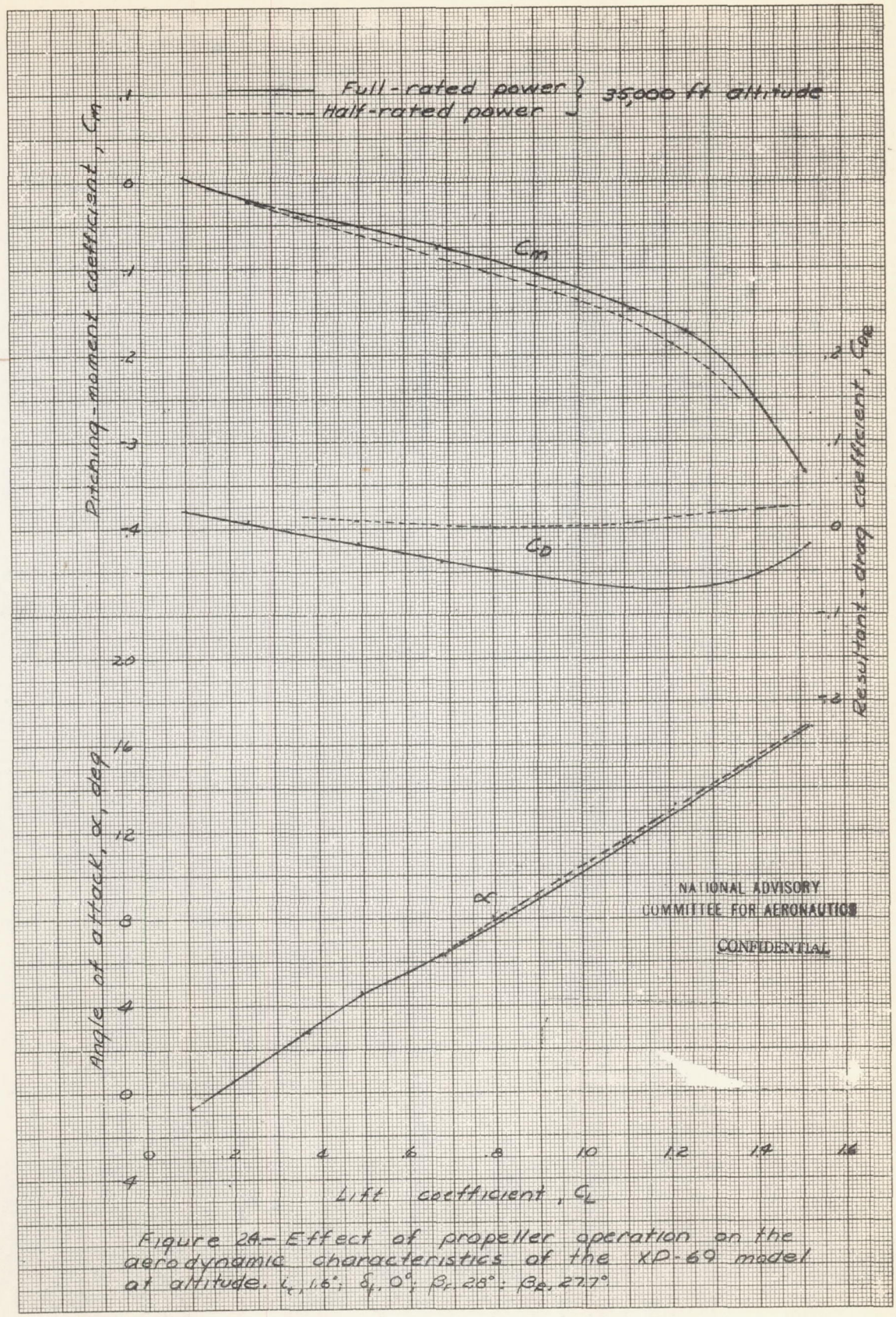

Figure 28.- Effect of propeller operation on the aerodynamic characteristics of the XP-69 model at altitude. i_t, 1.6°; δ_f, 0°; β_r, 28°; β_e, 27.7°.

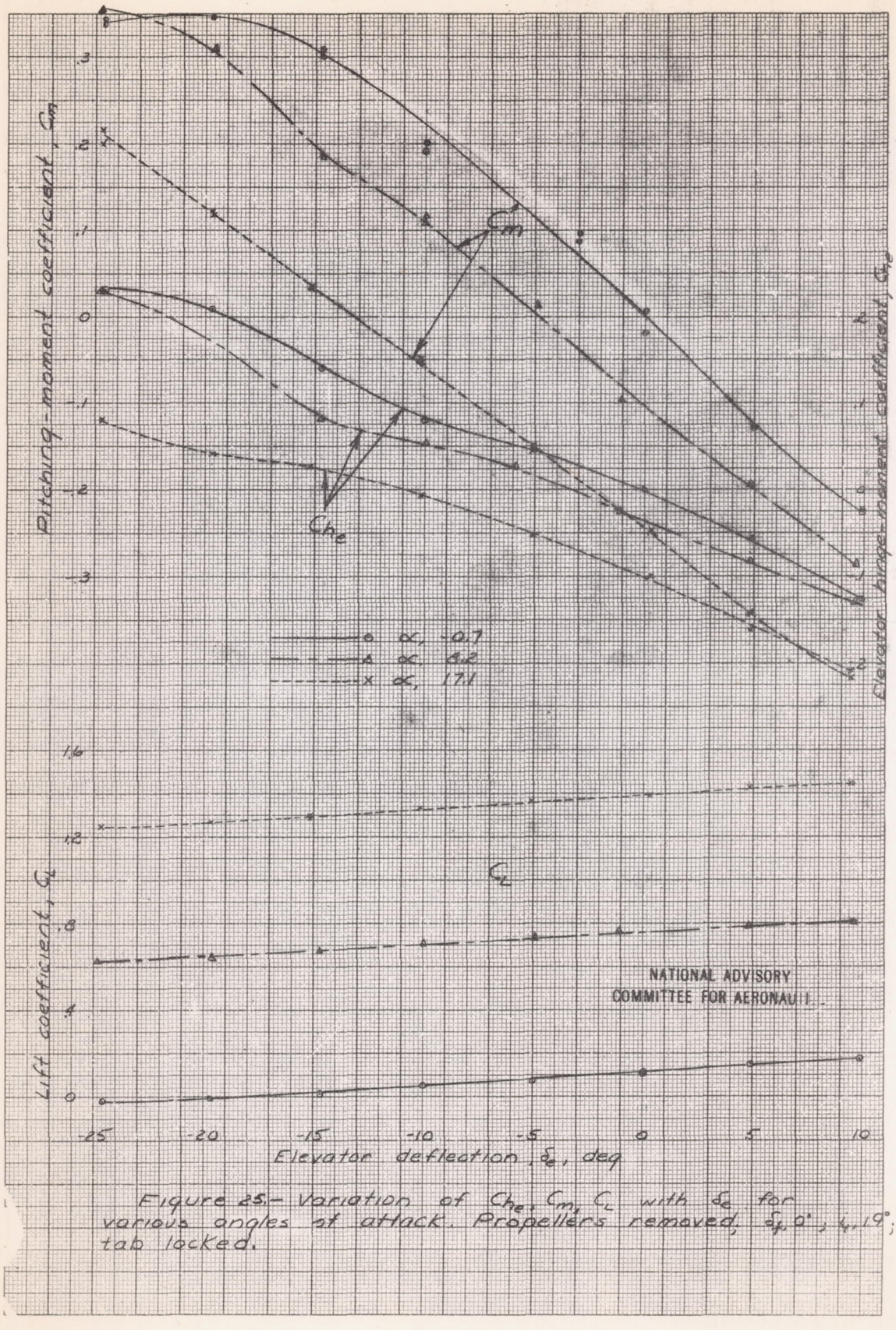

Figure 25.- Variation of C_{h_e}, C_m, C_L with δ_e for various angles of attack. Propellers removed, δ_f 0°, 4, 19°; tab locked.

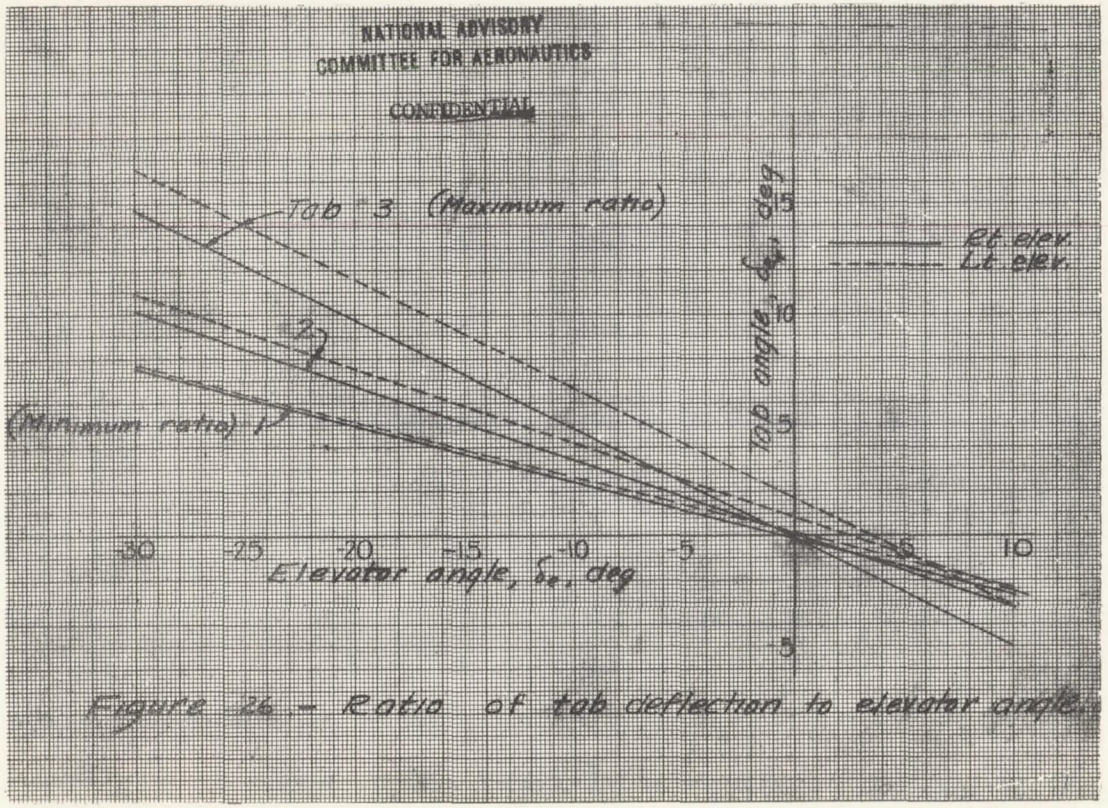

Figure 24. - Ratio of tab deflection to elevator angle.

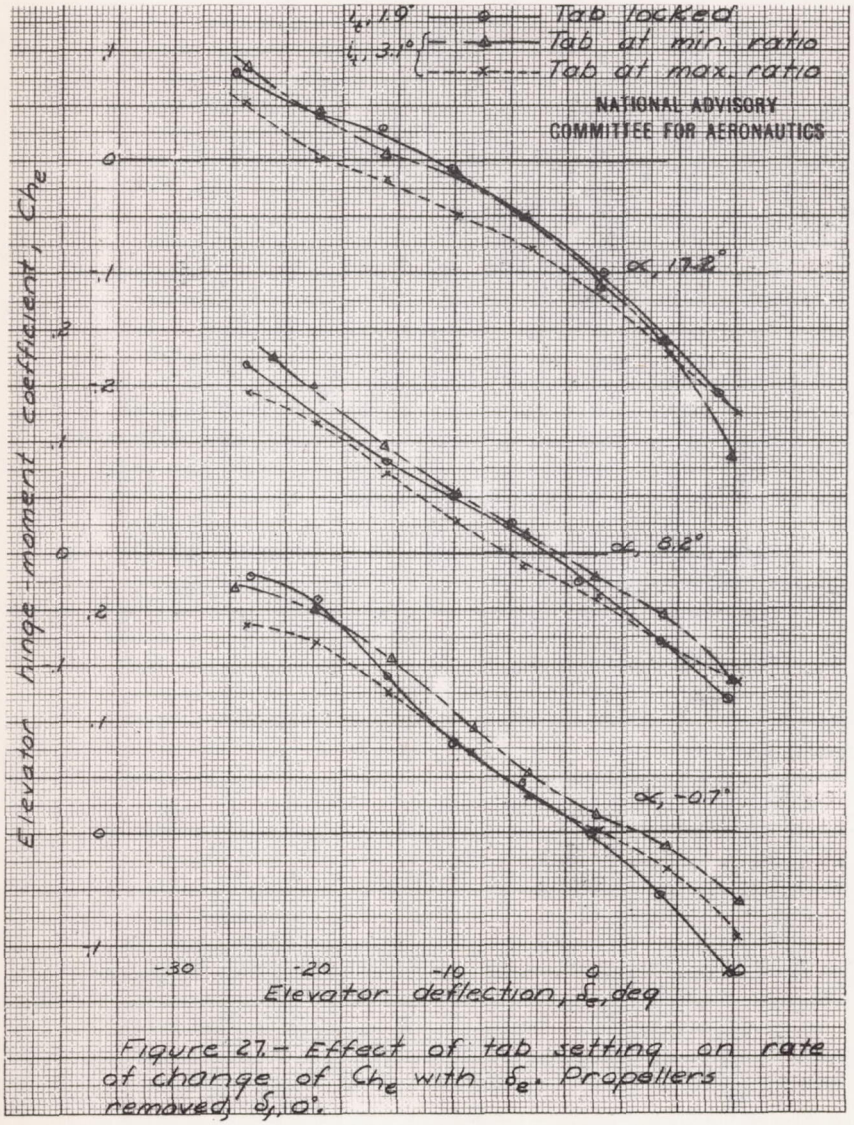

Figure 27.- Effect of tab setting on rate of change of C_{h_e} with δ_e. Propellers removed; δ_f, 0°.

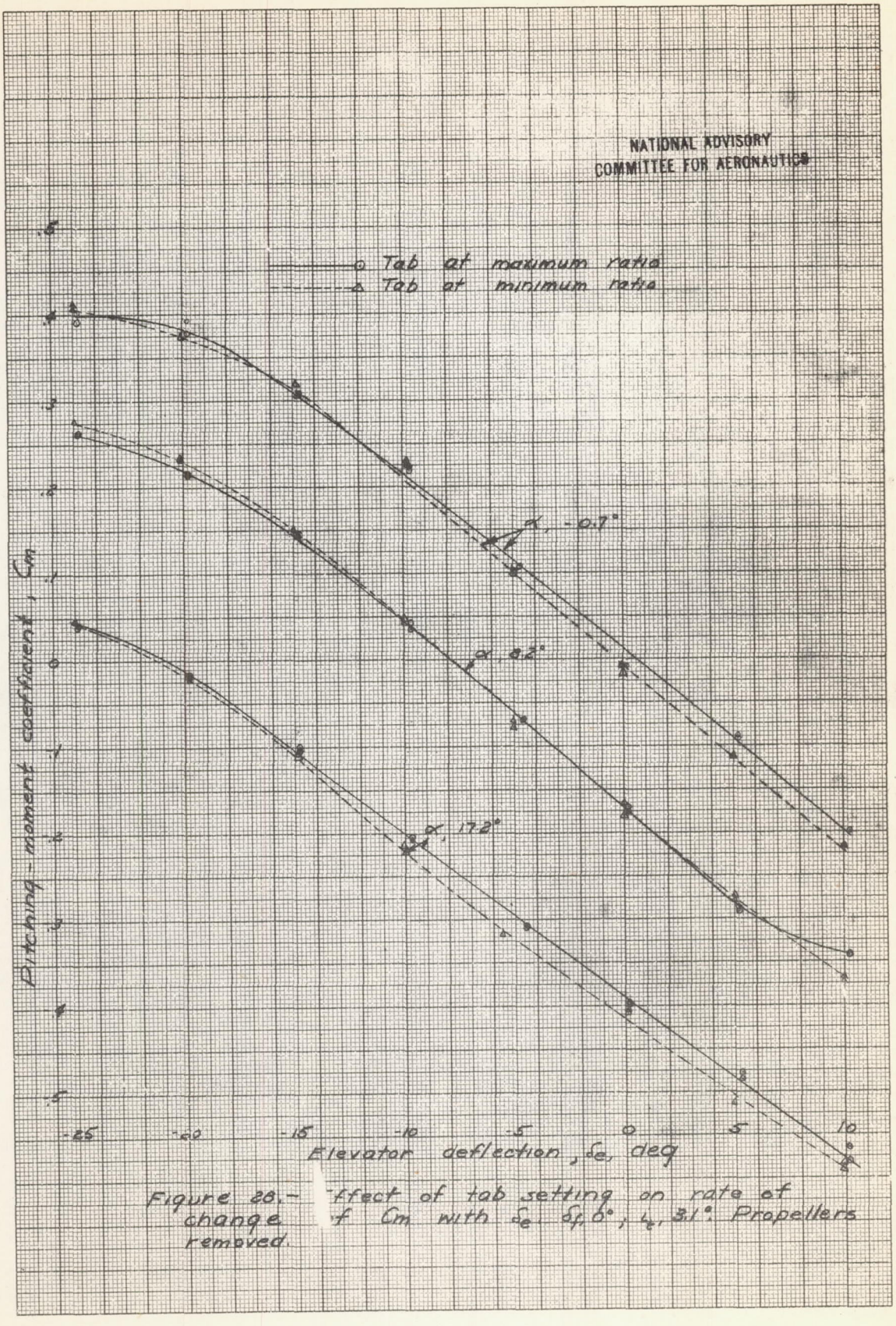

Figure 28.- Effect of tab setting on rate of change of C_m with δ_e. δ_f, 0°; i_t, 3.1°. Propellers removed.

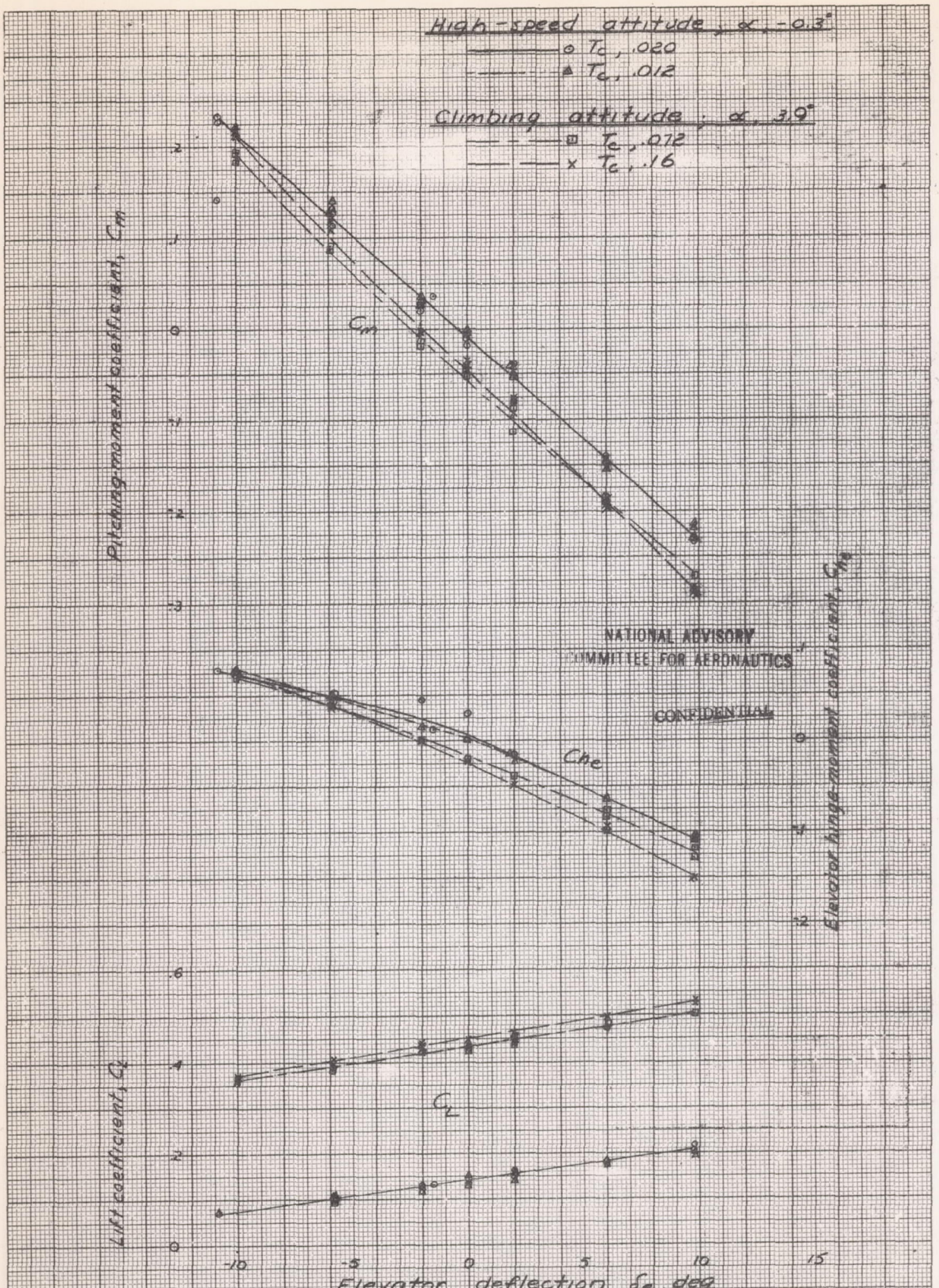

Figure 29.- Effect of elevator deflection on the aerodynamic characteristics of the XP-69 model for various power conditions. Elevator tab locked; δ_t, 0°; i_t, 16°

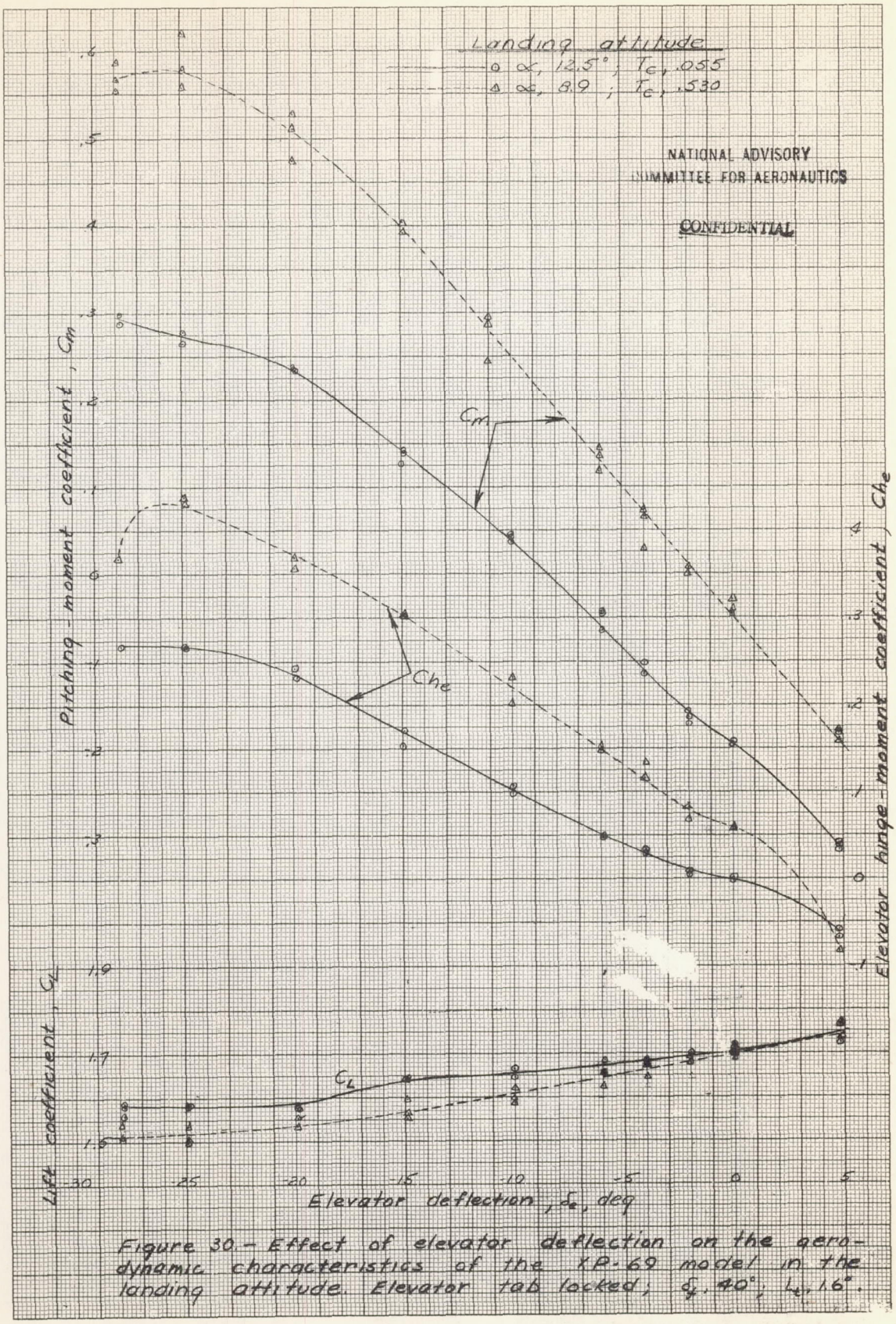

Figure 30.- Effect of elevator deflection on the aerodynamic characteristics of the XP-69 model in the landing attitude. Elevator tab locked; δ_t, 40°; L_e, 16".

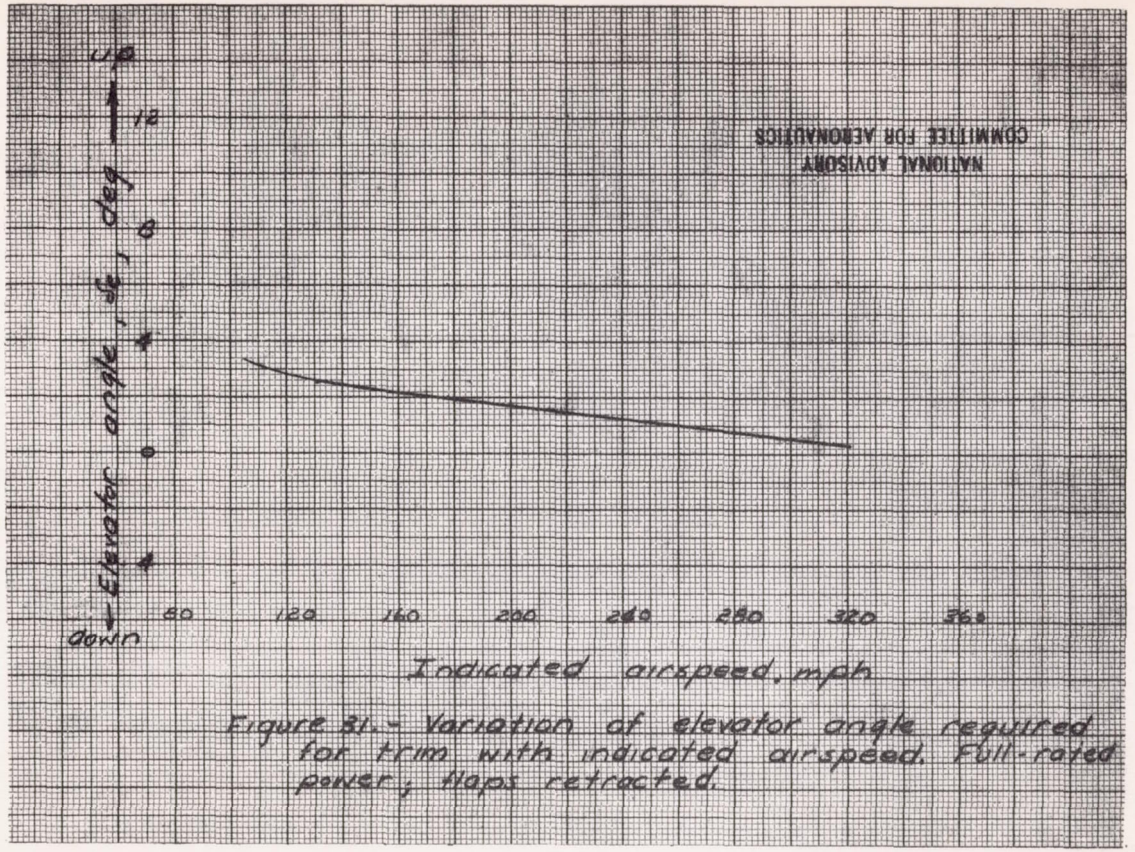

Figure 31.- Variation of elevator angle required for trim with indicated airspeed. Full-rated power; flaps retracted.

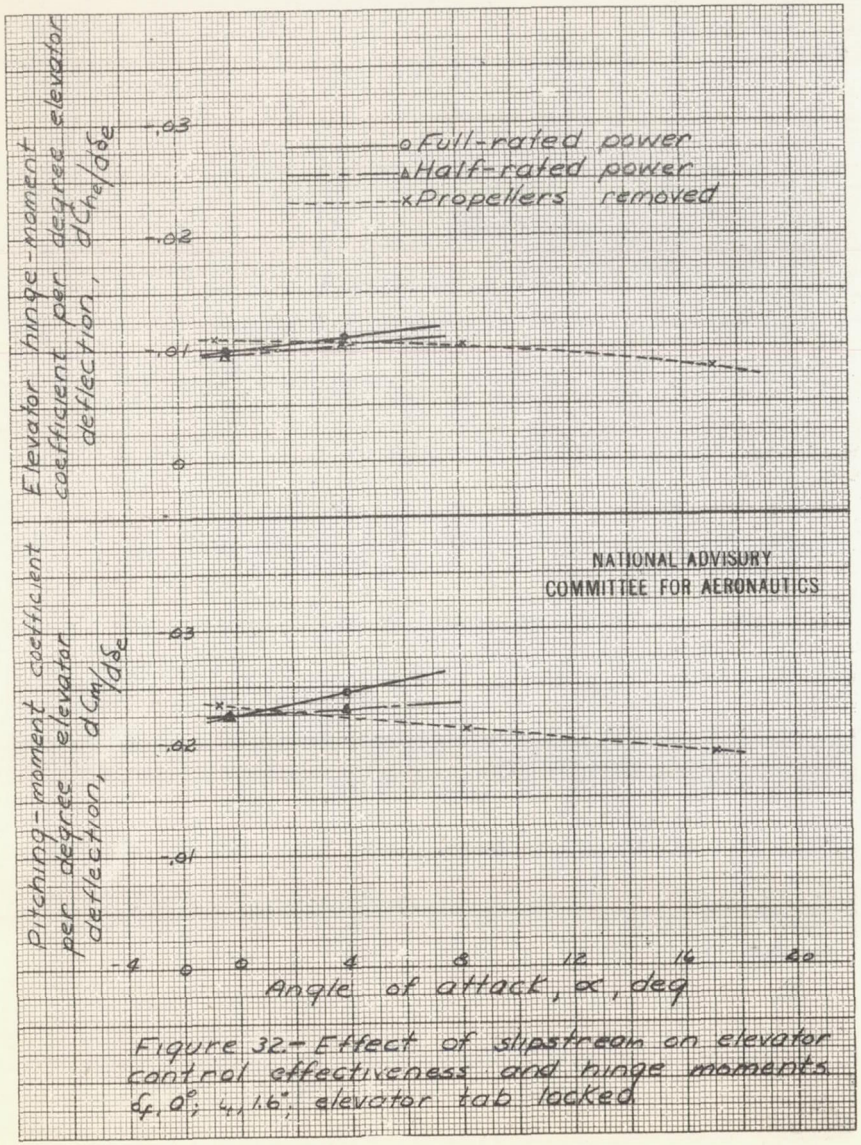

Figure 32.- Effect of slipstream on elevator control effectiveness and hinge moments. δ_f, 0°; i_t, 1.6°; elevator tab locked.

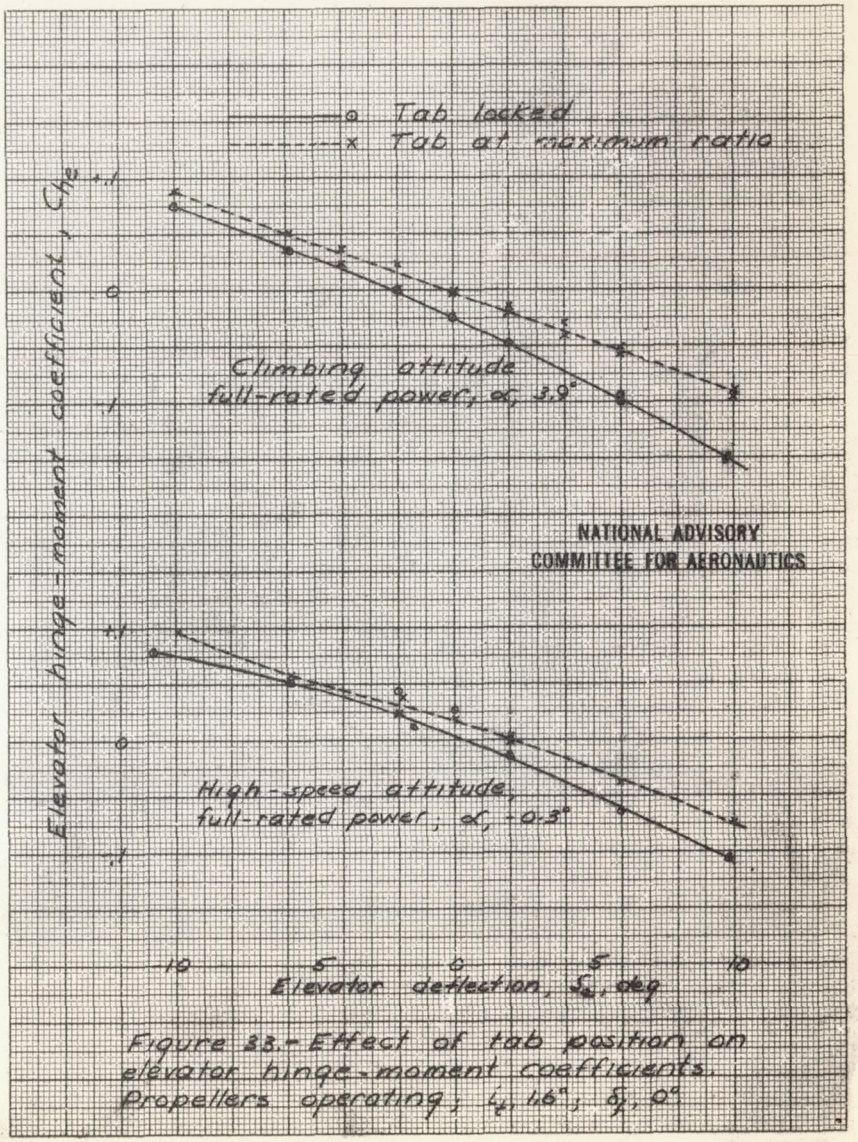

Figure 33.- Effect of tab position on elevator hinge-moment coefficients. Propellers operating; i_t, 1.6°; δ_f, 0°.

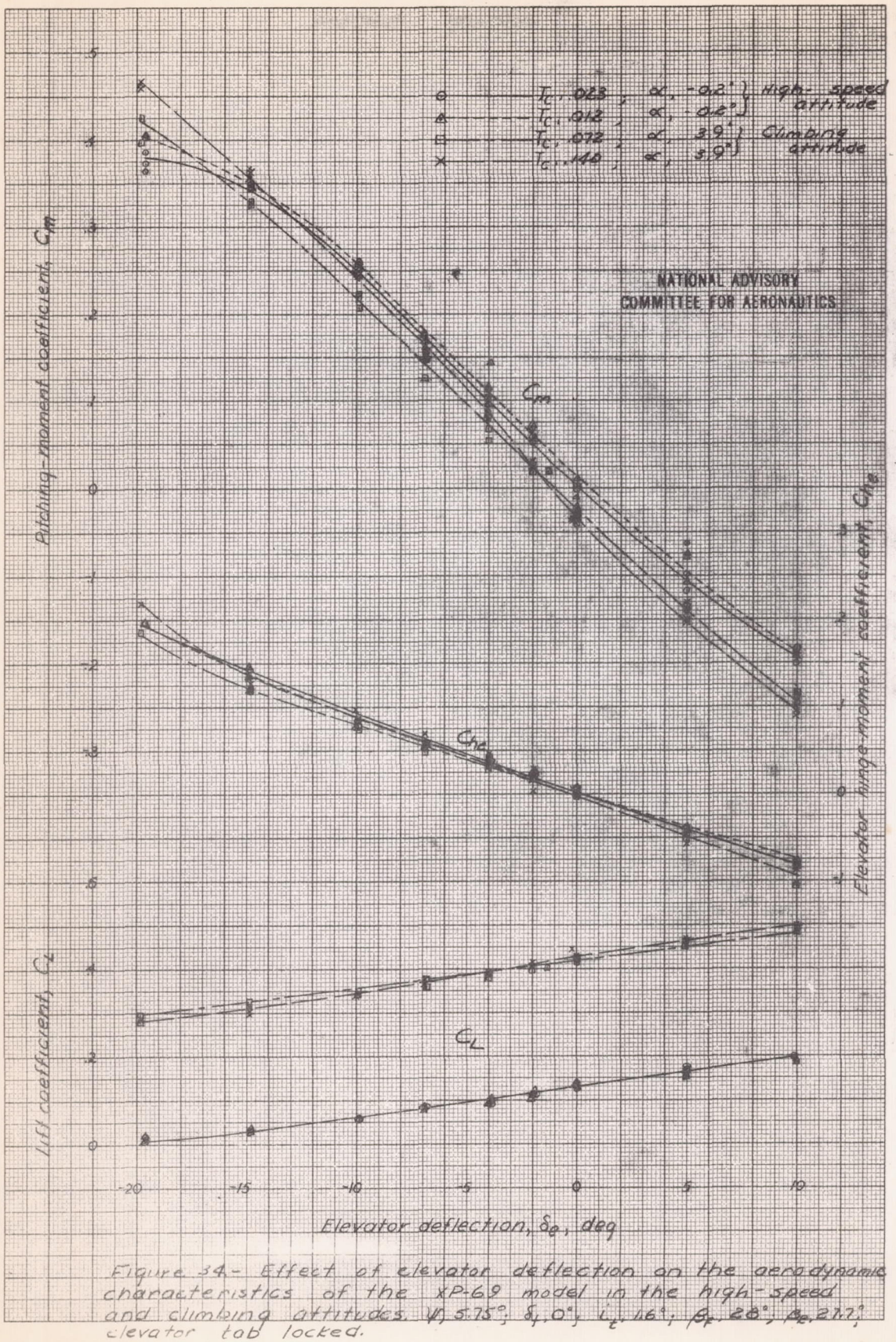

Figure 34.- Effect of elevator deflection on the aerodynamic characteristics of the XP-69 model in the high-speed and climbing attitudes. M, 5.75°; δ_f, 0°; i_t, 1.6°; β_p, 28°; α_e, 2.7°; elevator tab locked.

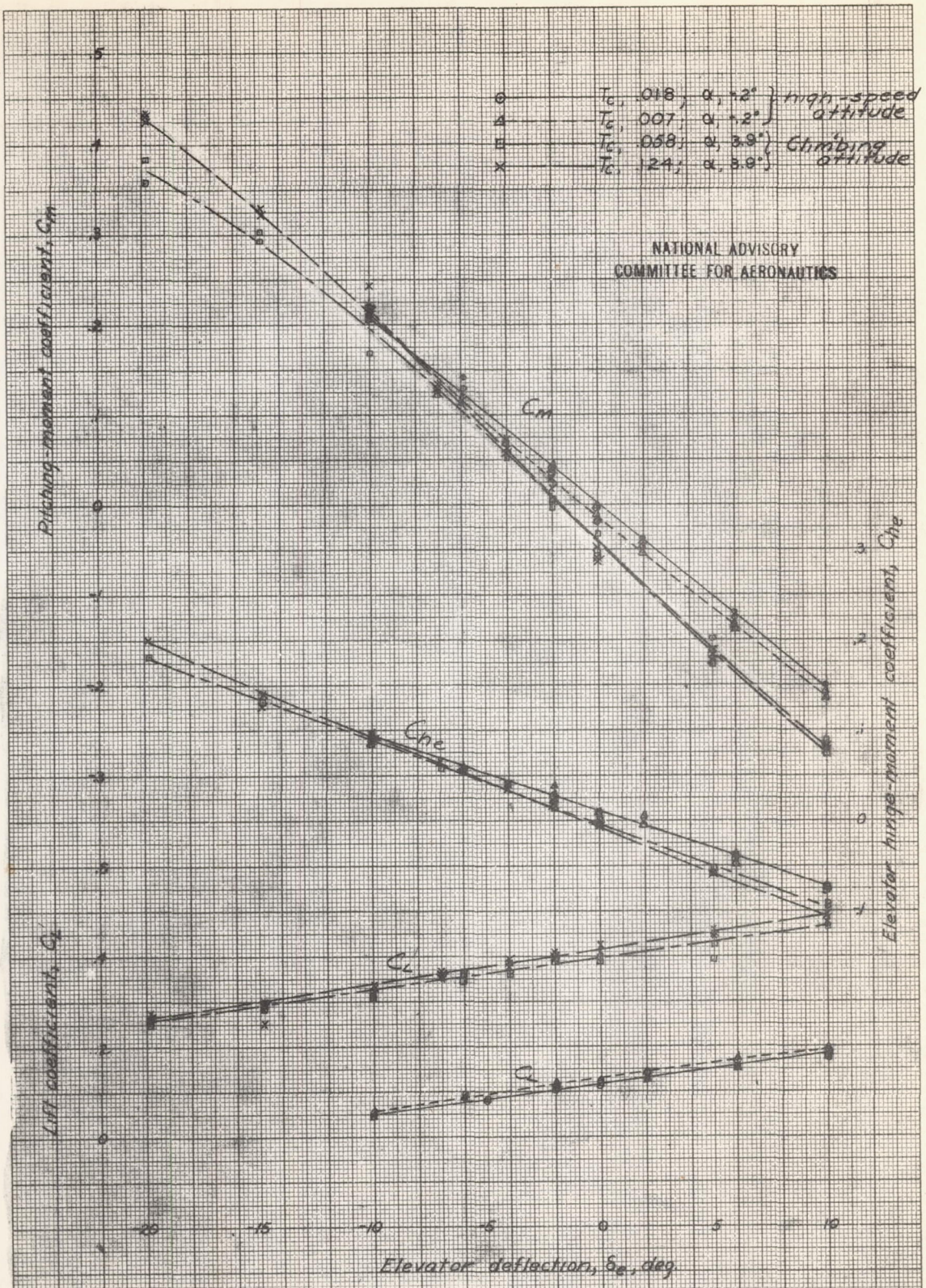

Figure 35.- Effect of elevator deflection on the aerodynamic characteristics of the XP-69 model in the high-speed and climbing attitudes. V_i, 15.1°; δ_f, 0°; i_t, 1.6°; β_t, 28°; β_e, 21.7°; elevator tab locked.

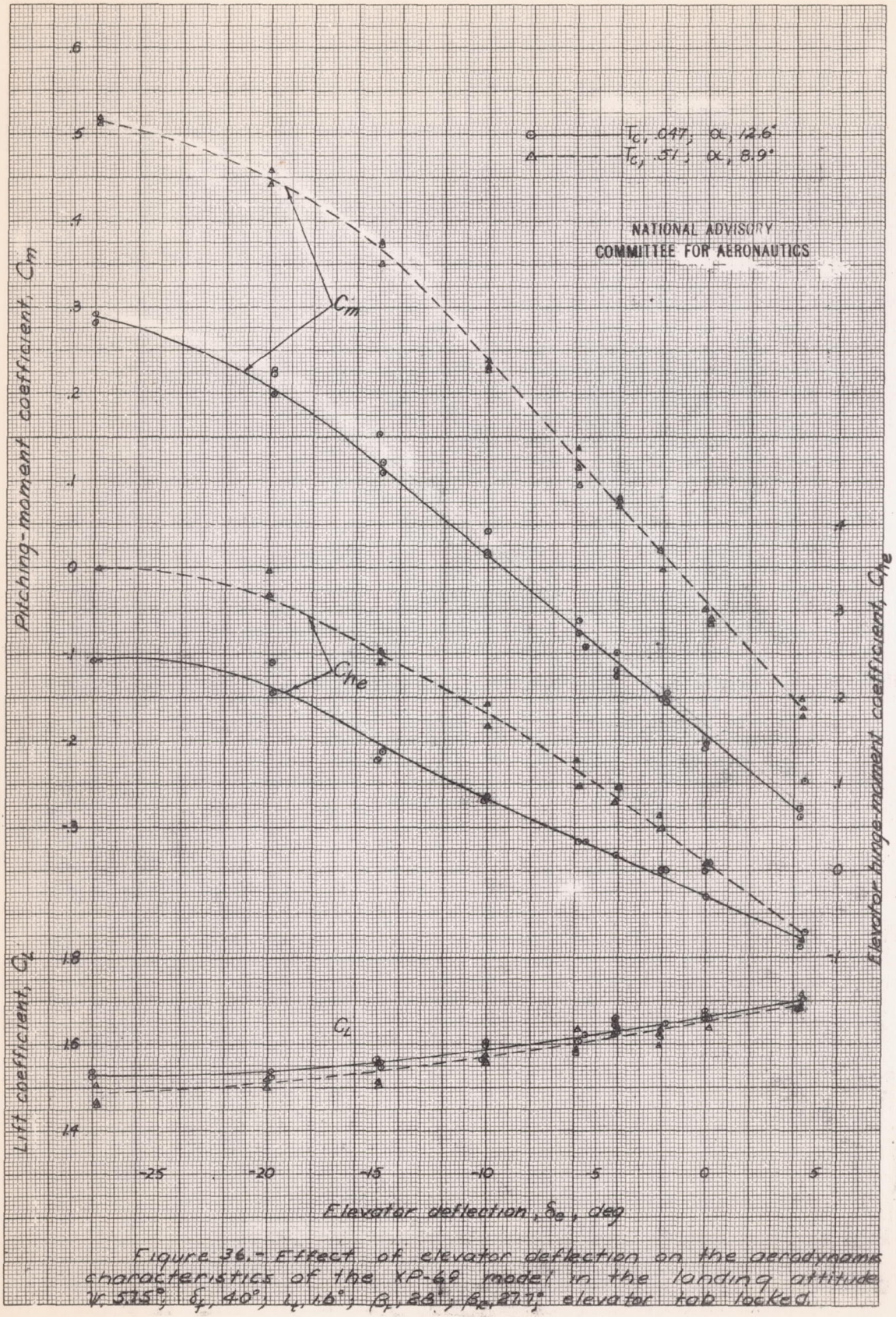

Figure 36.- Effect of elevator deflection on the aerodynamic characteristics of the XP-69 model in the landing attitude V_i, 535°; δ_f, 40°; i_t, 16°; β_1, 28°; β_2, 27.5°; elevator tab locked.

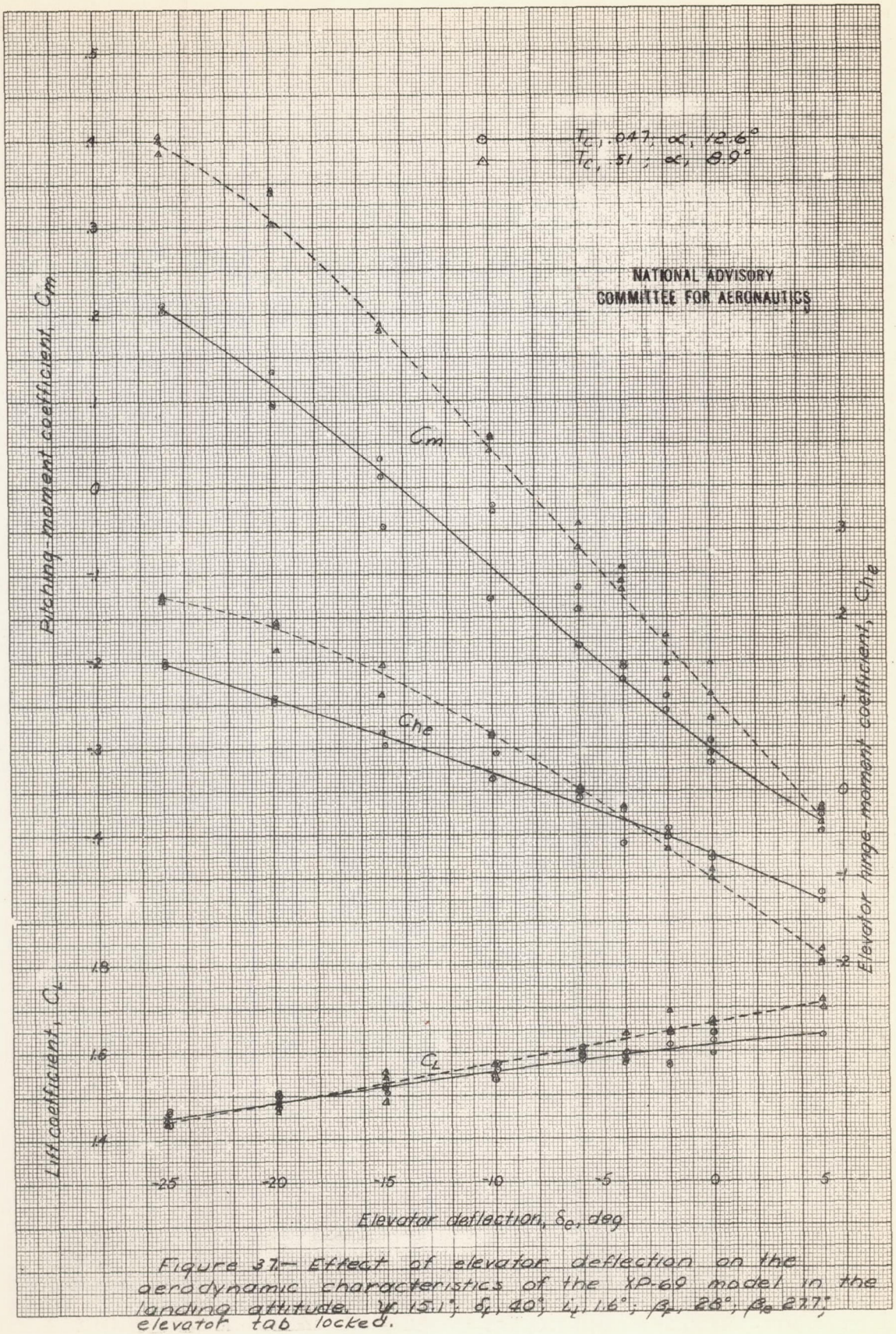

Figure 37.— Effect of elevator deflection on the aerodynamic characteristics of the XP-69 model in the landing attitude. V_p, 151; δ_f, 40°; i_t, 1.6°; β_p, 28°; β_e, 27.7°; elevator tab locked.

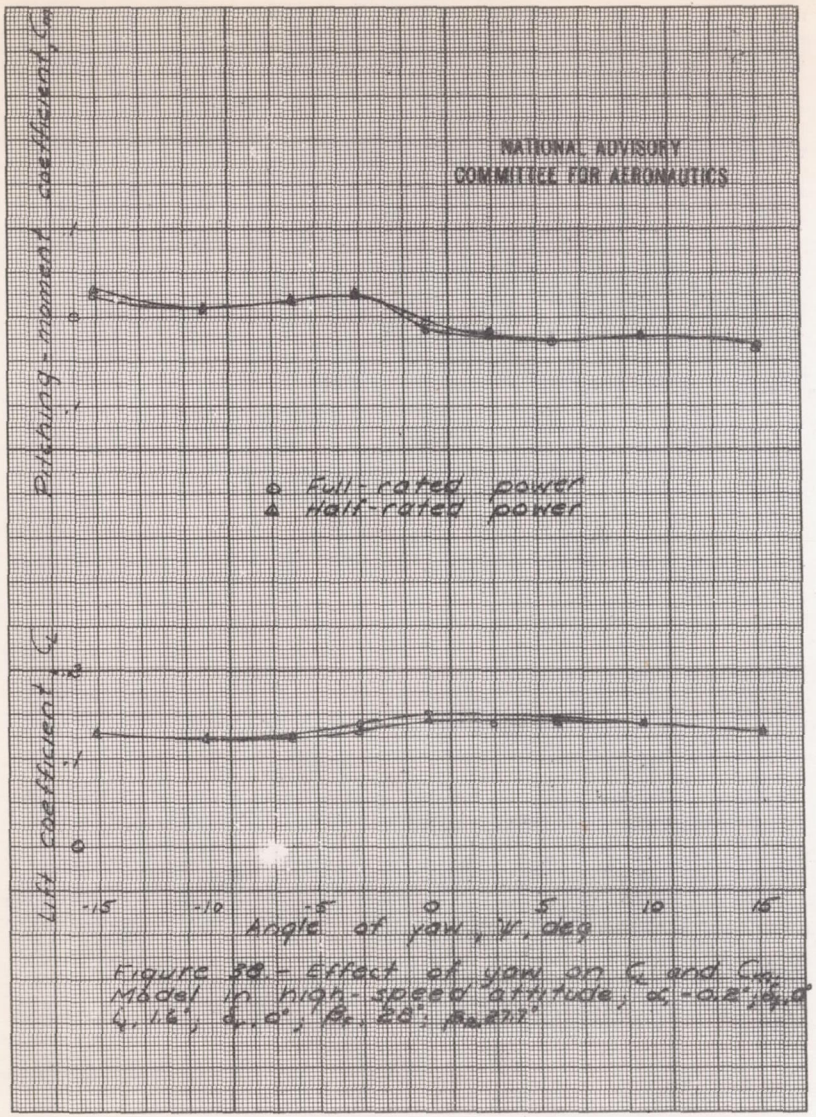

Figure 29.- Effect of yaw on C_L and C_m. Model in high-speed attitude, α_c -0.2°, i_t -2°, i_w 1.6°, i_h 0°, β_p 20°, β_w 20°.

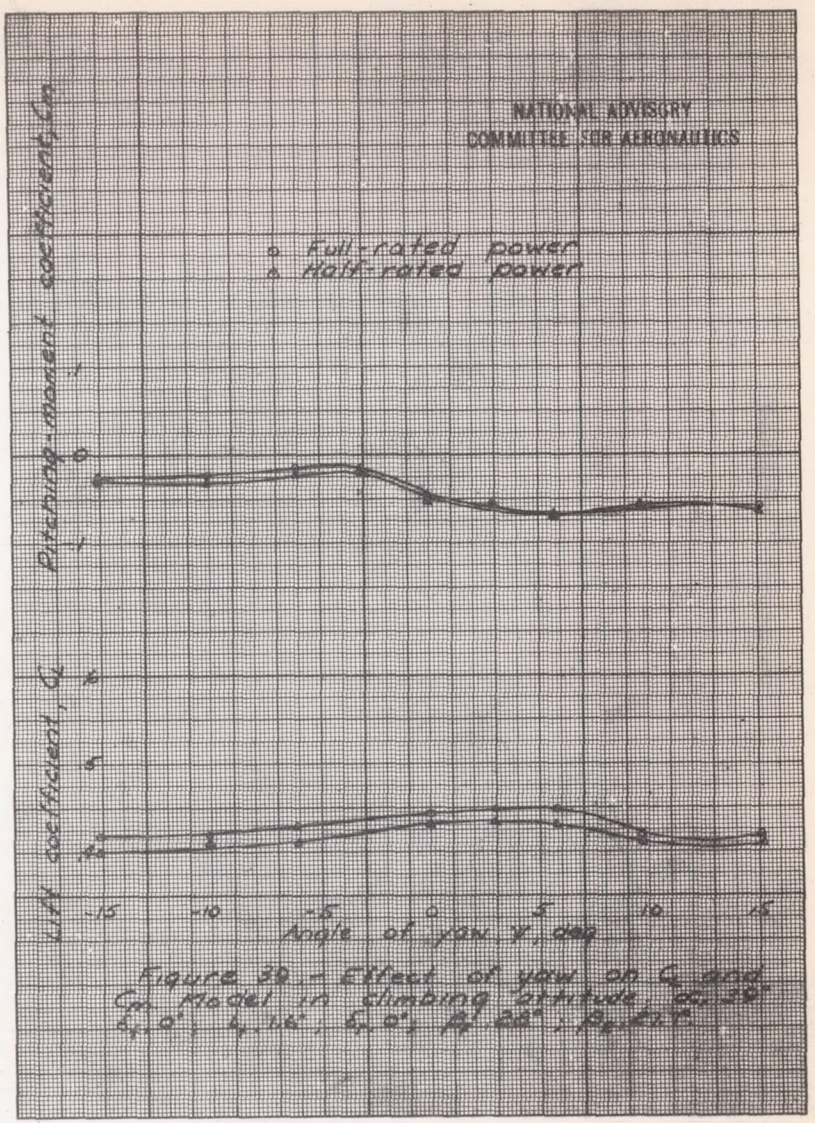

Figure 30.- Effect of yaw on C_L and C_m. Model in climbing attitude, α_c 2.8°, i_t 0°, i_w 1.6°, i_h 0°, β_p 20°, β_w 20°.

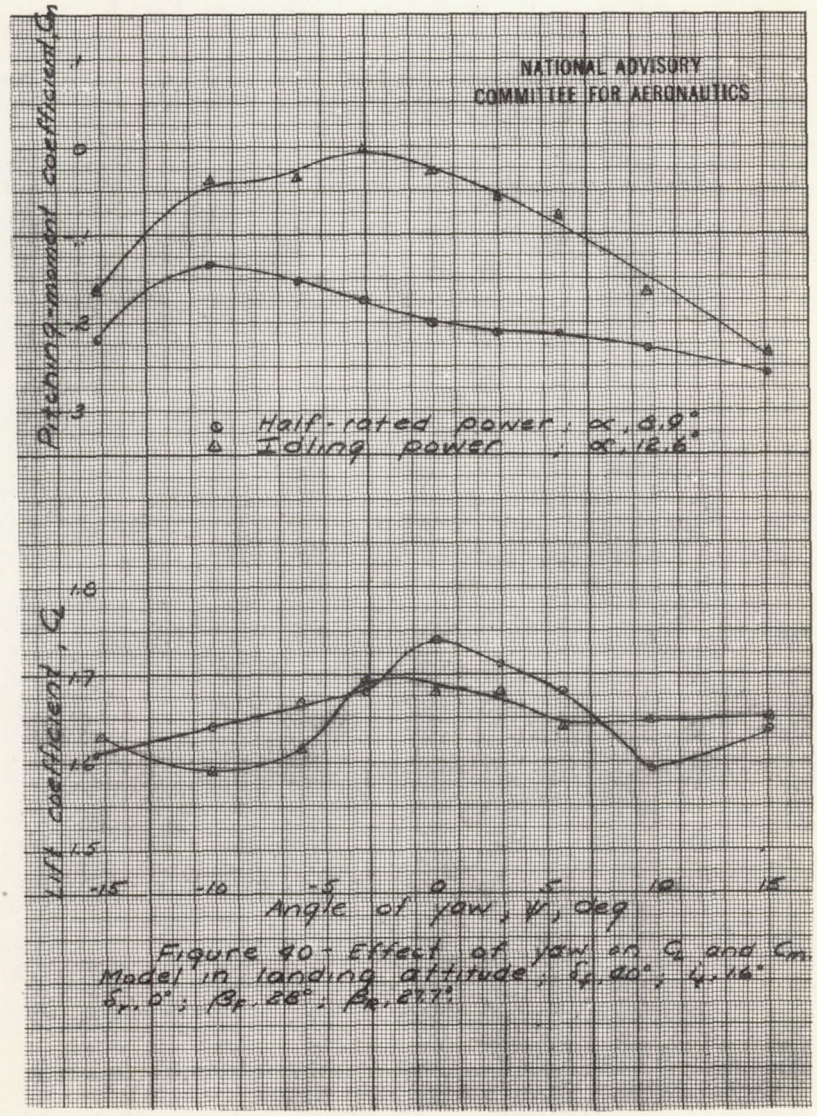

Figure 40.- Effect of yaw on C_L and C_m. Model in landing attitude; ζ_f, 40°; i_t, 16°; ζ_r, 0°; β_f, 28°; β_r, 27°.

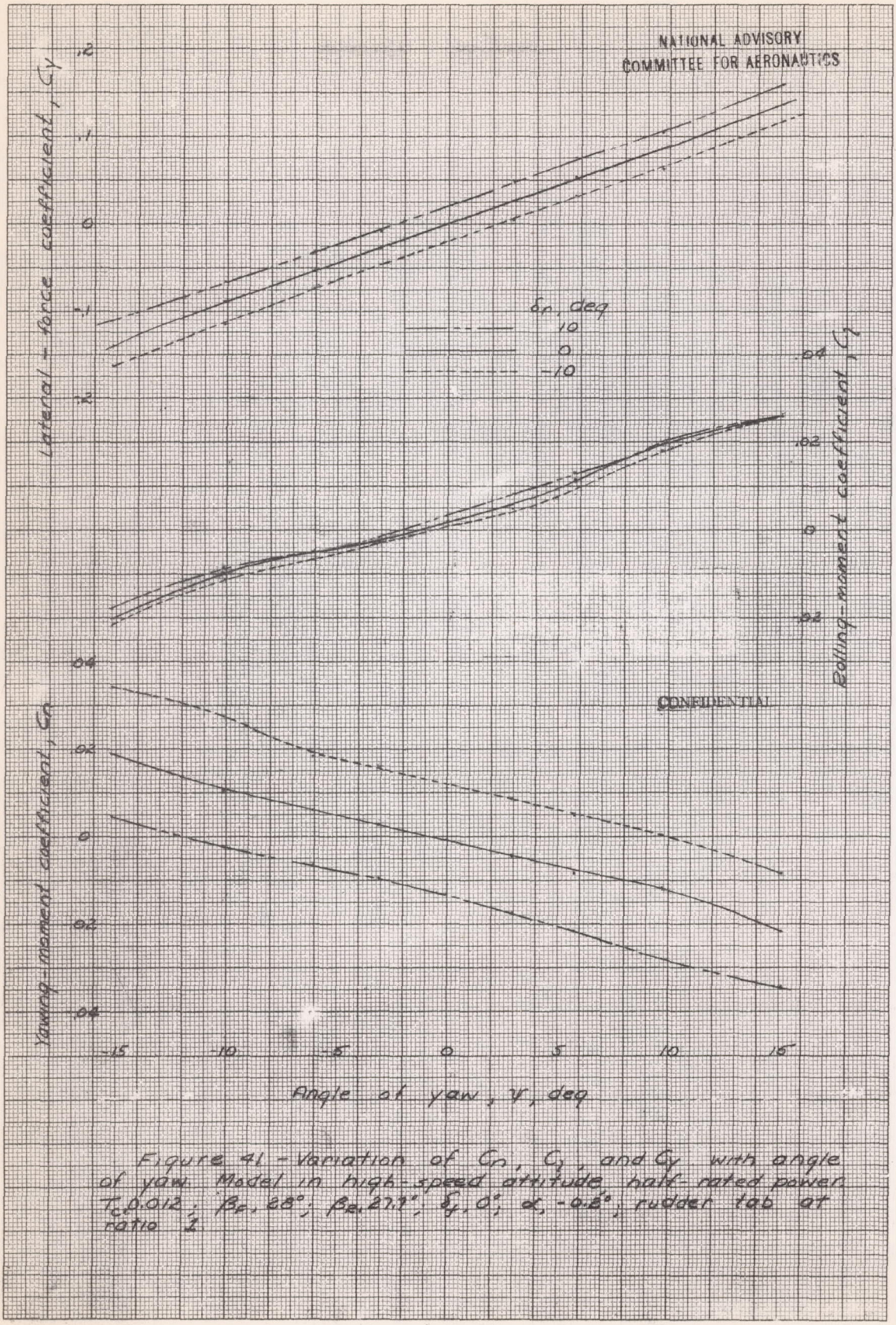

Figure 41 - Variation of C_n, C_l, and C_Y with angle of yaw. Model in high-speed attitude, half-rated power, T_c 0.012; β_F, 28°; β_R, 27.7°; δ_f, 0°; α, -0.8°; rudder tab at ratio 2.

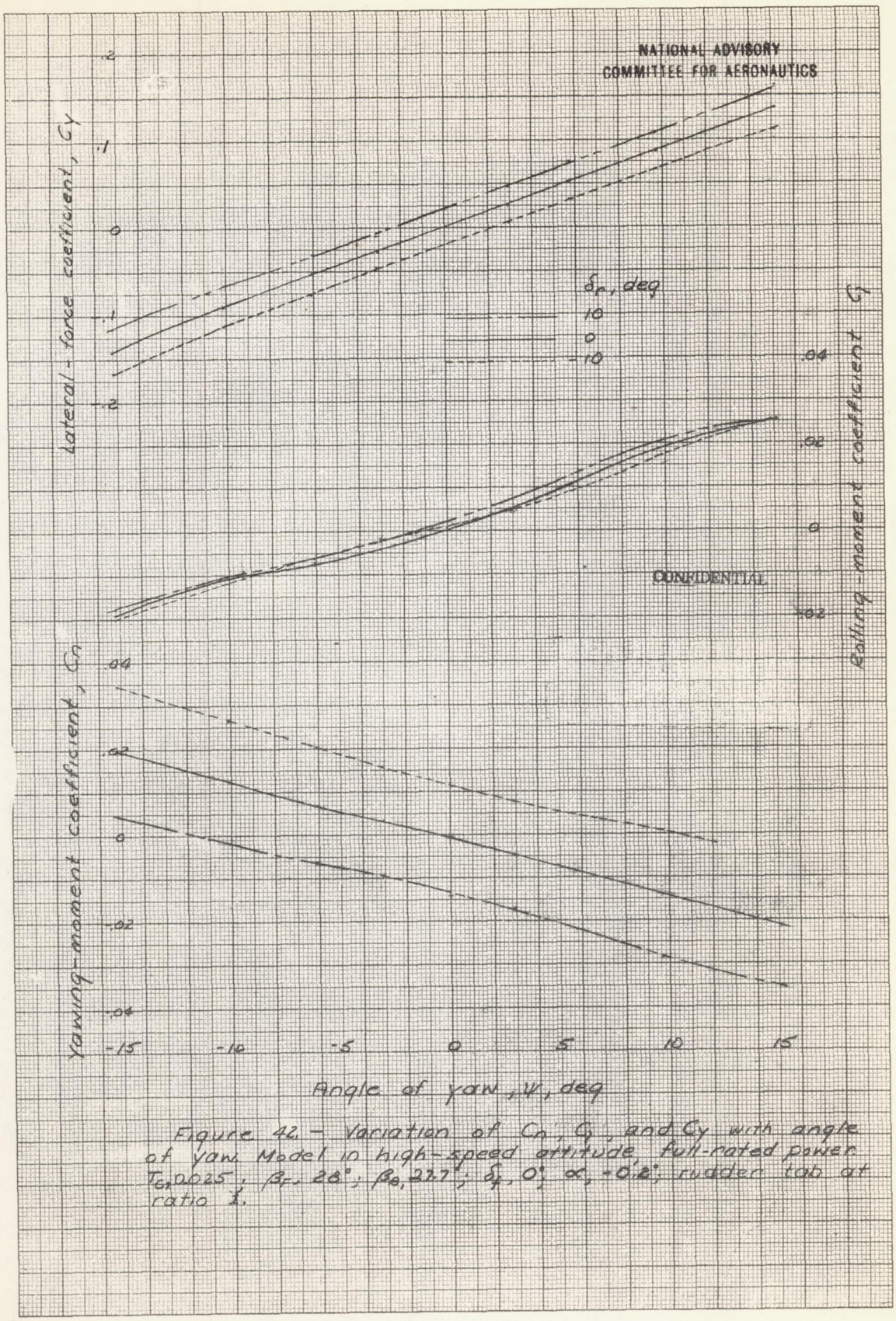

Figure 42. - Variation of C_n, C_l, and C_y with angle of yaw. Model in high-speed attitude, full-rated power T_c, 0.025; β_F, 28°; β_B, 22.7°; δ_f, 0°; α_t, -0.2°; rudder tab at ratio 1.

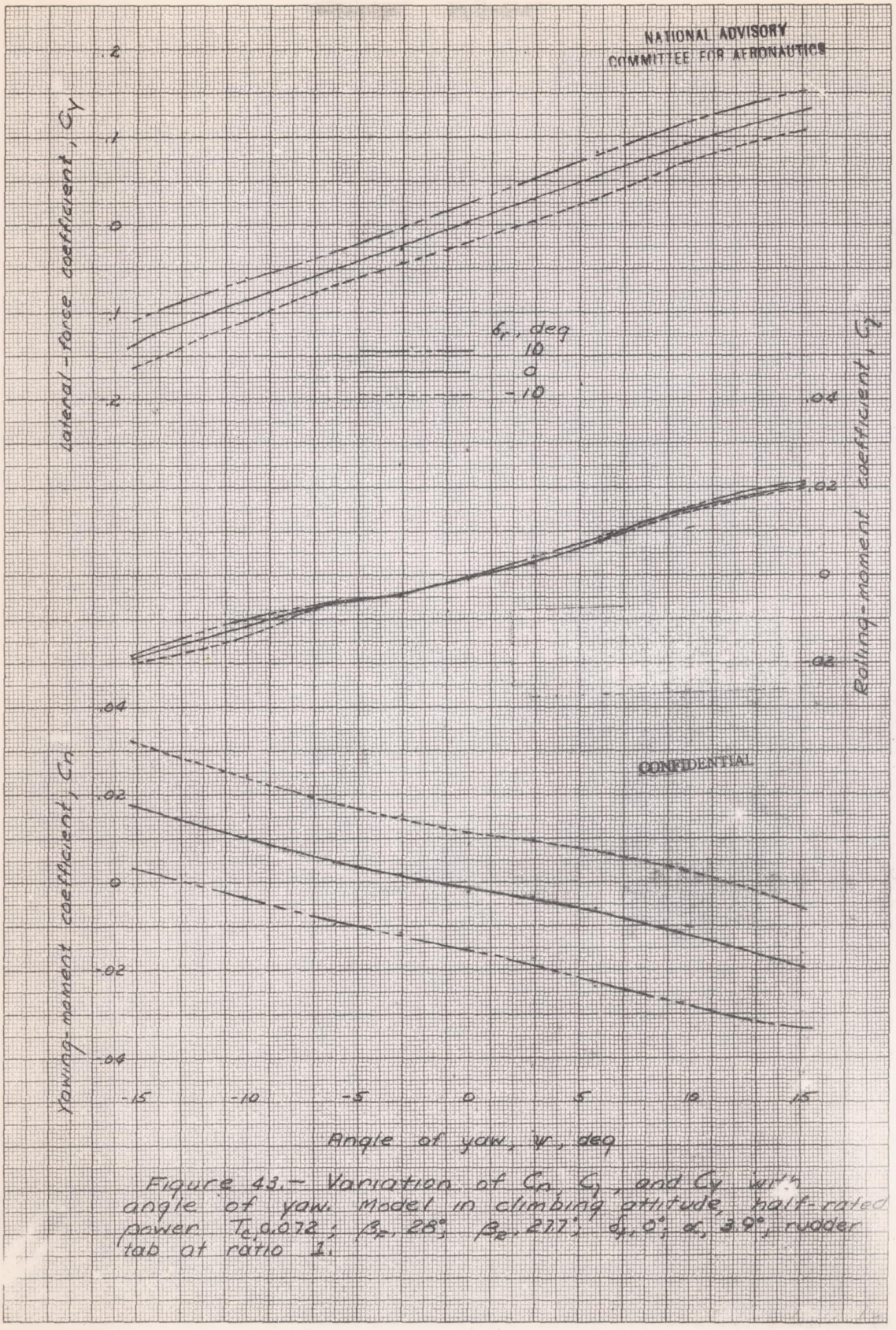

Figure 43.— Variation of C_n, C_l, and C_Y with angle of yaw. Model in climbing attitude, half-rated power, T_c 0.072; β_p, 28°; β_R, 21.7°; δ_f, 0°; α, 3.9°; rudder tab at ratio 1.

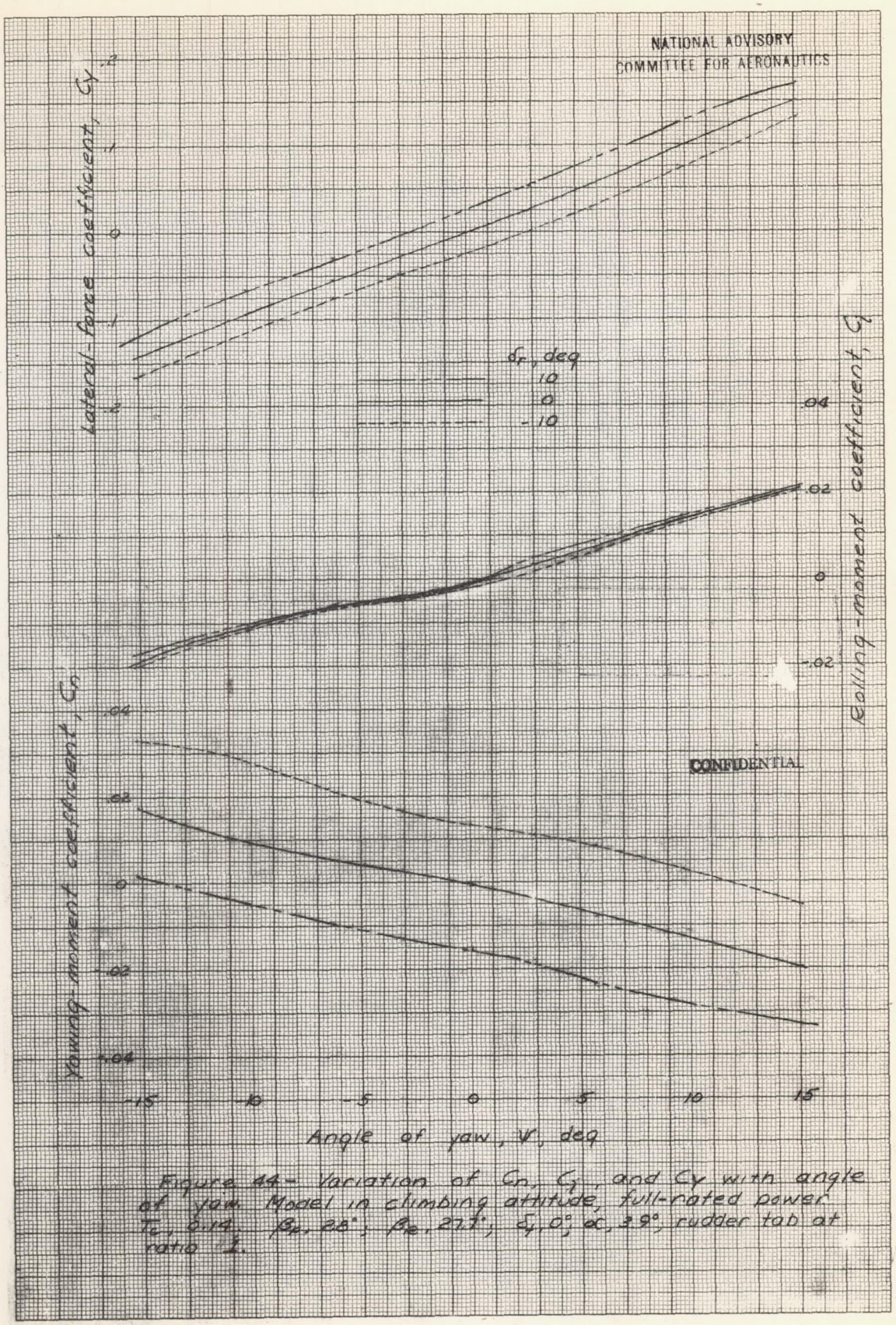

Figure 44.- Variation of C_n, C_l, and C_Y with angle of yaw. Model in climbing attitude, full-rated power (T_c, 0.14; β_p, 28°; β_e, 21.3°; δ_f, 0°; α, 3.9°; rudder tab at ratio 2.

CONFIDENTIAL

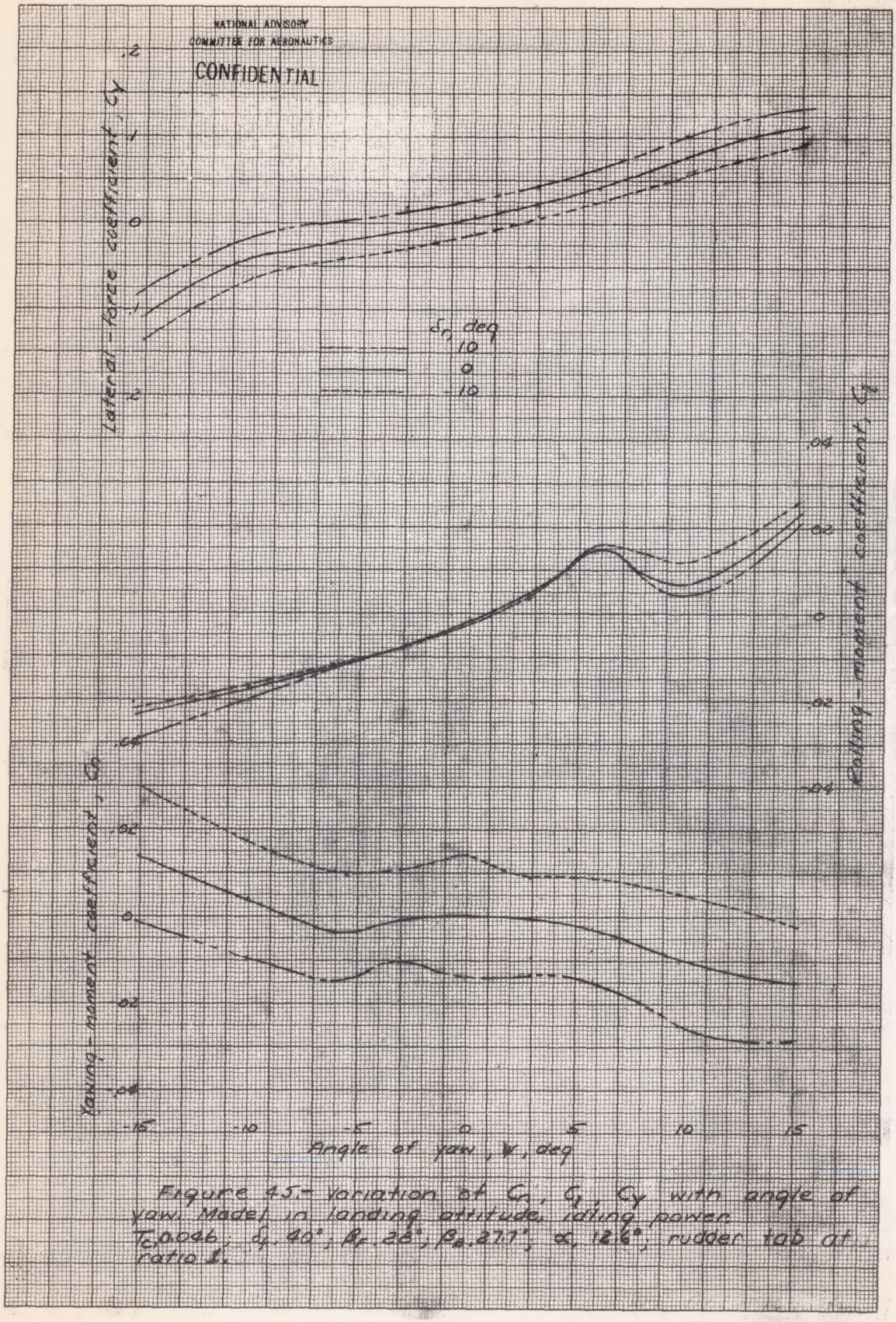

Figure 45.- Variation of C_n, C_l, C_Y with angle of yaw. Model in landing attitude, idling power. T_c 0.046; δ_f 40°; R_f 28°; R_e 27.1°; α_t 12.6°; rudder tab at ratio 1.

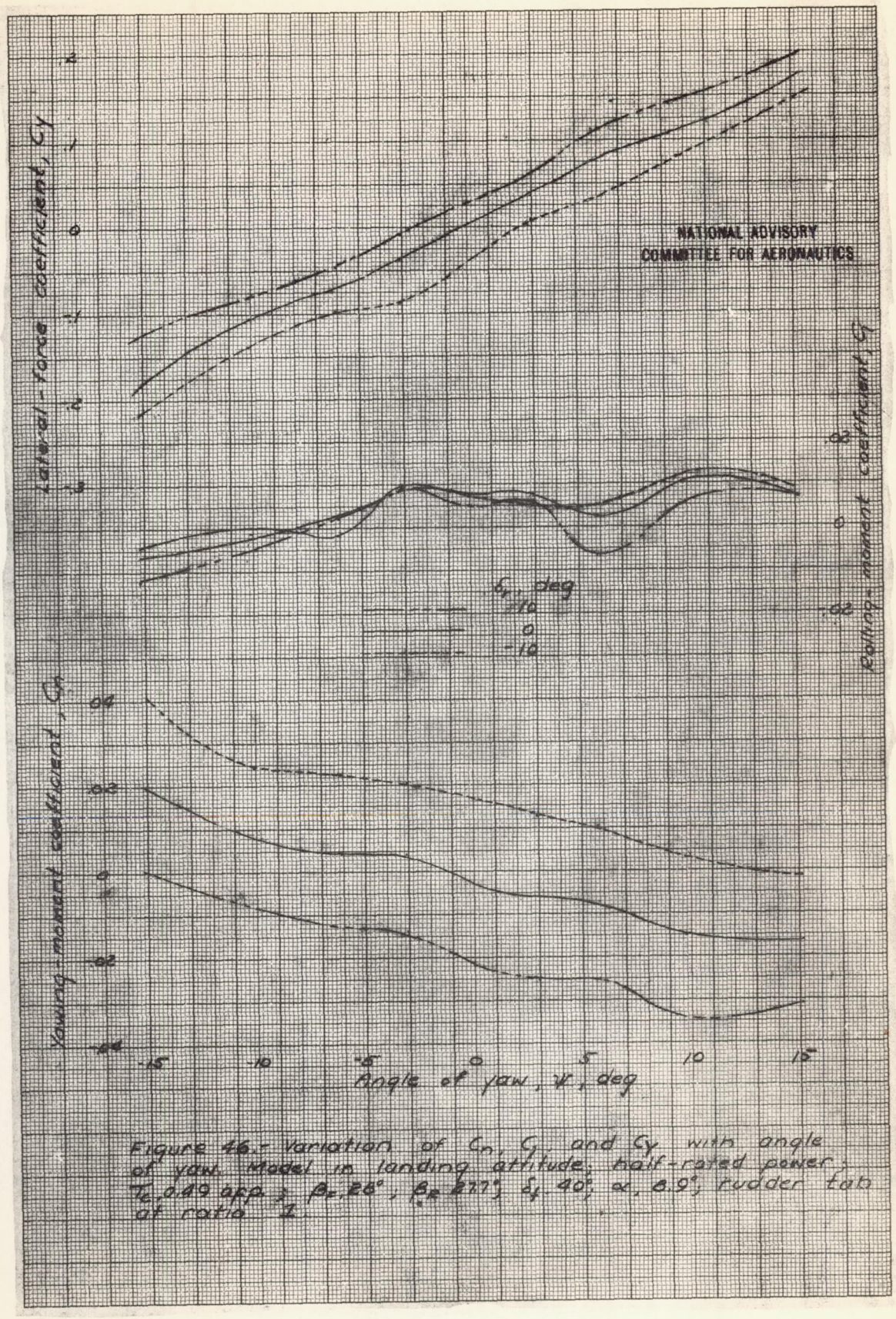

Figure 46.- Variation of C_n, C_l, and C_Y with angle of yaw. Model in landing attitude; half-rated power; T_c, 0.19 app.; β_p, 28°; β_R, 27.7°; δ_f, 40°; α, 8.9°; rudder tab of ratio .2.

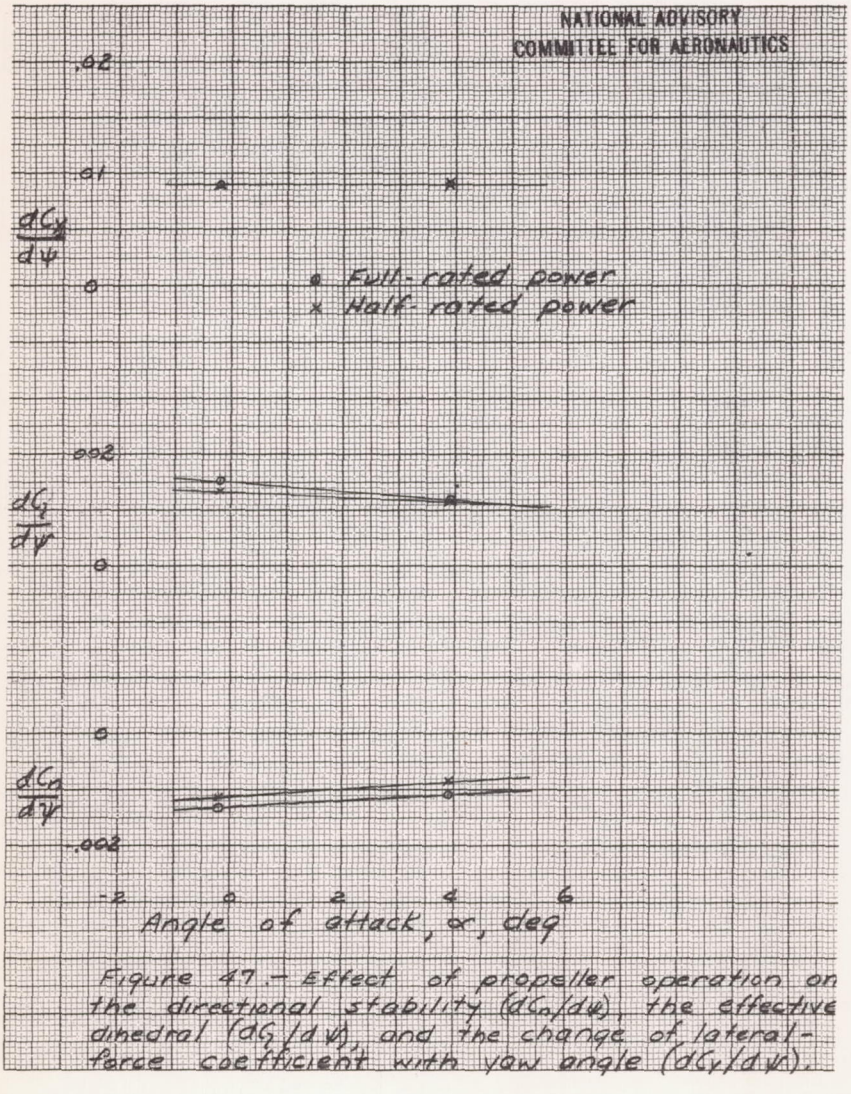

Figure 47.- Effect of propeller operation on the directional stability ($dC_n/d\psi$), the effective dihedral ($dC_l/d\psi$), and the change of lateral-force coefficient with yaw angle ($dC_Y/d\psi$).

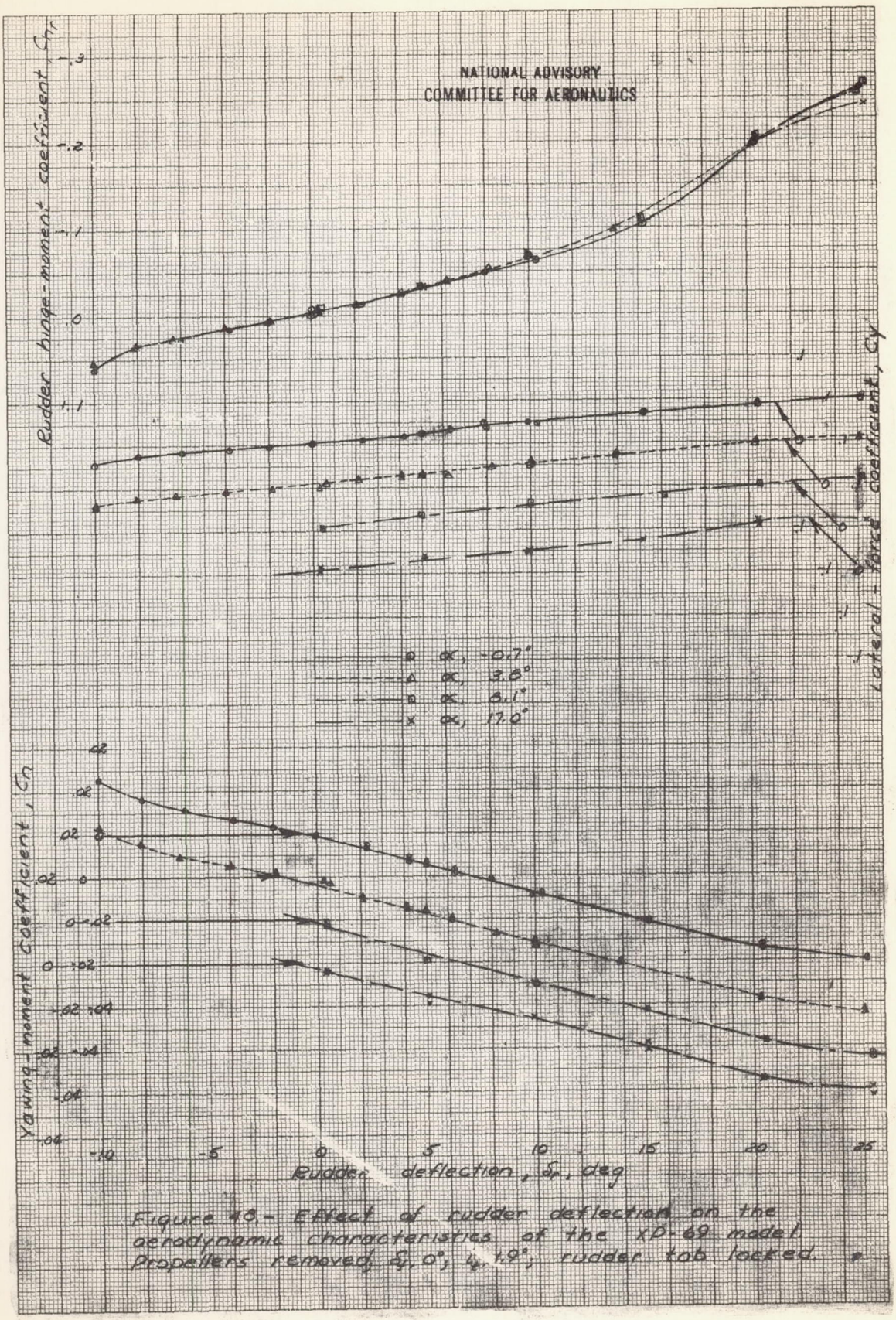

Figure 13.- Effect of rudder deflection on the aerodynamic characteristics of the XP-69 model. Propellers removed; δ_e, 0°; i_t, 1.9°; rudder tab locked.

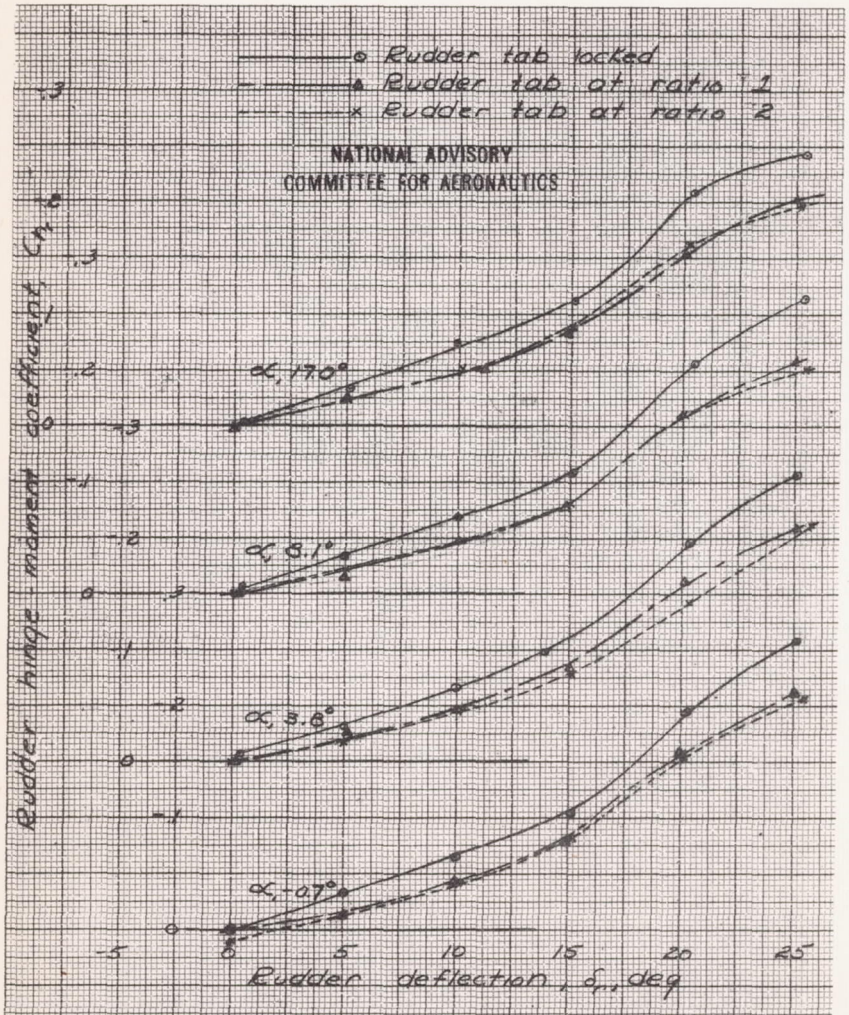

Figure 49.- Effect of tab setting on rate of change of C_{h_r} with δ_r. Propellers removed, δ_f, 0°; ψ, 0°.

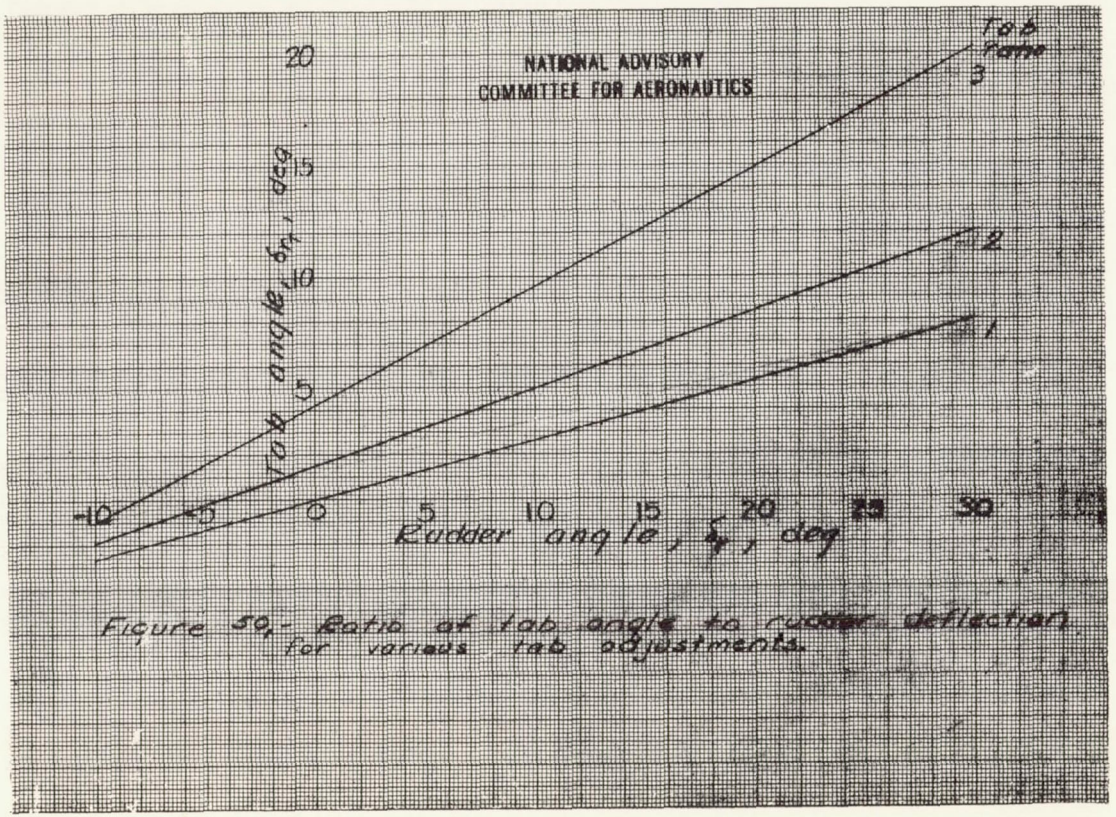

Figure 30.- Ratio of tab angle to rudder deflection for various tab adjustments.

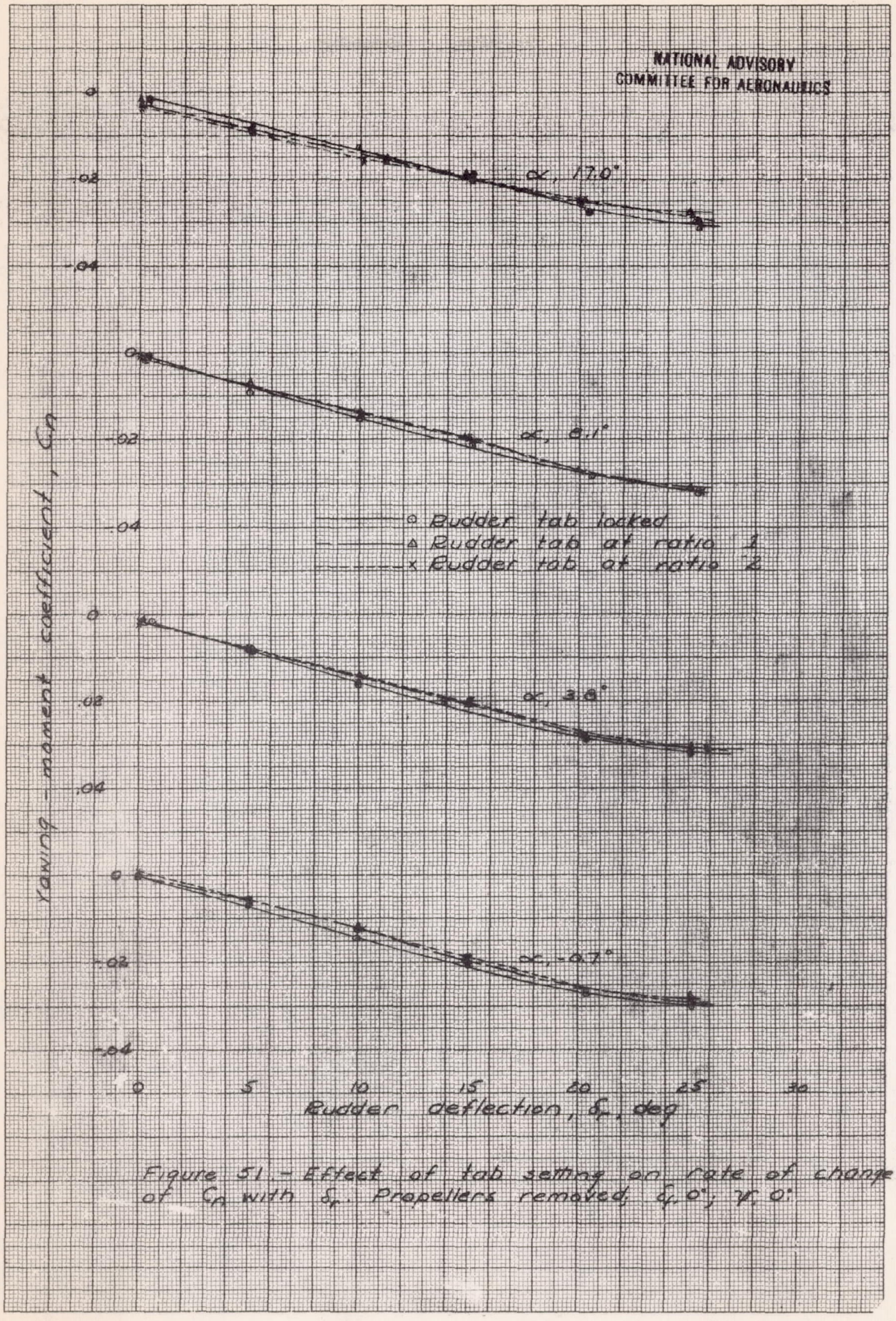

Figure 51 - Effect of tab setting on rate of change of C_n with δ_r. Propellers removed; δ_e 0°; γ_t 0°.

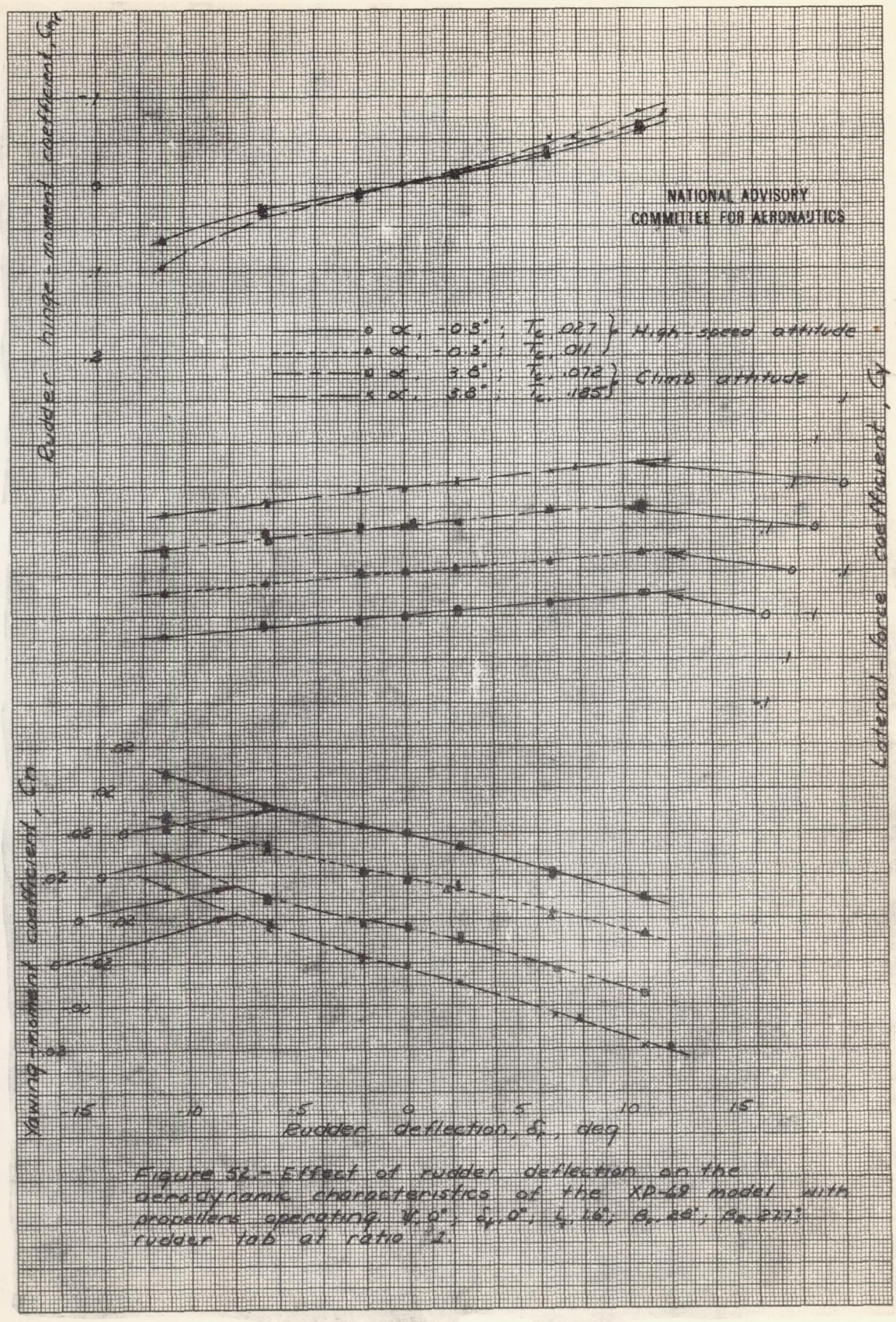

Figure 32.- Effect of rudder deflection on the aerodynamic characteristics of the XP-69 model with propellers operating. i_t, 0°; δ_f, 0°; i_r, 1.6°; β_p, 28°; R_p, 2773; rudder tab at ratio 2.

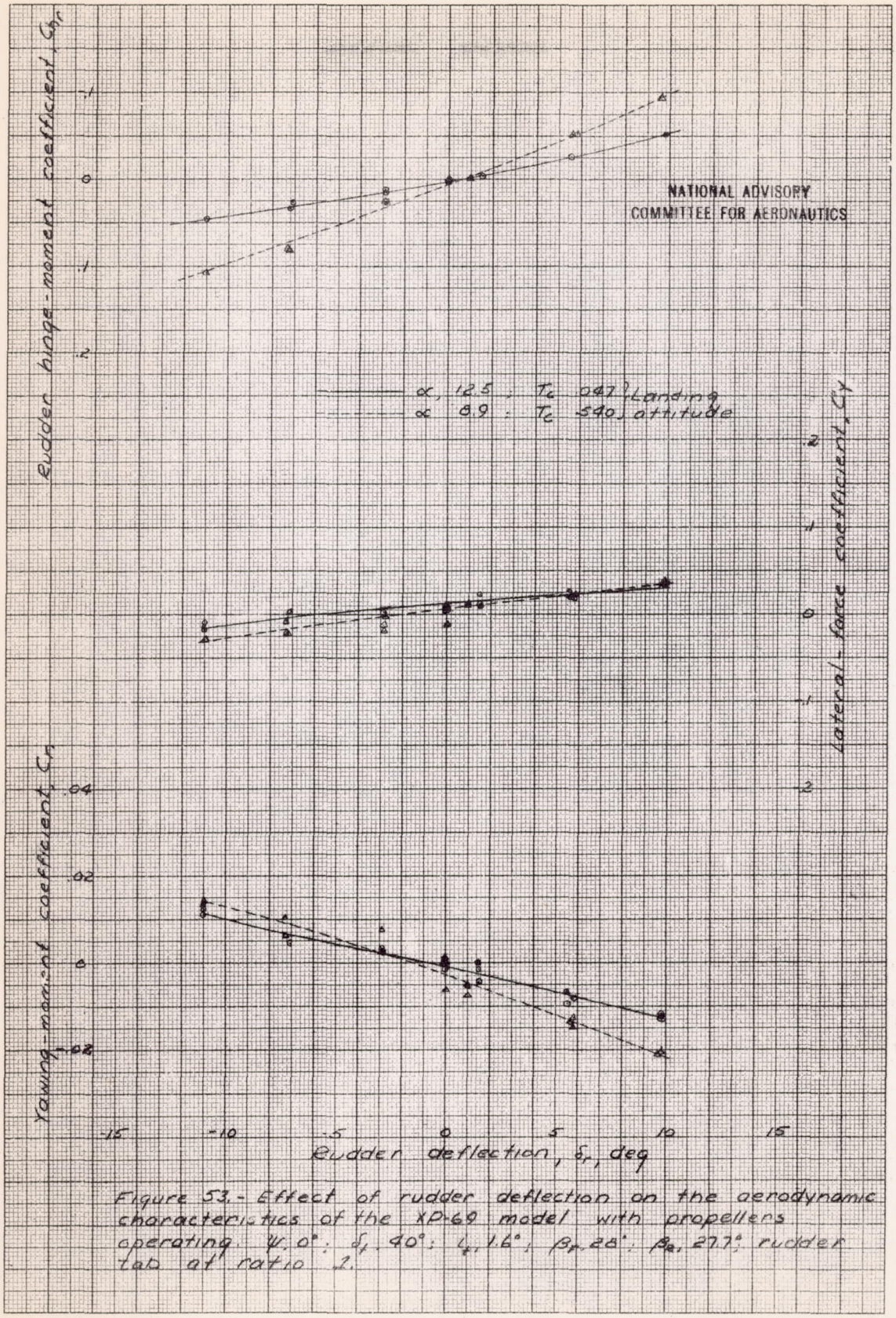

Figure 53.- Effect of rudder deflection on the aerodynamic characteristics of the XP-69 model with propellers operating. Ψ, 0°; δ_f, 40°; i_t, 1.6°; $\beta_{P.R.}$, 28°; $\beta_{P.L.}$, 27.7°; rudder tab at ratio 2.

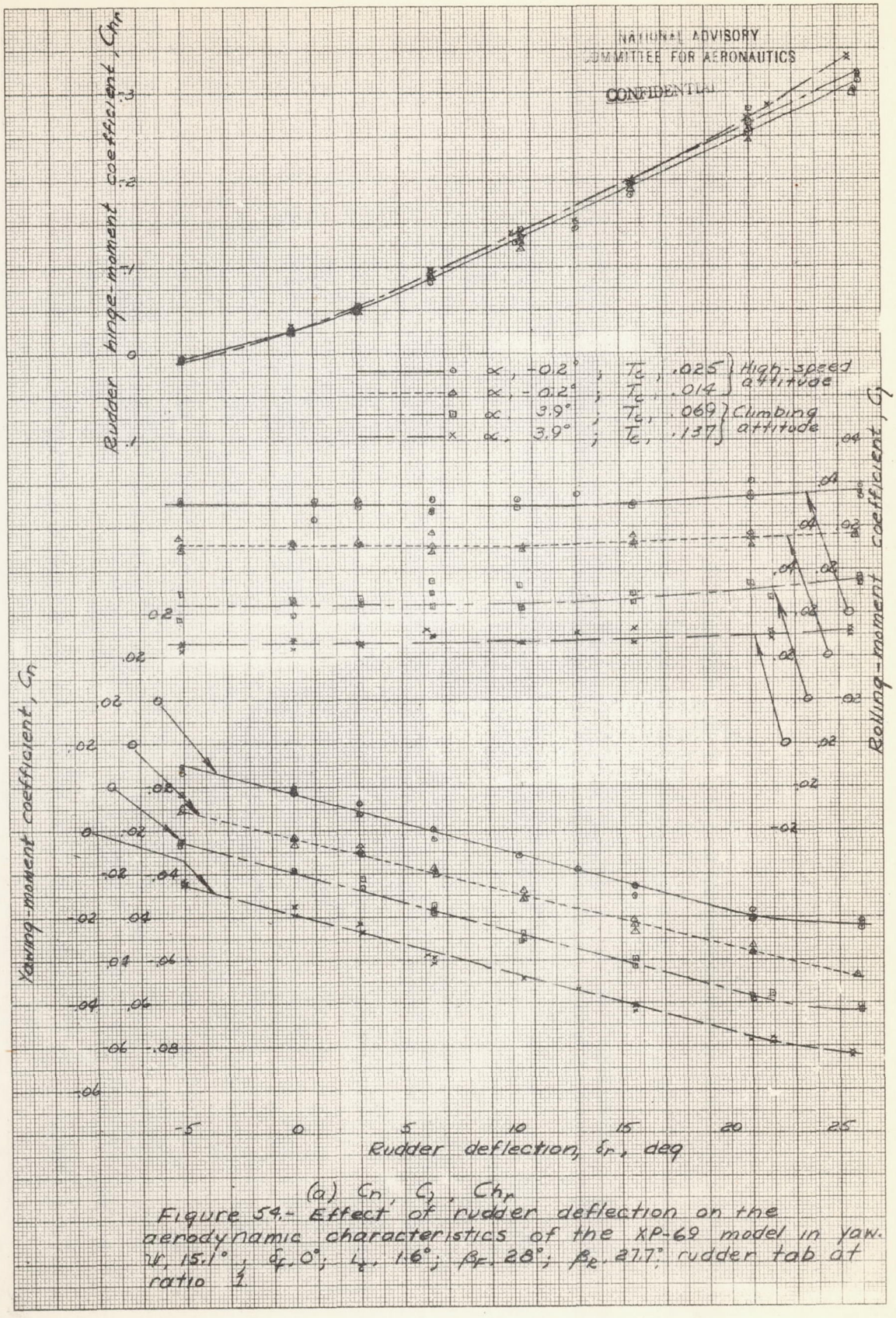

(a) C_n, C_l, C_{h_r}

Figure 54.- Effect of rudder deflection on the aerodynamic characteristics of the XP-69 model in yaw. V, 15.1°; δ_f, 0°; i_t, 1.6°; β_f, 28°; β_t, 27.7°; rudder tab at ratio 1.

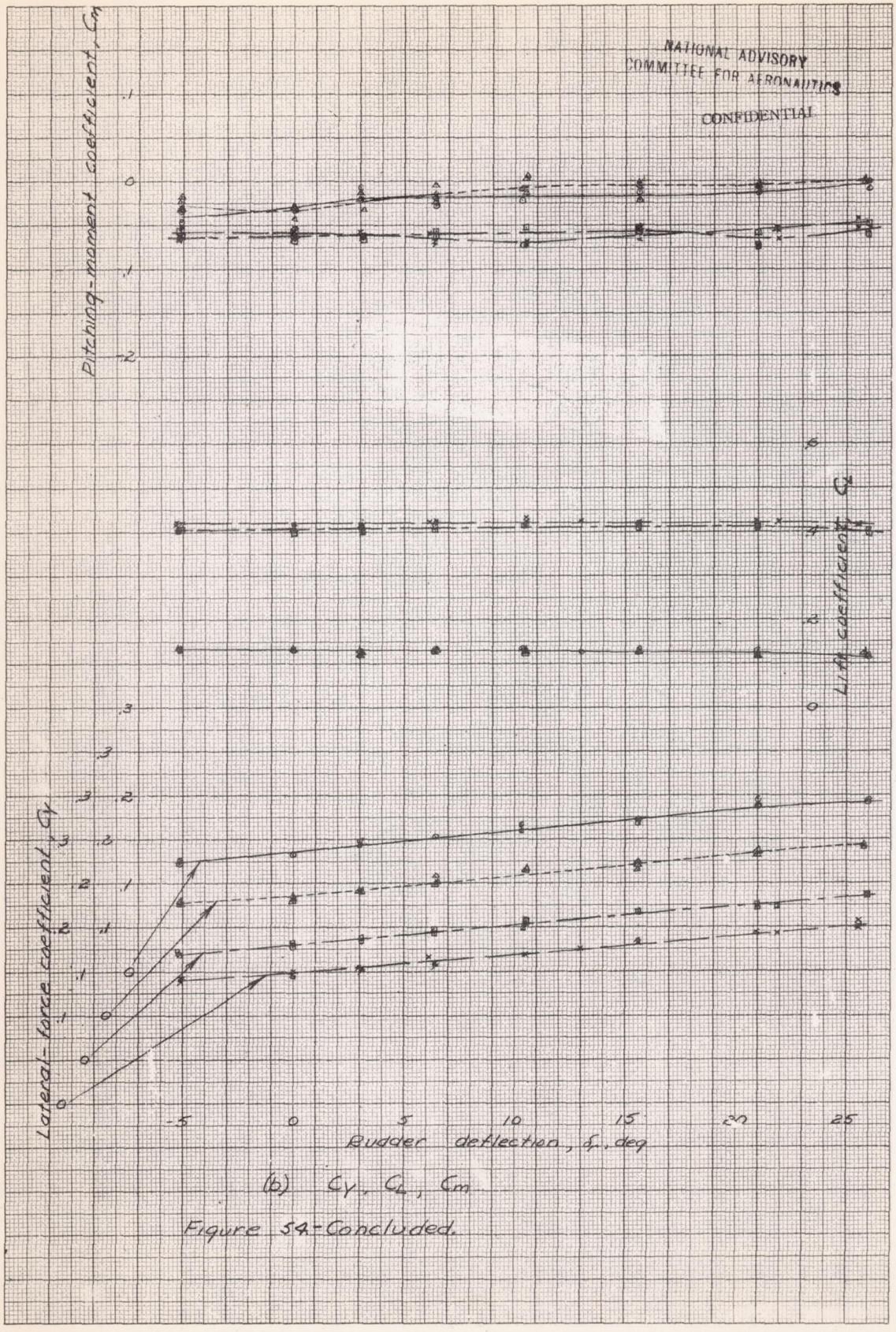

(b) C_y, C_L, C_m

Figure 54.- Concluded.

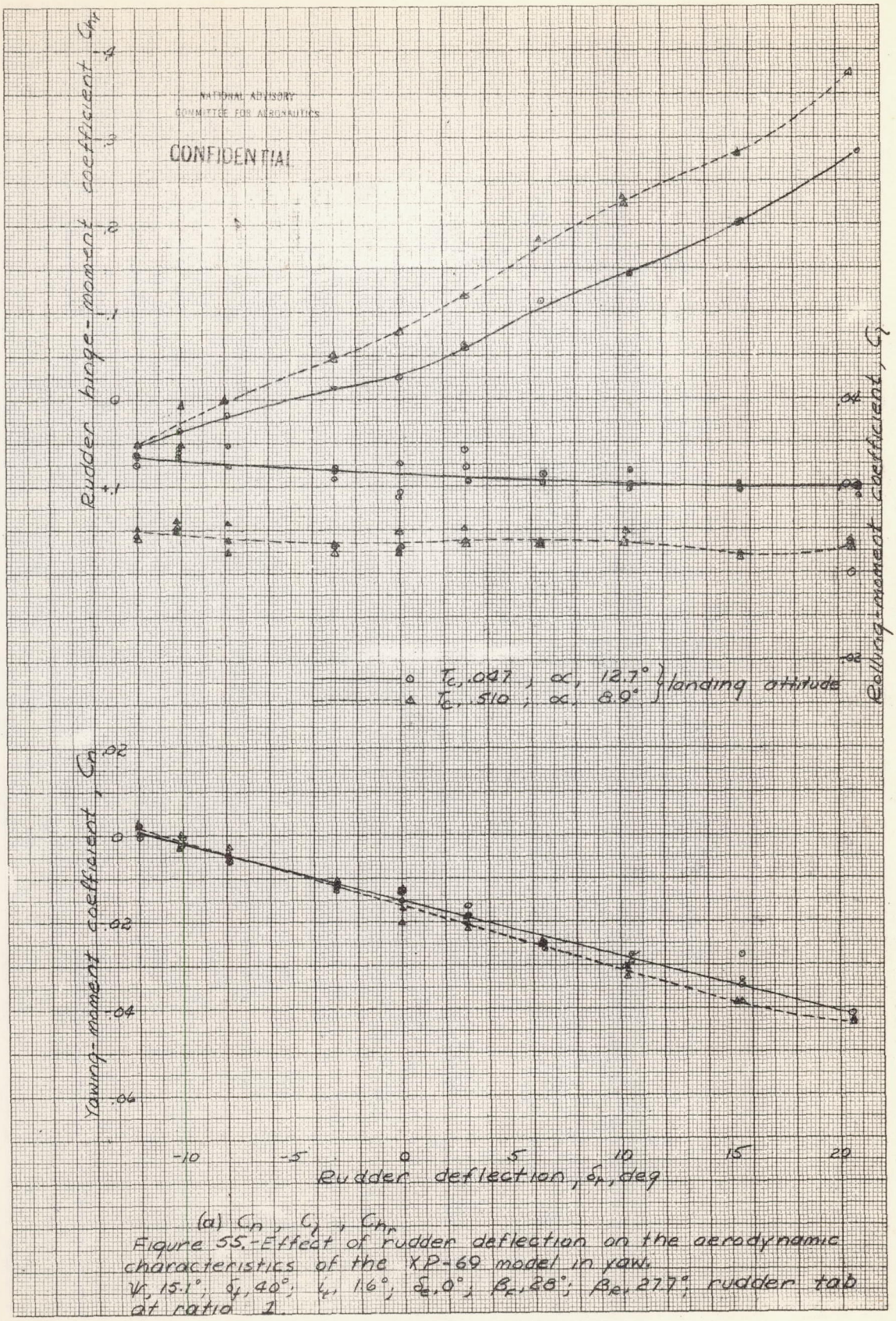

(a) C_n, C_l, C_{h_r}

Figure 55.- Effect of rudder deflection on the aerodynamic characteristics of the XP-69 model in yaw. ψ, 15.1°; δ_f, 40°; i_t, 1.6°; ξ, 0°; β_c, 28°; β_e, 27.7°; rudder tab at ratio 1.

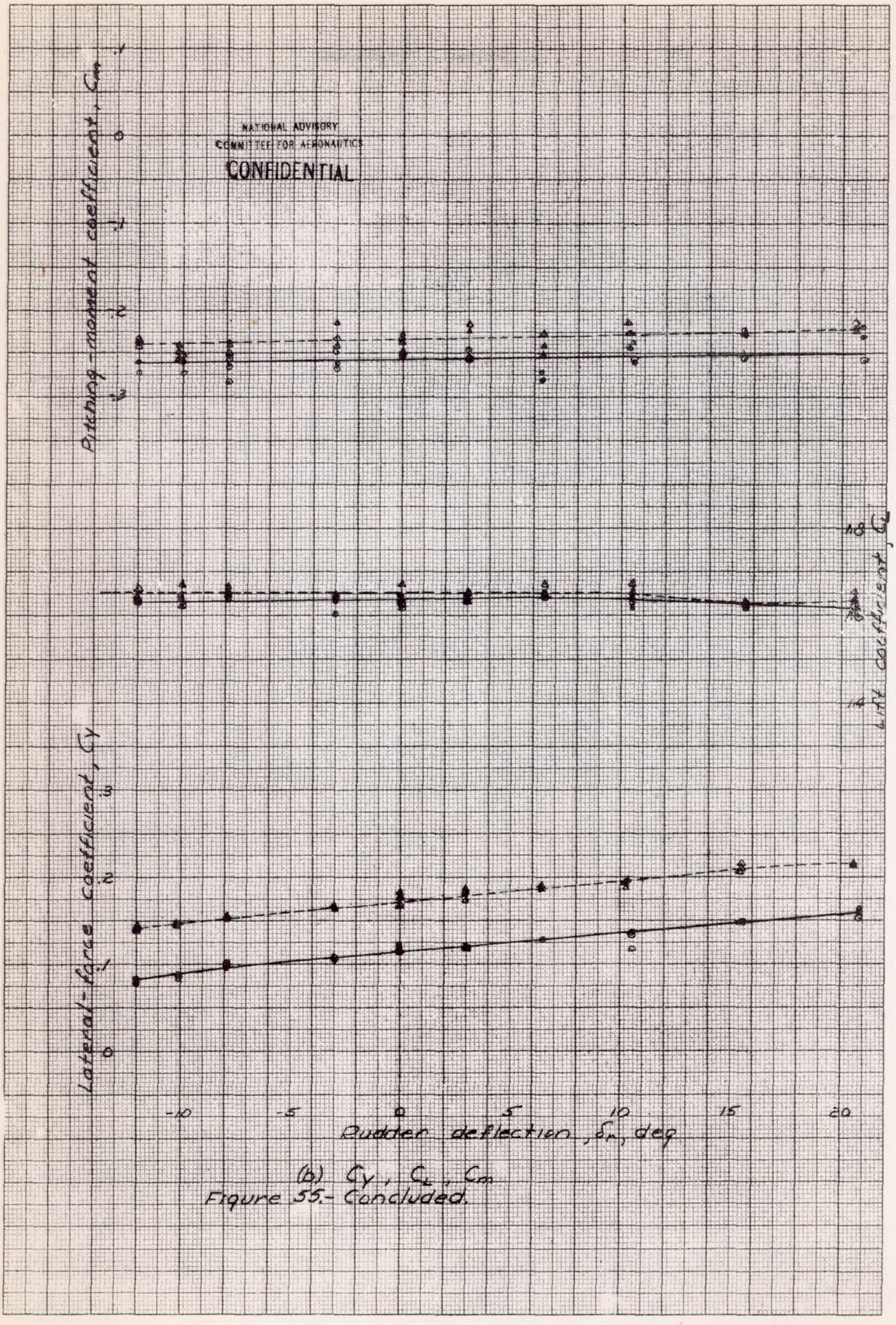

(b) C_Y, C_l, C_m

Figure 55.- Concluded.

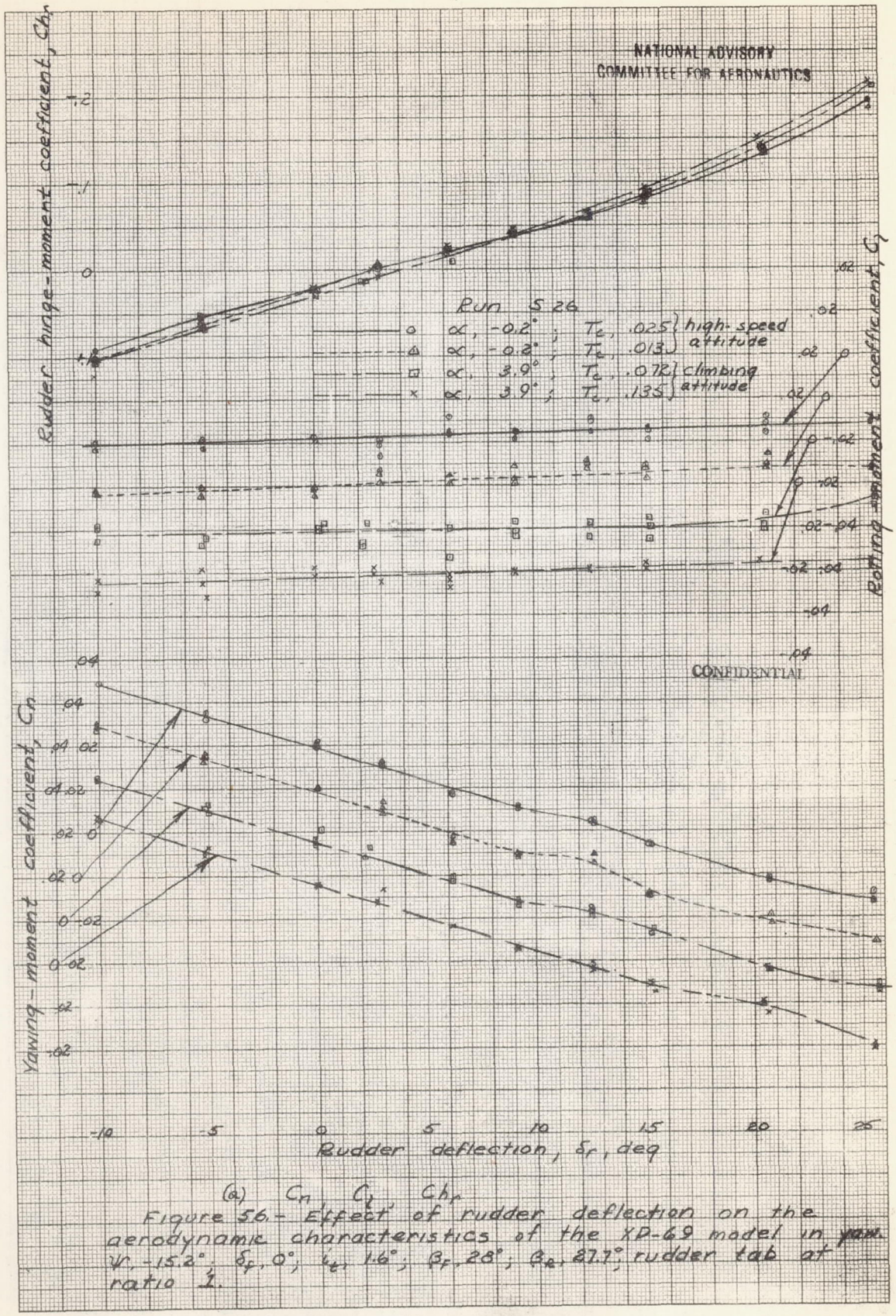

(a) C_n C_l C_{h_r}

Figure 56.- Effect of rudder deflection on the aerodynamic characteristics of the XP-69 model in yaw. Ψ, -15.2°; δ_f, 0°; i_t, 1.6°; β_f, 28°; β_e, 27.7°; rudder tab at ratio 1.

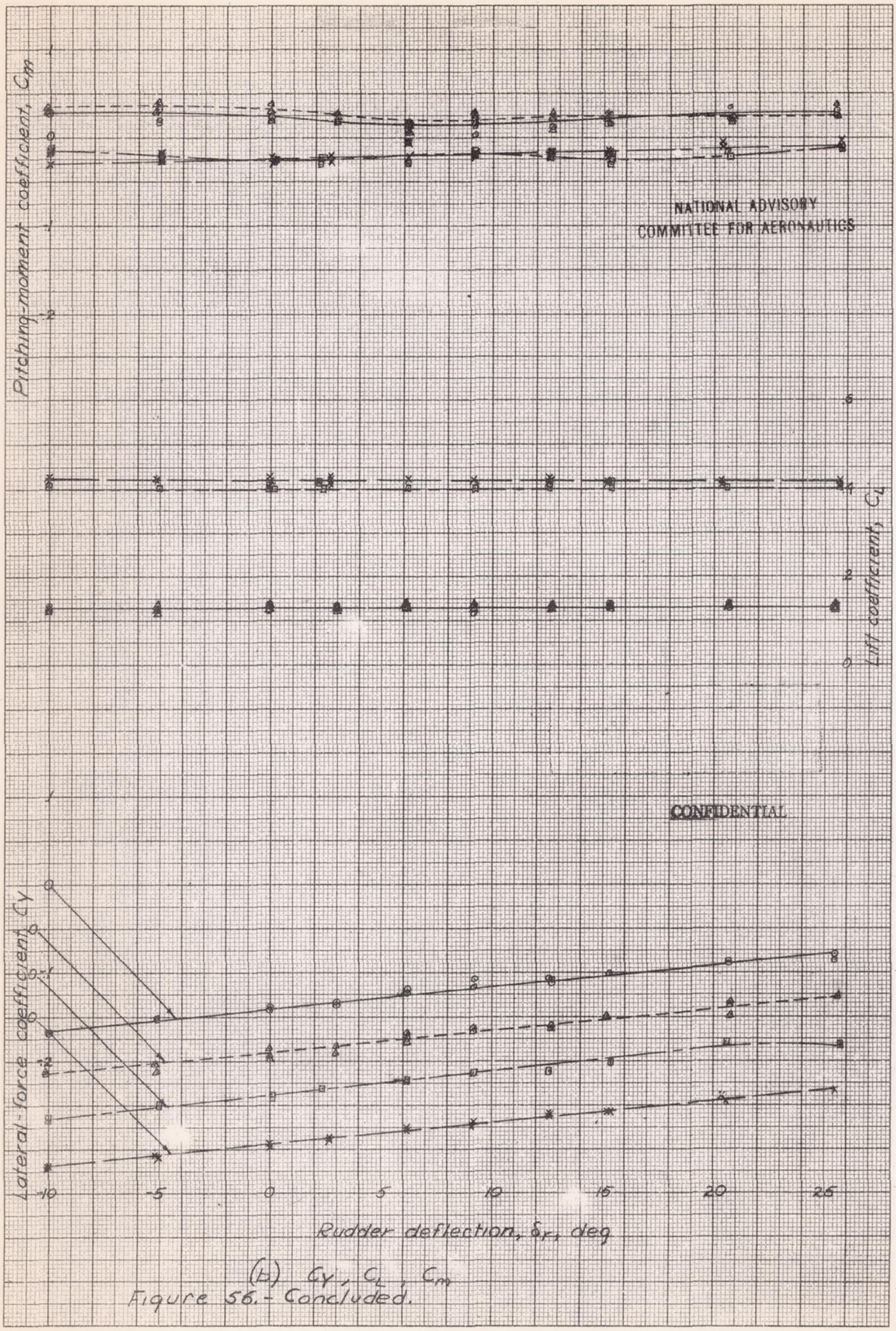

(b) C_Y, C_L, C_m

Figure 56.- Concluded.

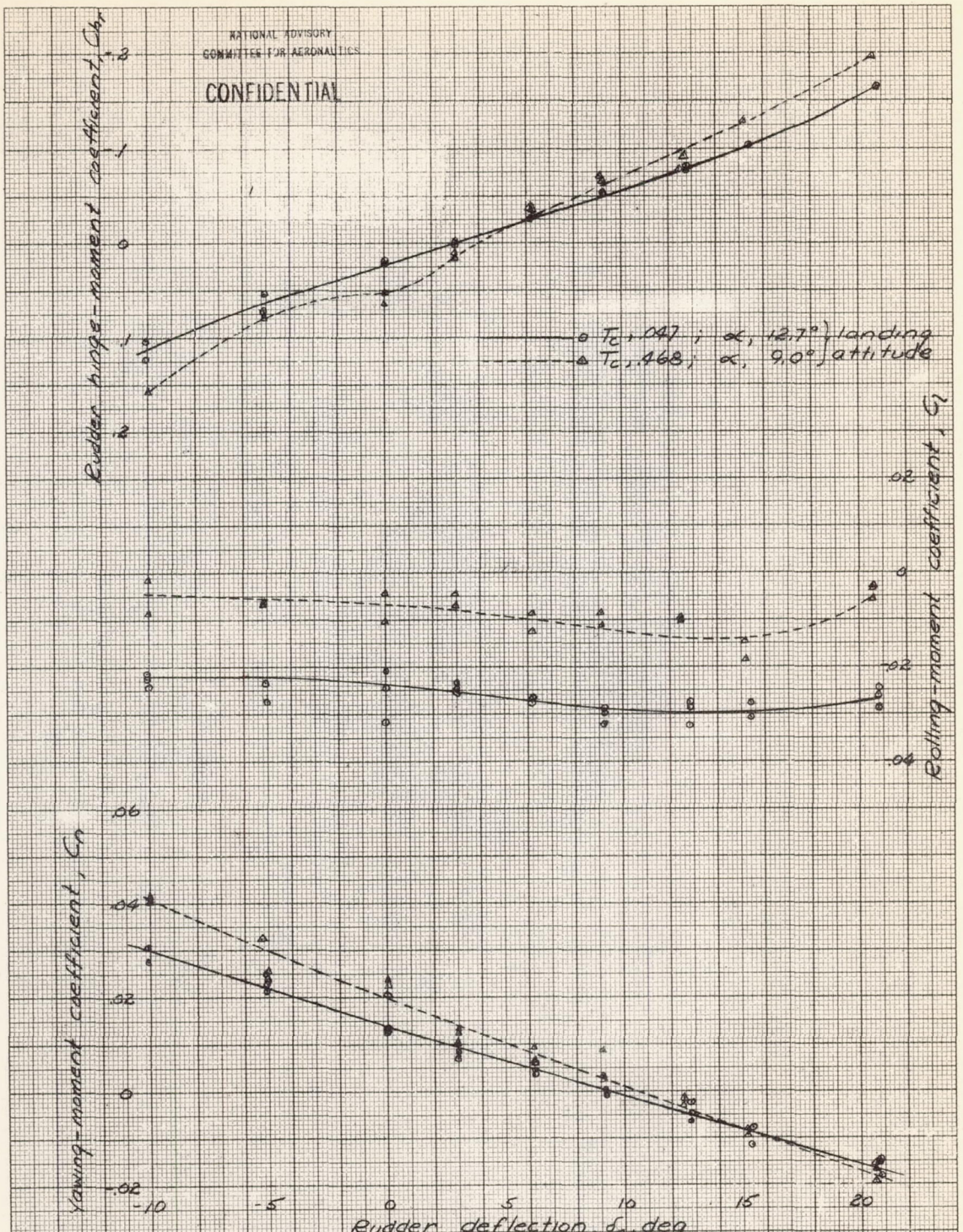

(a) C_n, C_l, C_{h_r}

Figure 51.- Effect of rudder deflection on the aerodynamic characteristics of the XP-69 model in yaw. ψ, -15.2°; δ_f, 40°; i_t, 1.6°; δ_e, 0°; β_r, .28°; β_e, 27.7°; rudder tab at ratio 1.

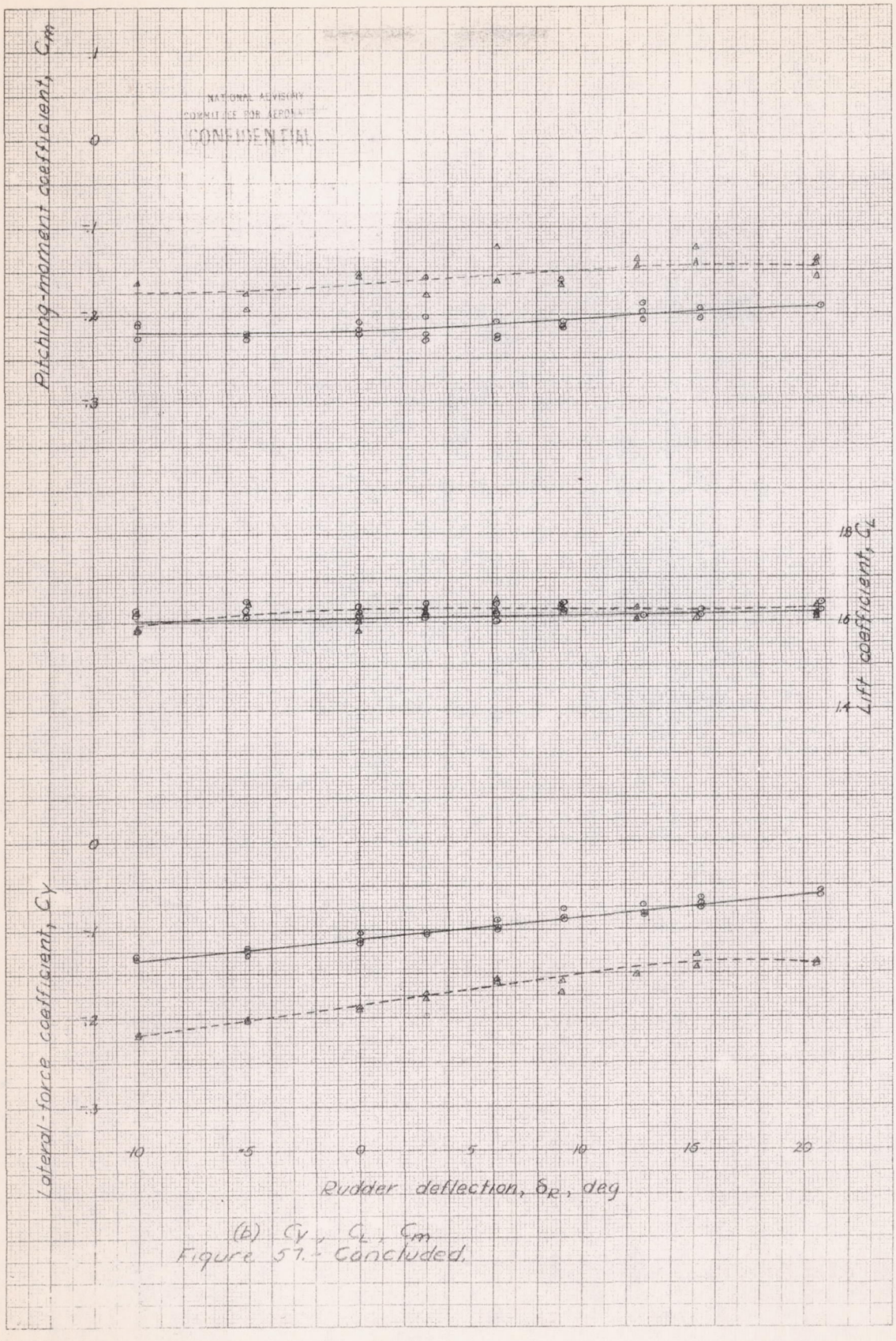

(b) C_Y, C_L, C_m

Figure 57.- Concluded.

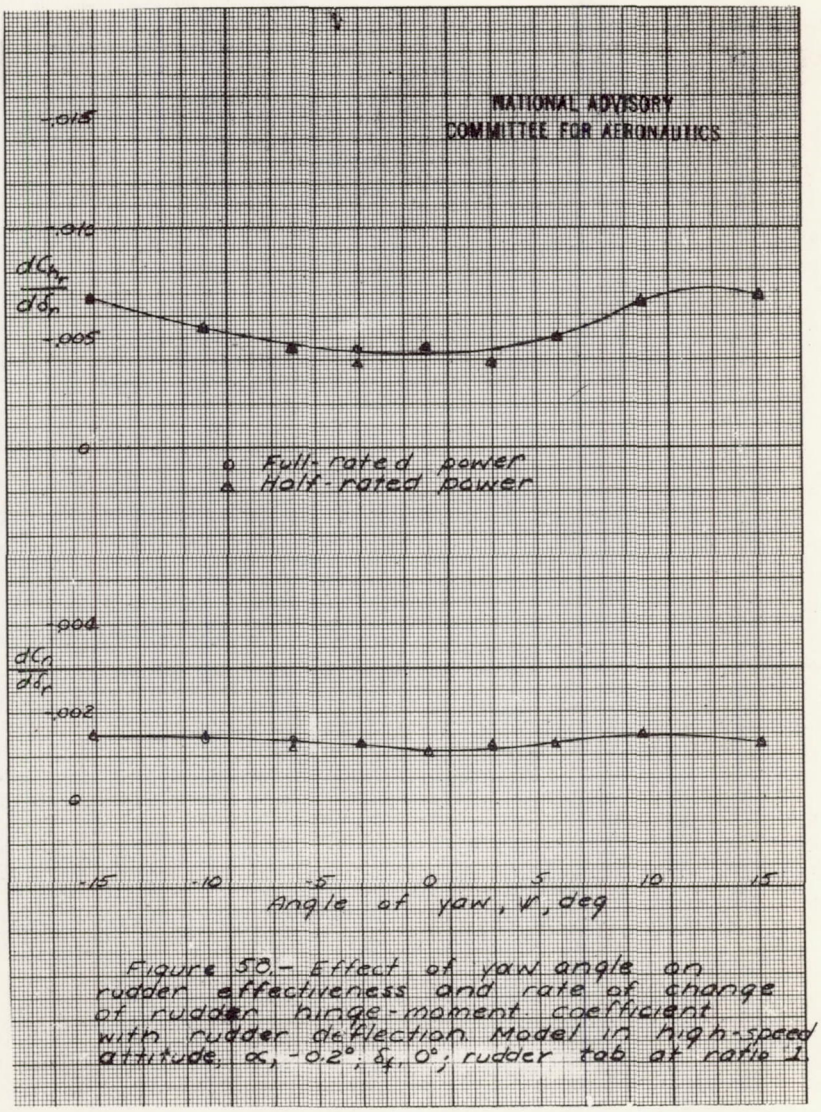

Figure 58.- Effect of yaw angle on rudder effectiveness and rate of change of rudder hinge-moment coefficient with rudder deflection. Model in high-speed attitude, α, -0.2°; δ_t, 0°; rudder tab at ratio 1.

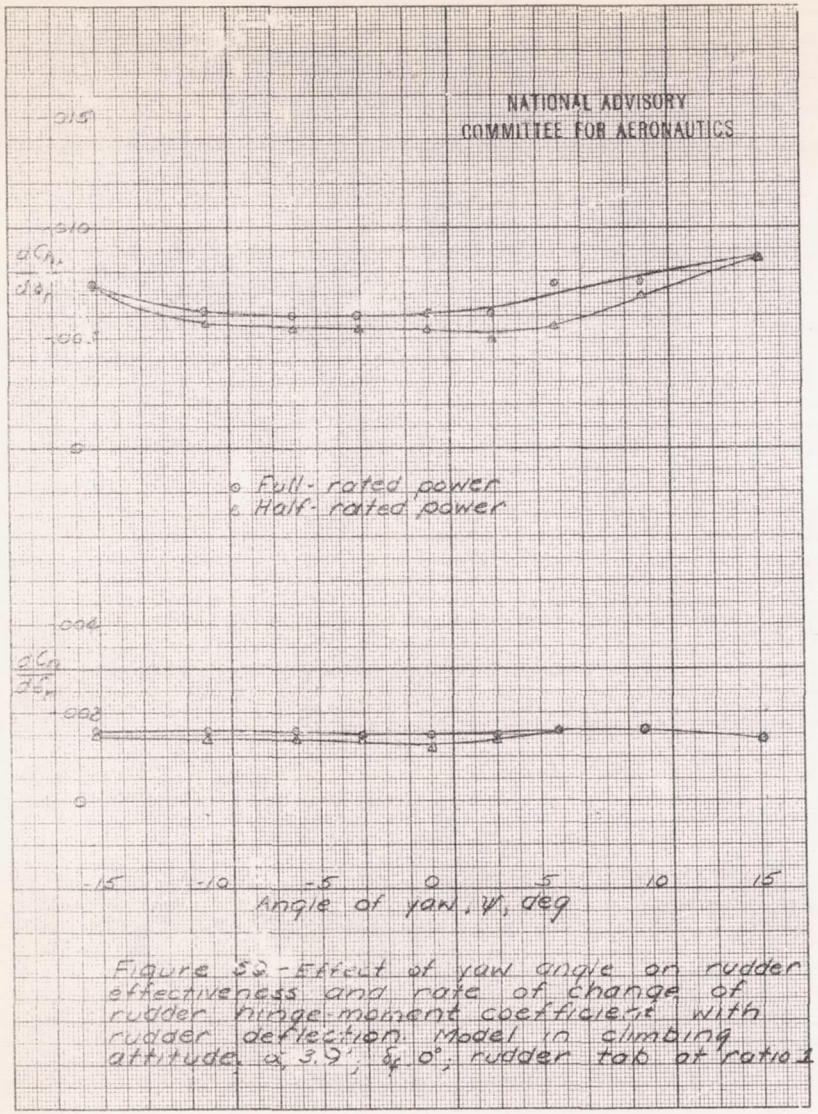

Figure 59.- Effect of yaw angle on rudder effectiveness and rate of change of rudder hinge-moment coefficient with rudder deflection. Model in climbing attitude, α, 3.9°; δ_t, 0°; rudder tab at ratio 1.

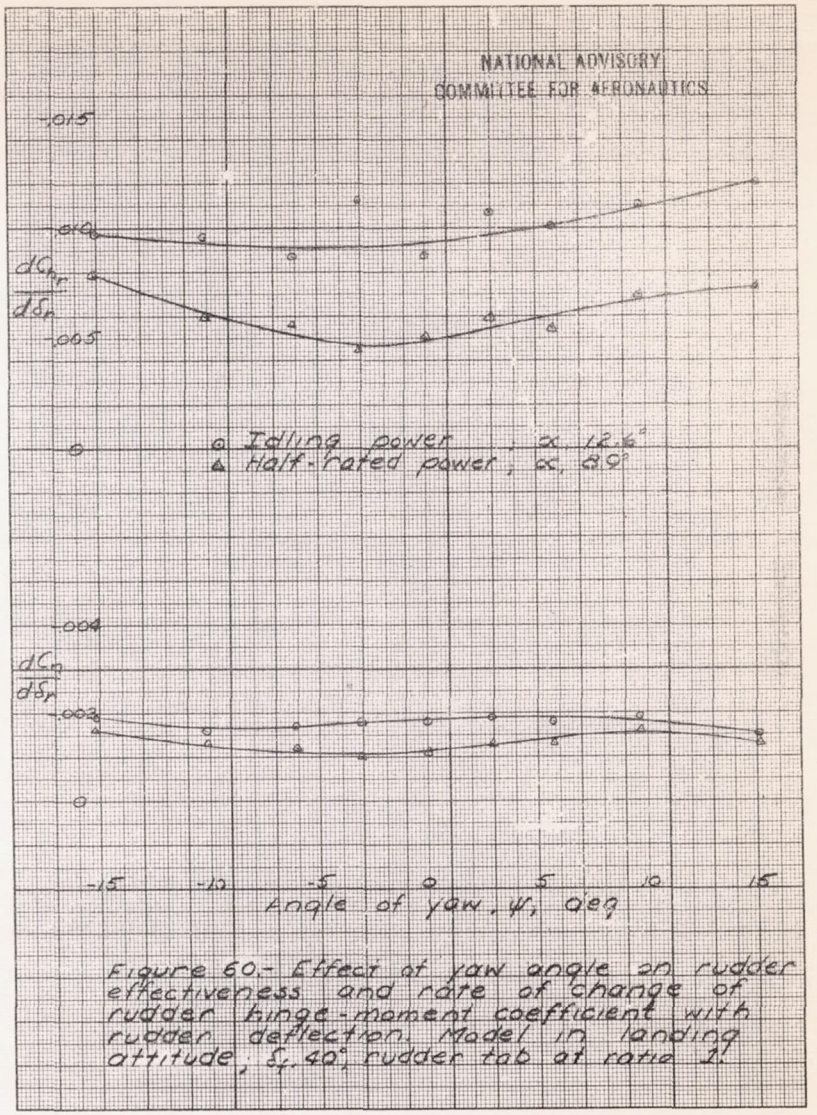

Figure 60.- Effect of yaw angle on rudder effectiveness and rate of change of rudder hinge-moment coefficient with rudder deflection. Model in landing attitude, δ_t, 40°; rudder tab at ratio 1.

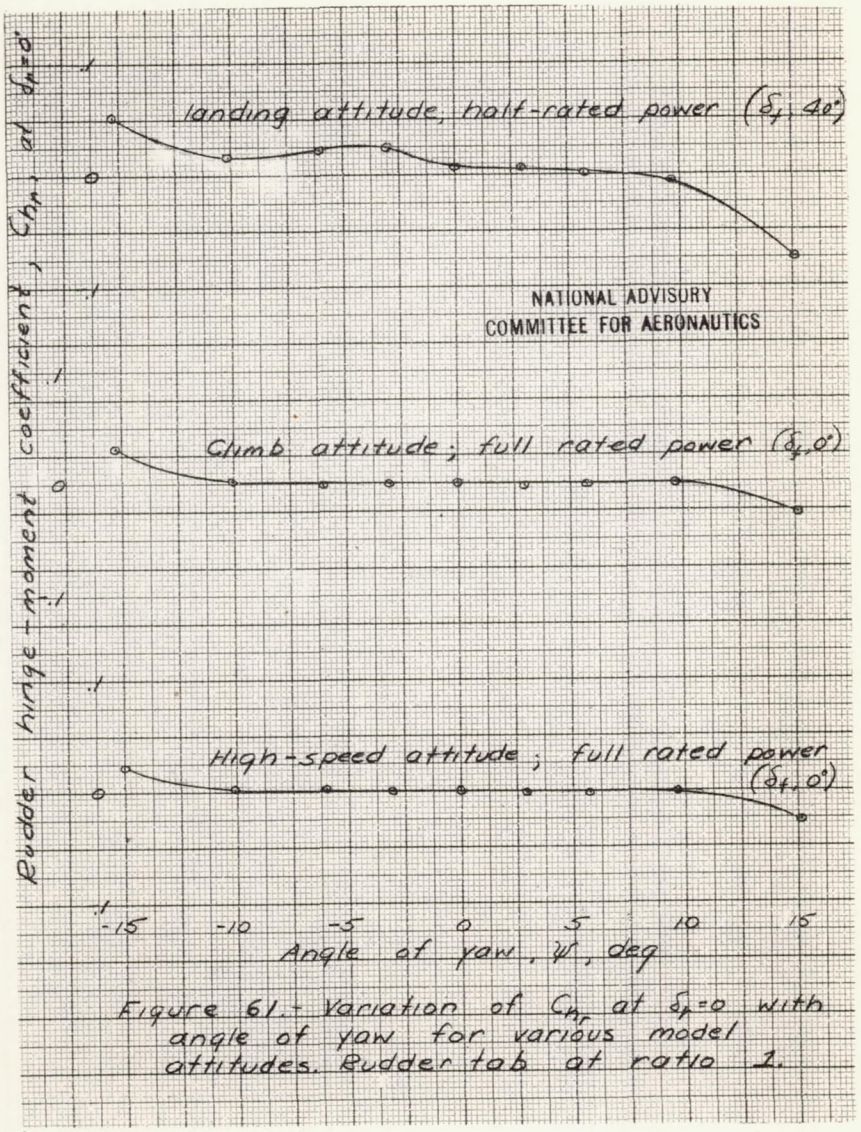

Figure 61.- Variation of C_{h_r} at $\delta_r = 0$ with angle of yaw for various model attitudes. Rudder tab at ratio 1.

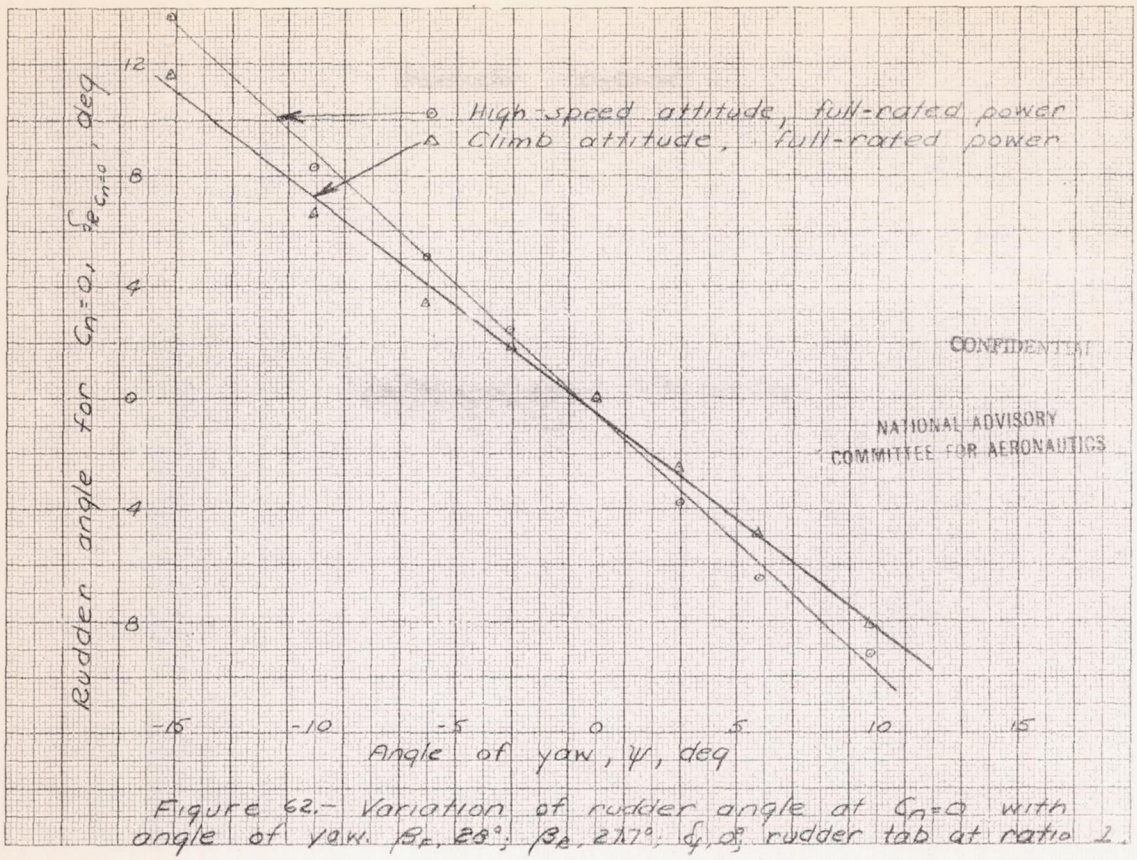

Figure 62.- Variation of rudder angle at $C_n=0$ with angle of yaw. β_r, 28°; β_e, 27.1°; δ_t, 0°; rudder tab at ratio 2.

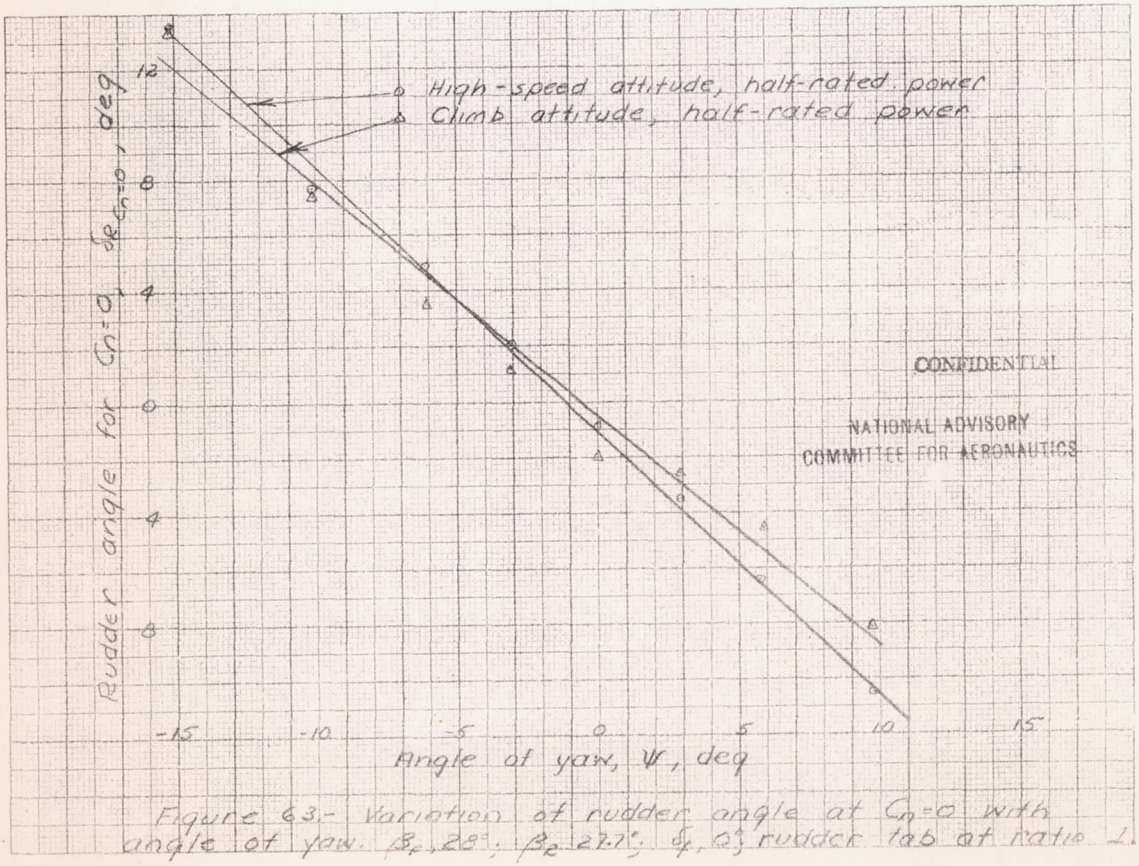

Figure 63.- Variation of rudder angle at $C_n=0$ with angle of yaw. β_r, 28°; β_e 27.1°; δ_t, 0°; rudder tab at ratio 2.

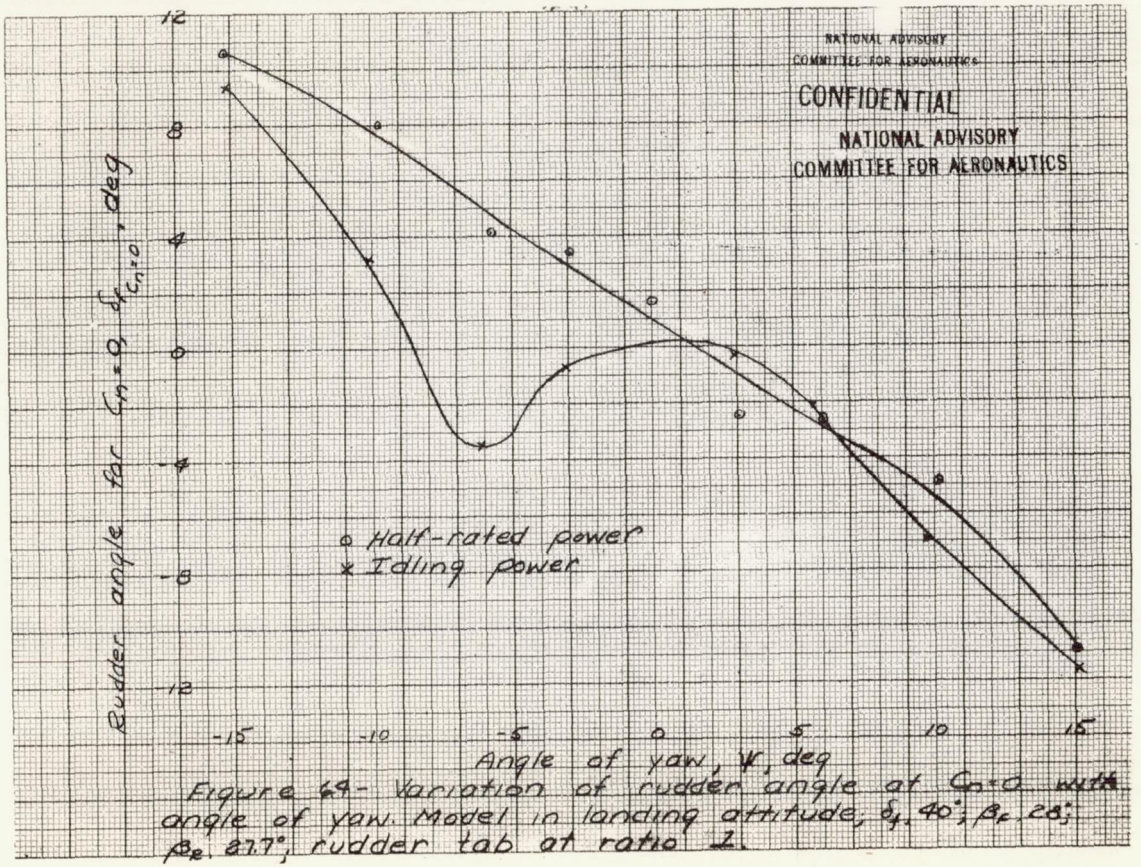

Figure 69- Variation of rudder angle at $C_n = 0$ with angle of yaw. Model in landing attitude, δ_f, 40°; β_f, 28°; β_e, 27.7°; rudder tab at ratio 1.

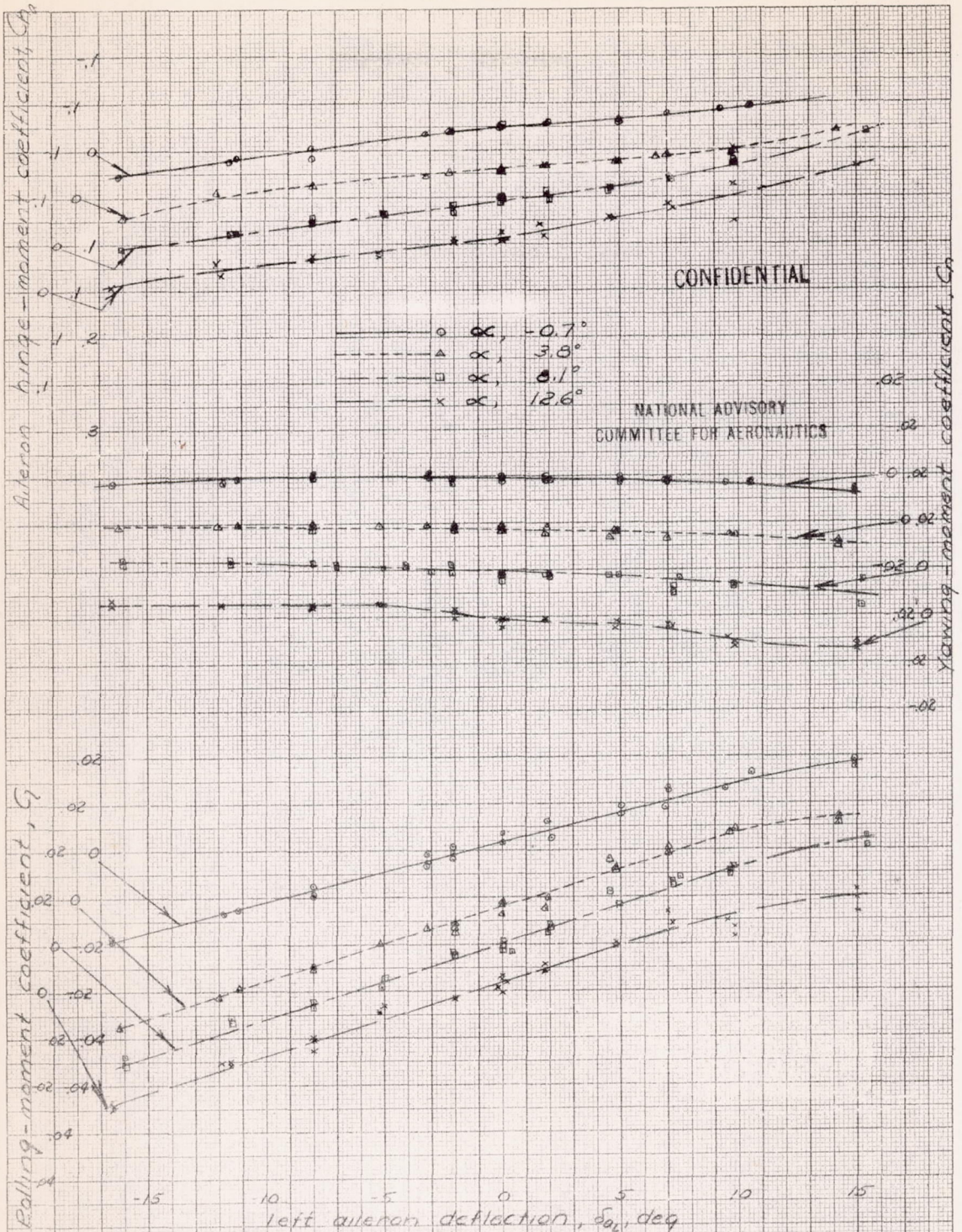

Figure 65.- Effect of aileron deflection on the aerodynamic characteristics of the XP-69 model. Propellers removed, right aileron locked, left aileron tab locked; ψ, 0°; δ_f, 0°; i_t, 1.6°

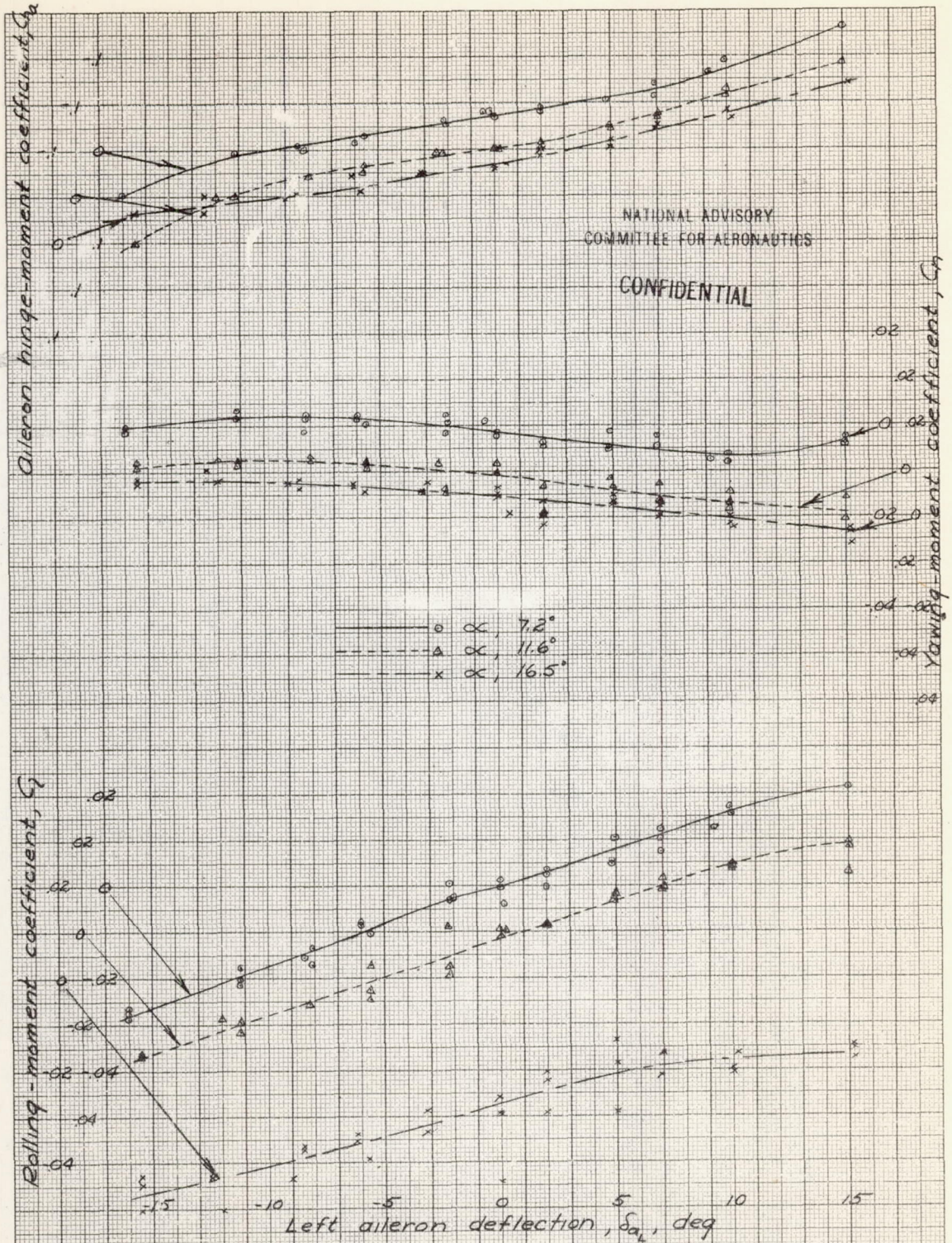

Figure 66.- Effect of aileron deflection on the aileron deflection on the aerodynamic characteristics of the XP-69 model. Propellers removed; right aileron locked, left aileron tab locked; ψ, 0°; δ_f, 40°; i_t, 1.6°

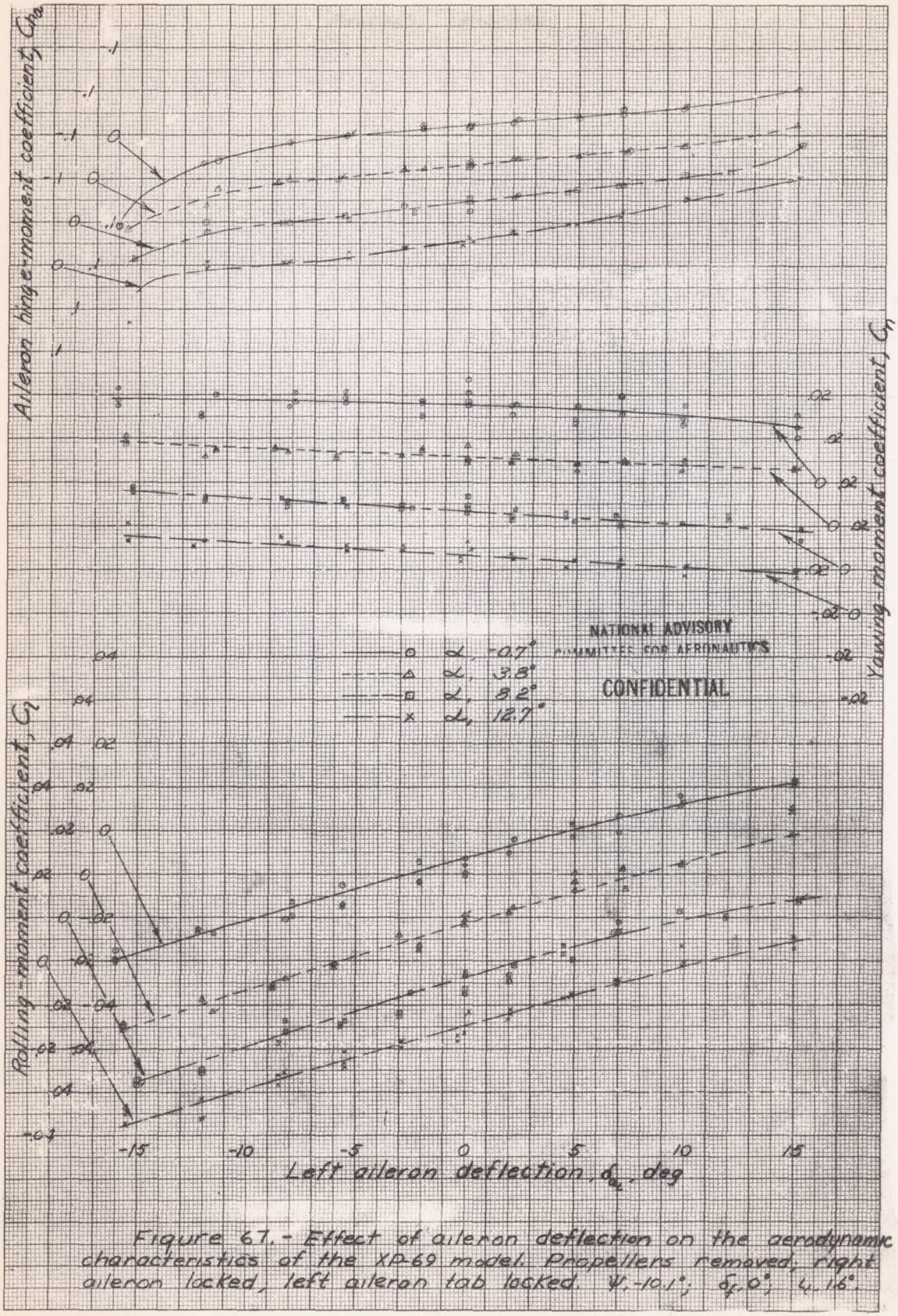

Figure 67.- Effect of aileron deflection on the aerodynamic characteristics of the XP-69 model. Propellers removed, right aileron locked, left aileron tab locked. ψ, -10.1°; δ_f, 0°; i_t, 1.6°.

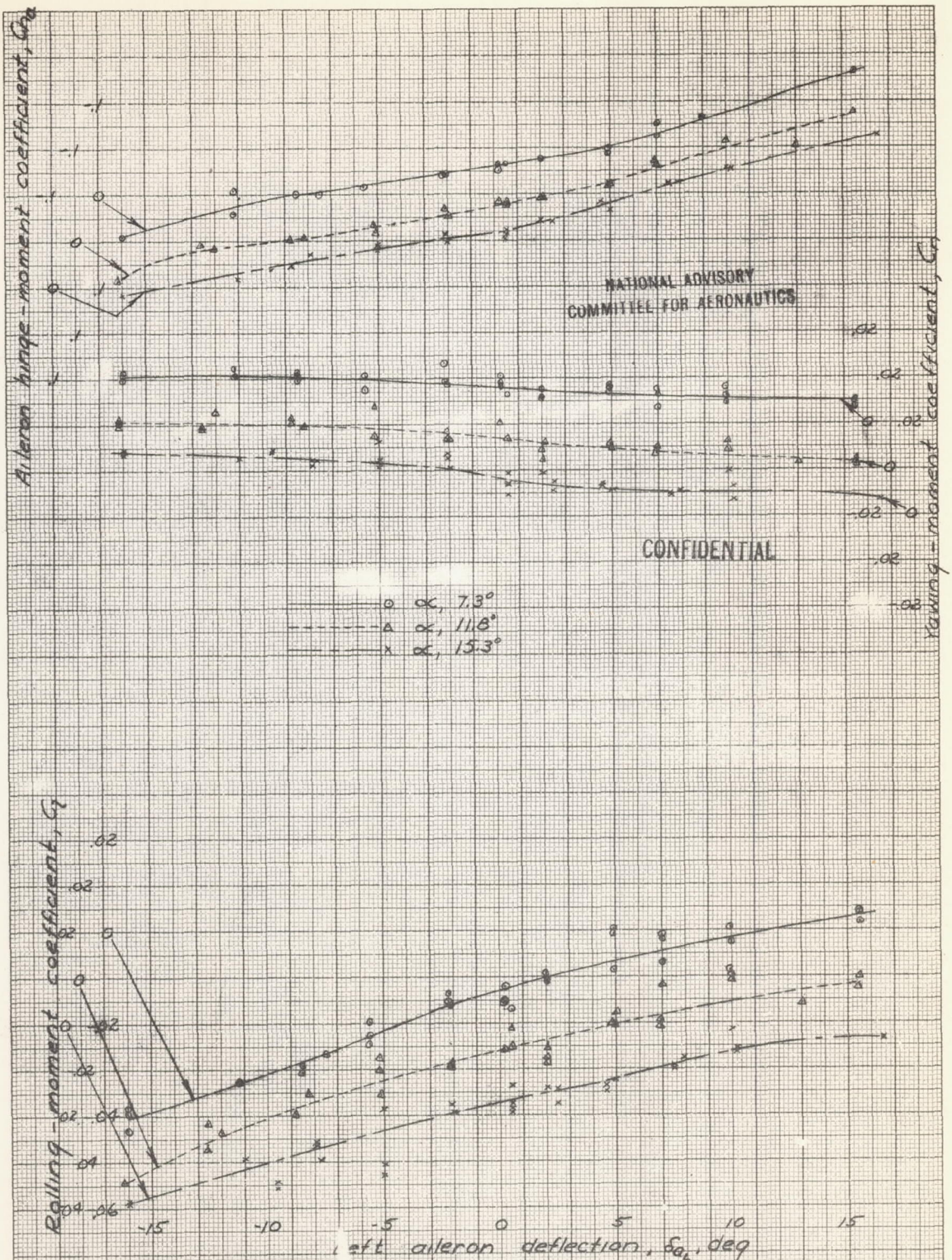

Figure 68.- Effect of aileron deflection on the aerodynamic characteristics of the XP-69 model. Propellers removed; right aileron locked; left aileron tab locked. ψ, -10.1°; δ_f, 40°; i_t, 1.6°.

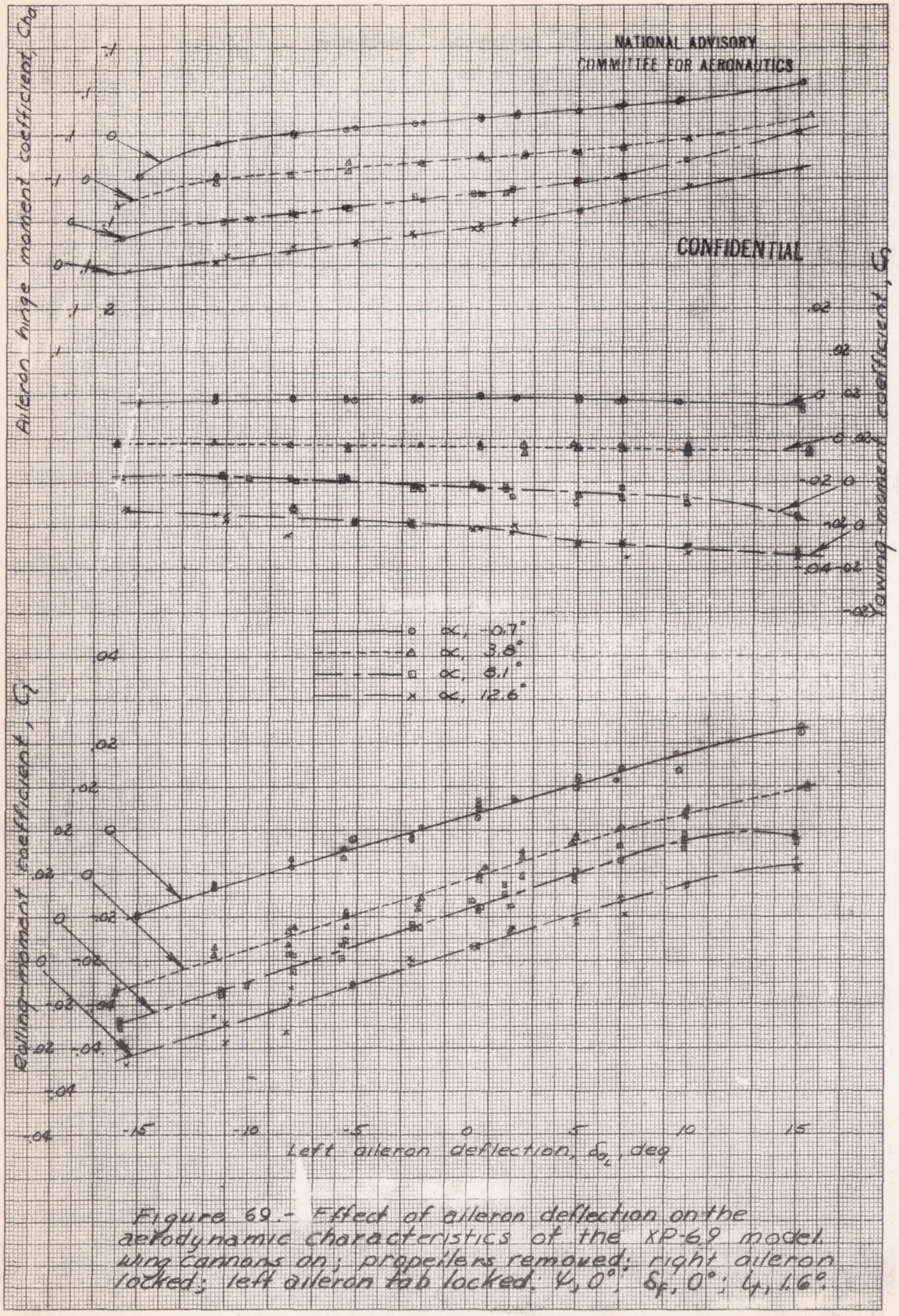

Figure 69.- Effect of aileron deflection on the aerodynamic characteristics of the XP-69 model. Wing cannons on; propellers removed; right aileron locked; left aileron tab locked. i_t, 0°; δ_f, 0°; i_t, 1.6°.

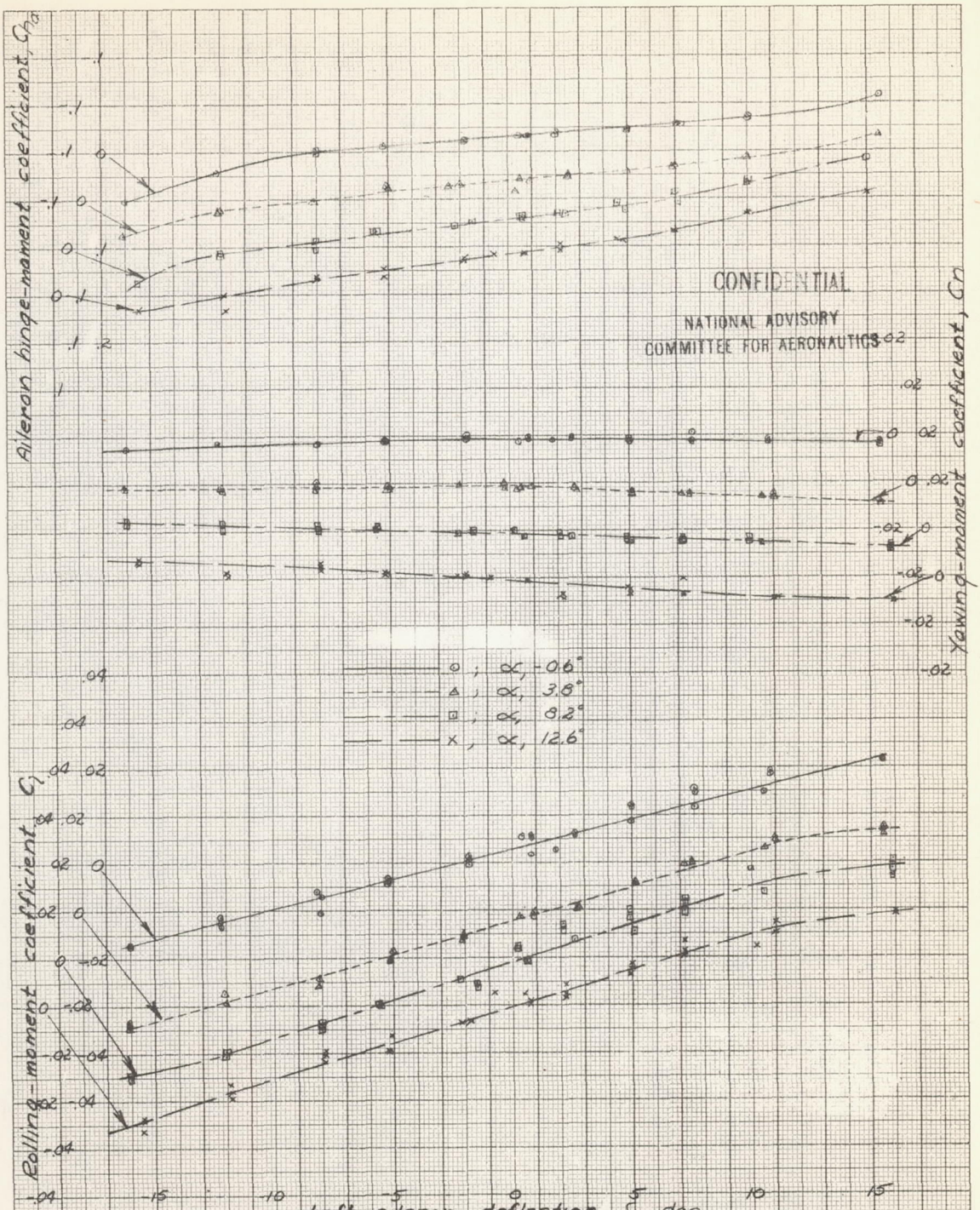

Figure 70.- Effect of aileron deflection on the aerodynamic characteristics of the XP-69 model. Propellers removed, wing tanks on, right aileron locked, left aileron tab locked. ψ, 0°; δ_f, 0°; i_t, 1.6°.

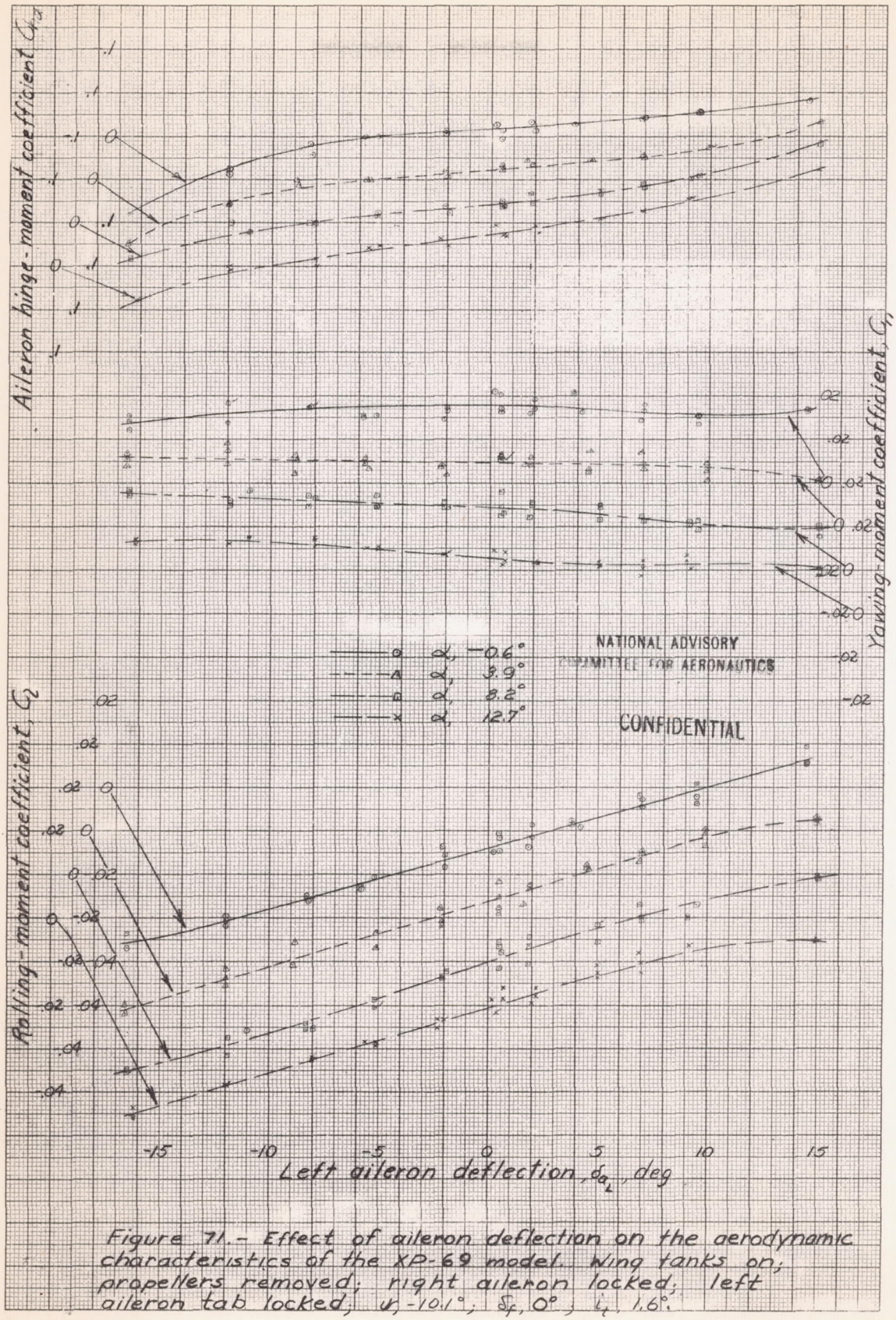

Figure 71.- Effect of aileron deflection on the aerodynamic characteristics of the XP-69 model. Wing tanks on; propellers removed; right aileron locked; left aileron tab locked; i_t, -10.1°; δ_f, 0°; i_t, 1.6°.

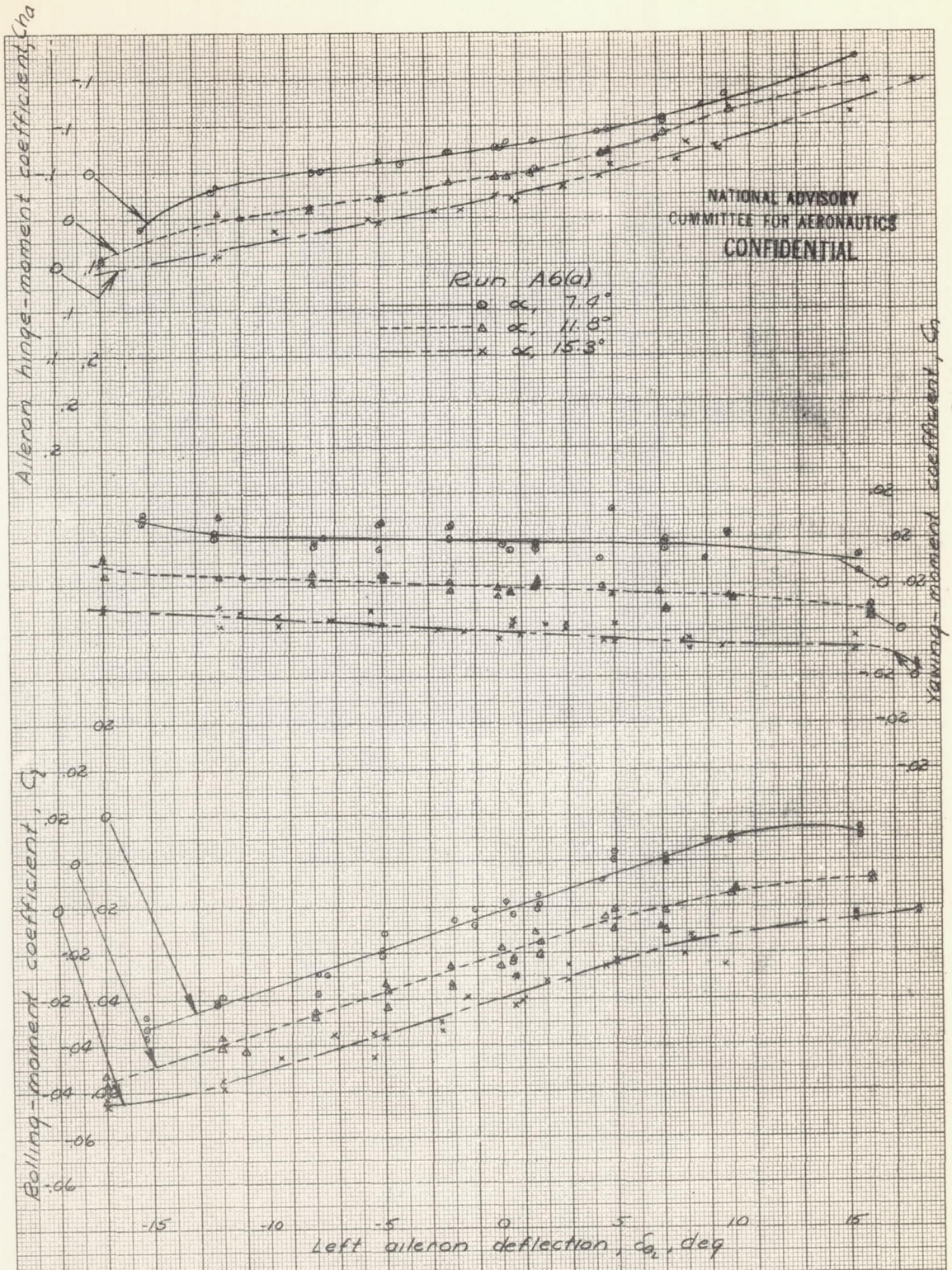

Figure 72.- Effect of aileron deflection on the aerodynamic characteristics of the XP-69 model. Propellers removed; wing tanks on; right aileron locked; left aileron tab locked. ψ_c, +10.1°; δ_e, 4.0°; i_t, 1.6°.

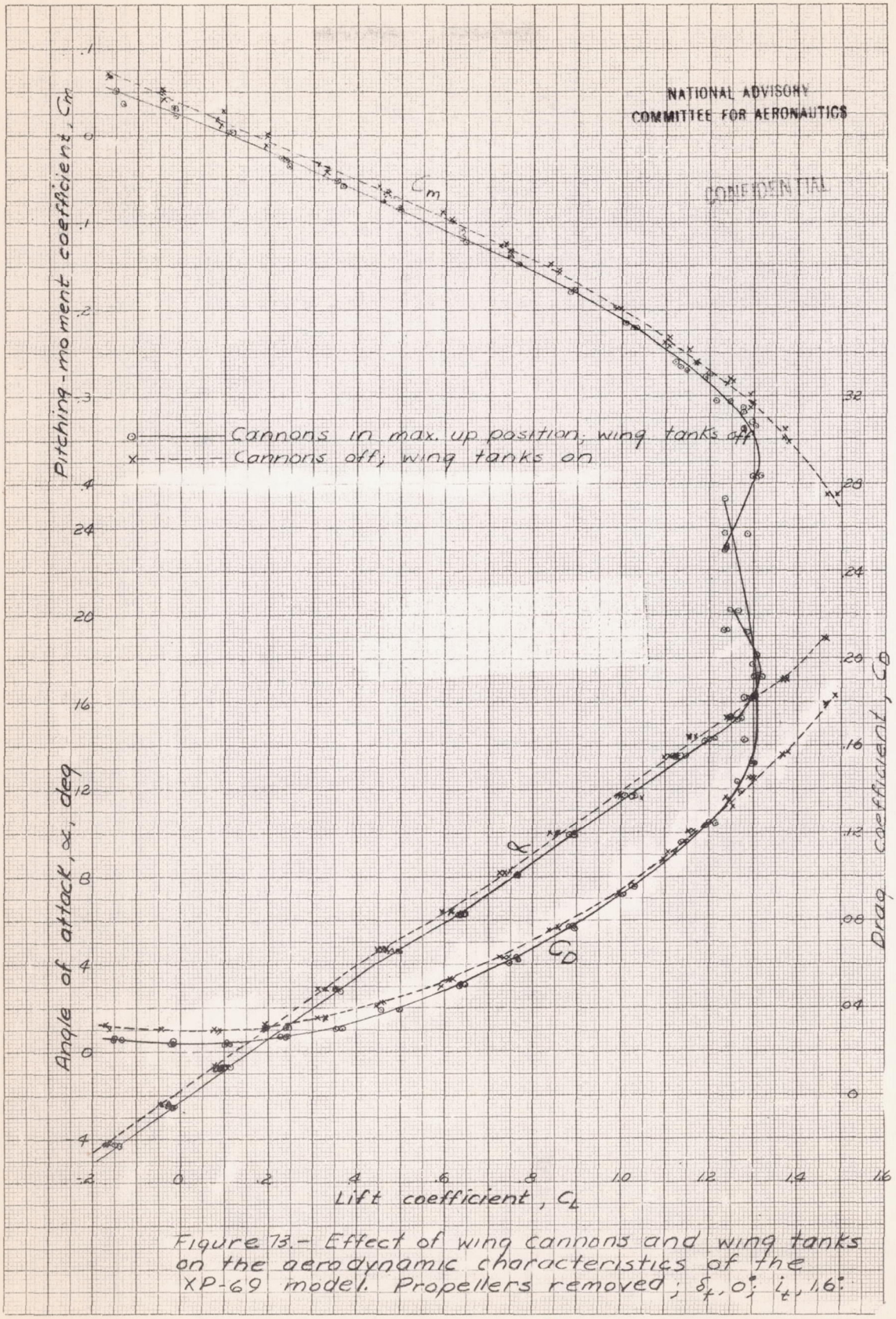

Figure 73.- Effect of wing cannons and wing tanks on the aerodynamic characteristics of the XP-69 model. Propellers removed; δ_f, 0°; i_t, 1.6°.

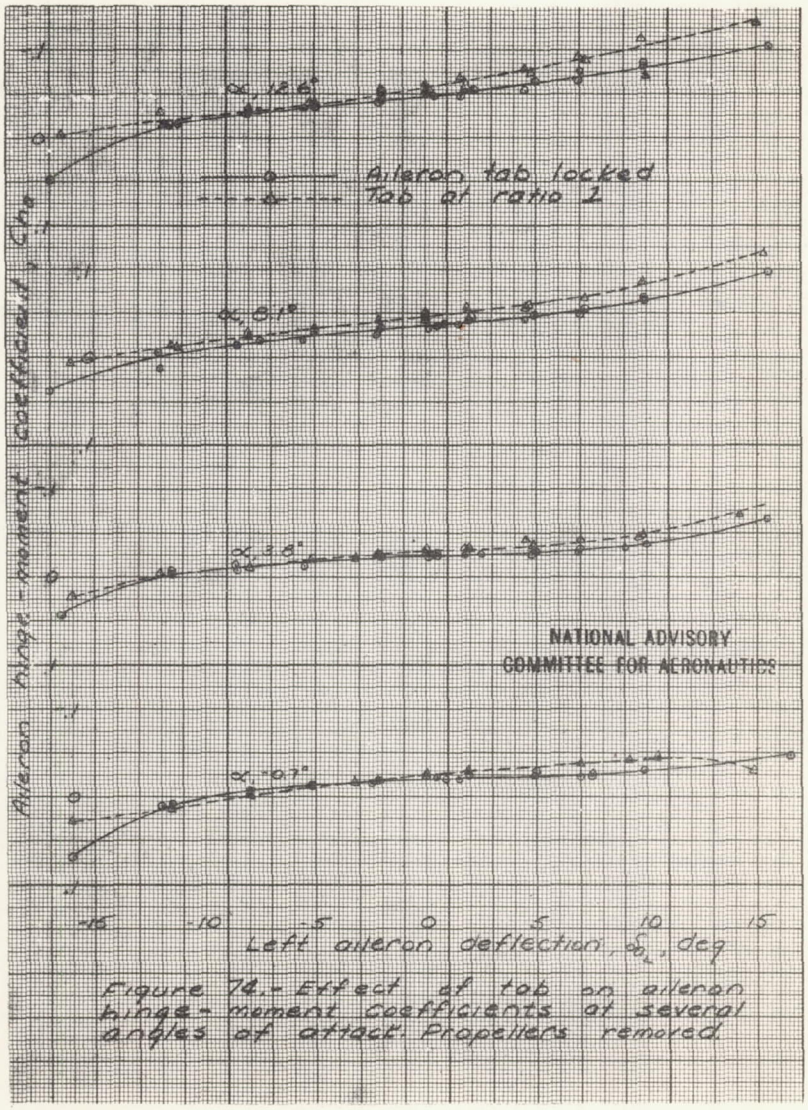

Figure 74.- Effect of tab on aileron hinge-moment coefficients at several angles of attack. Propellers removed.

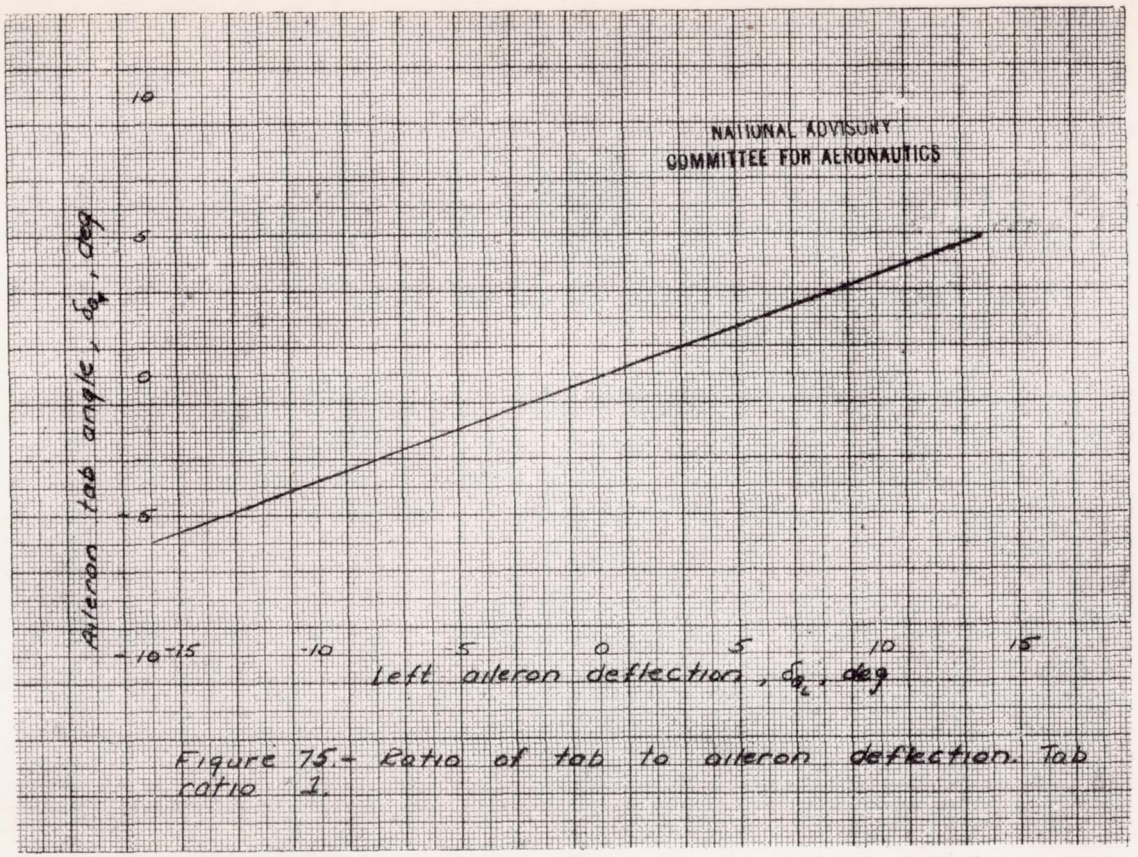

Figure 75.- Ratio of tab to aileron deflection. Tab ratio .1.

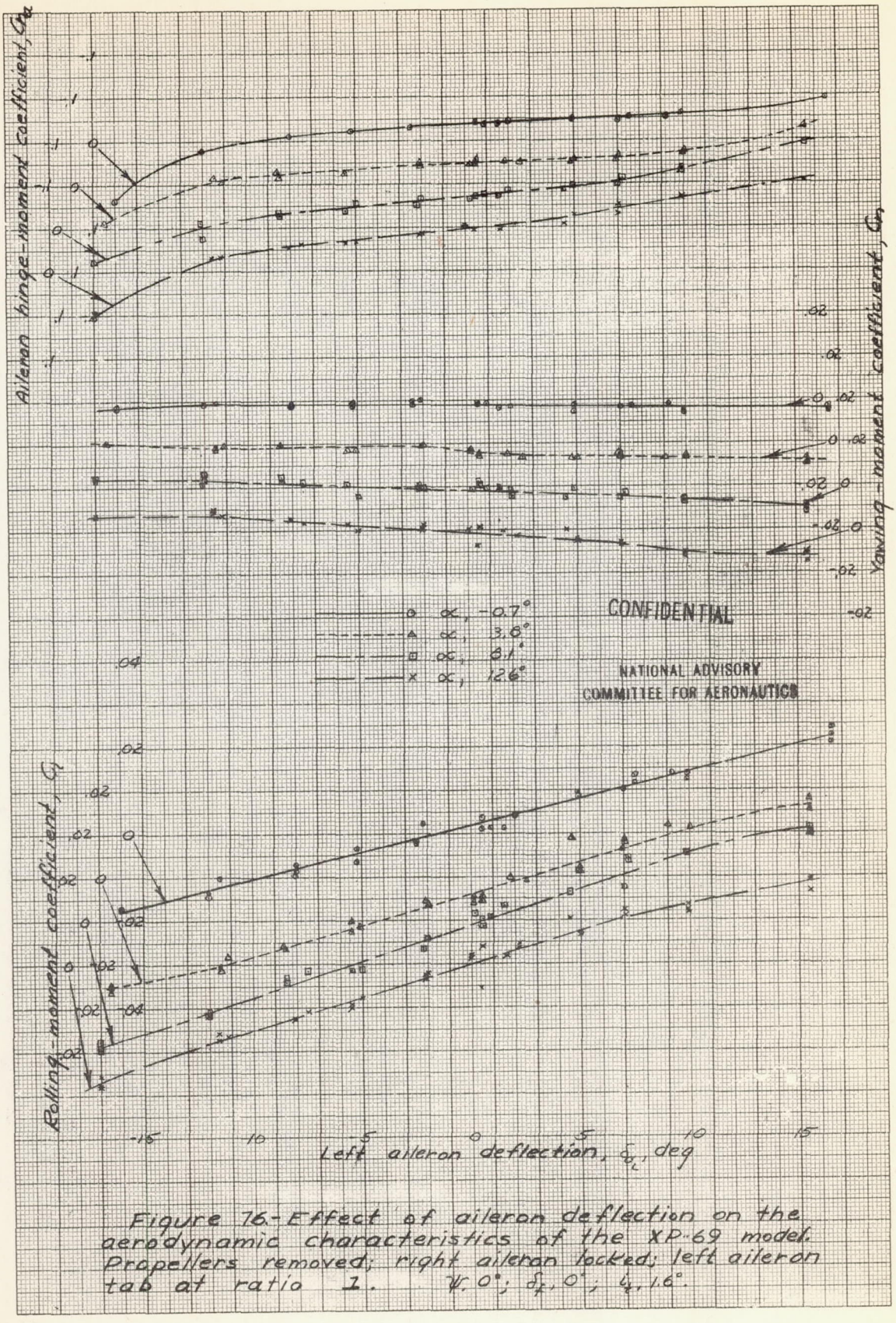

Figure 76.- Effect of aileron deflection on the aerodynamic characteristics of the XP-69 model. Propellers removed; right aileron locked; left aileron tab at ratio 1. ψ, 0°; δ_f, 0°; i_t, 1.6°.

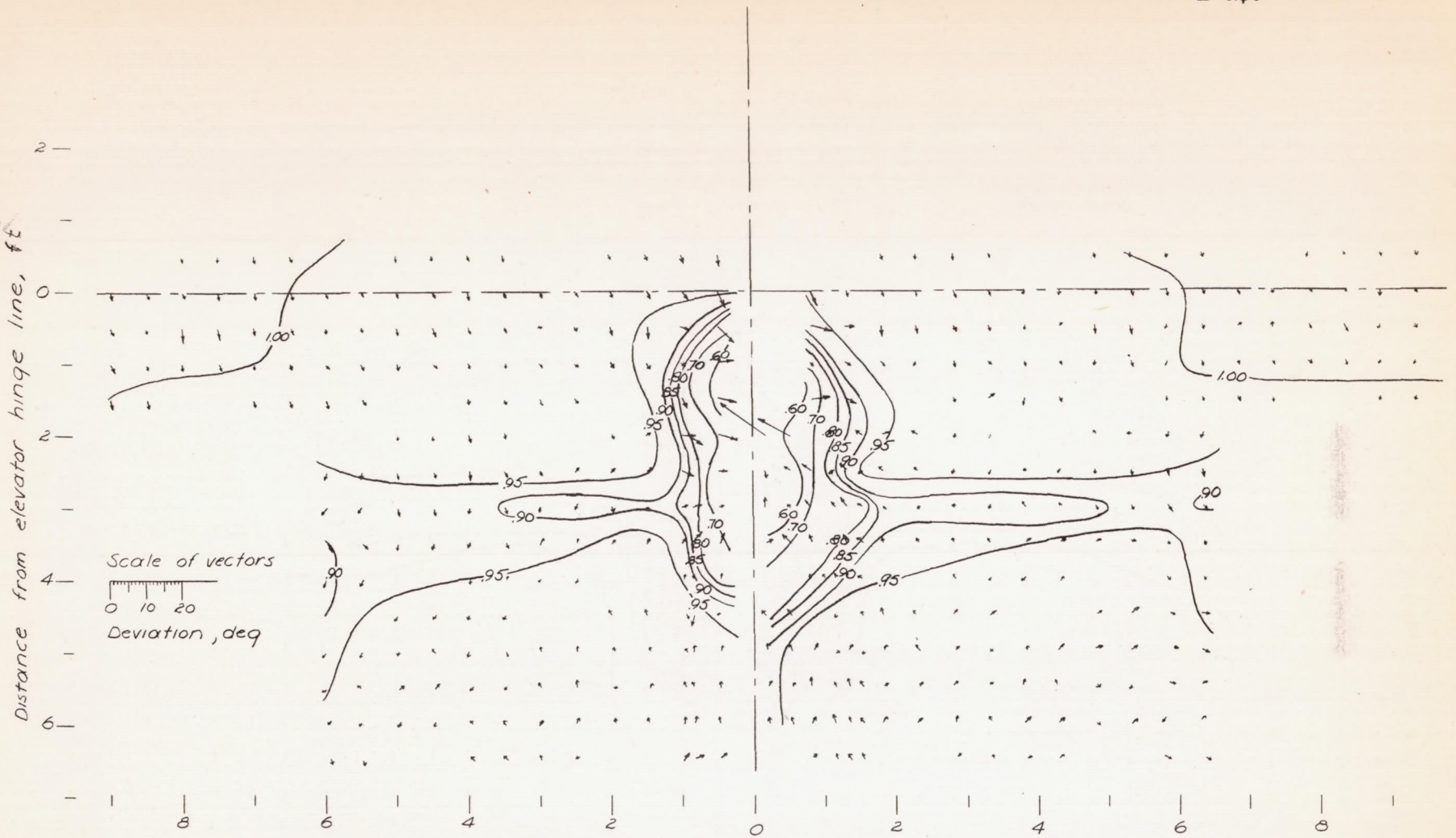

(a) $\alpha = -0.7°$

Figure 77.- Dynamic pressure (q/q₀) contours and inclination of the air stream in the plane of the elevator hinge line. Vectors show angular deviation of air flow from free-stream direction. View looking forward. Propellers removed; flaps retracted; horizontal and vertical tail surfaces removed.

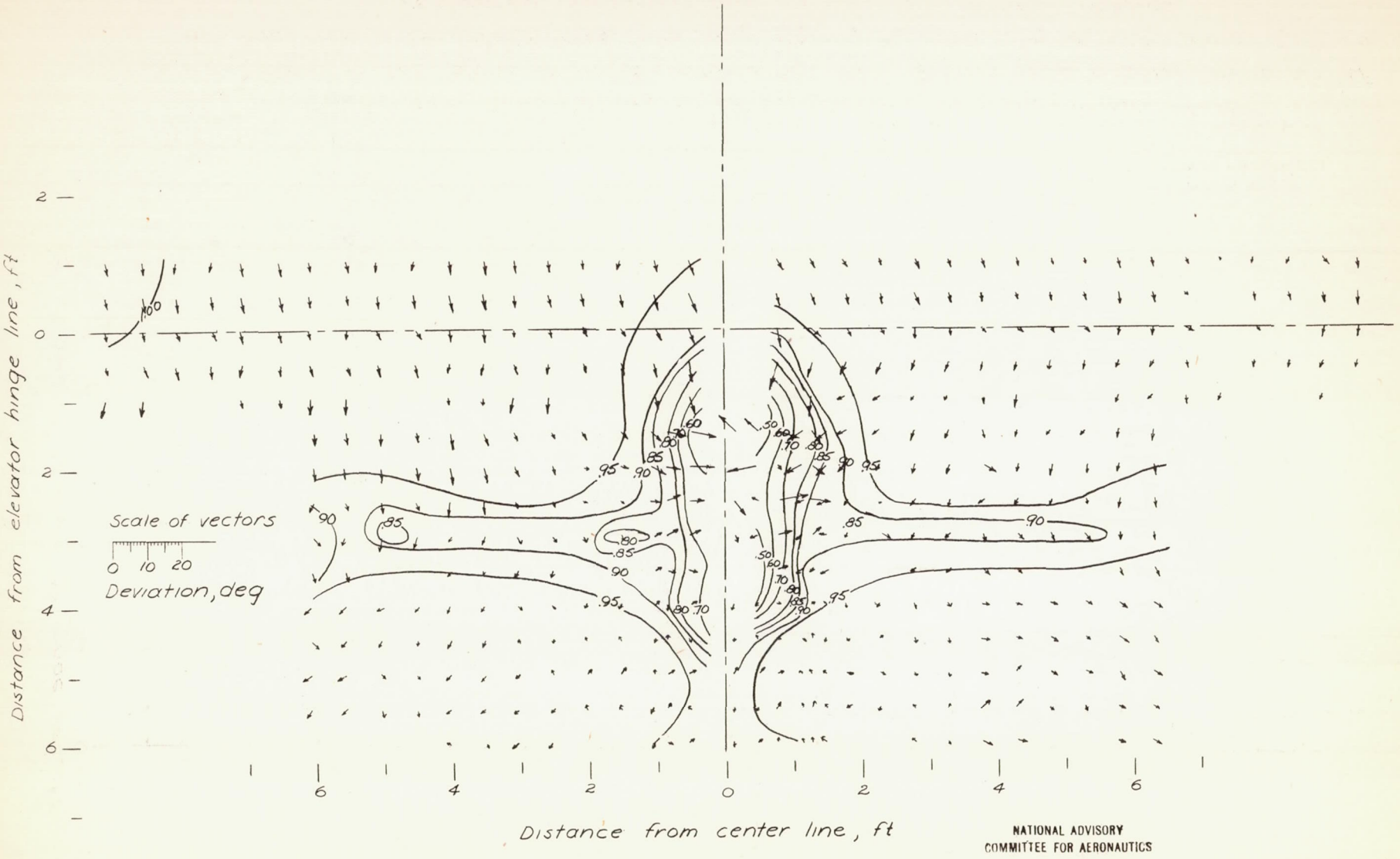

(b) $\alpha = 3.7°$

Figure 77.- Continued.

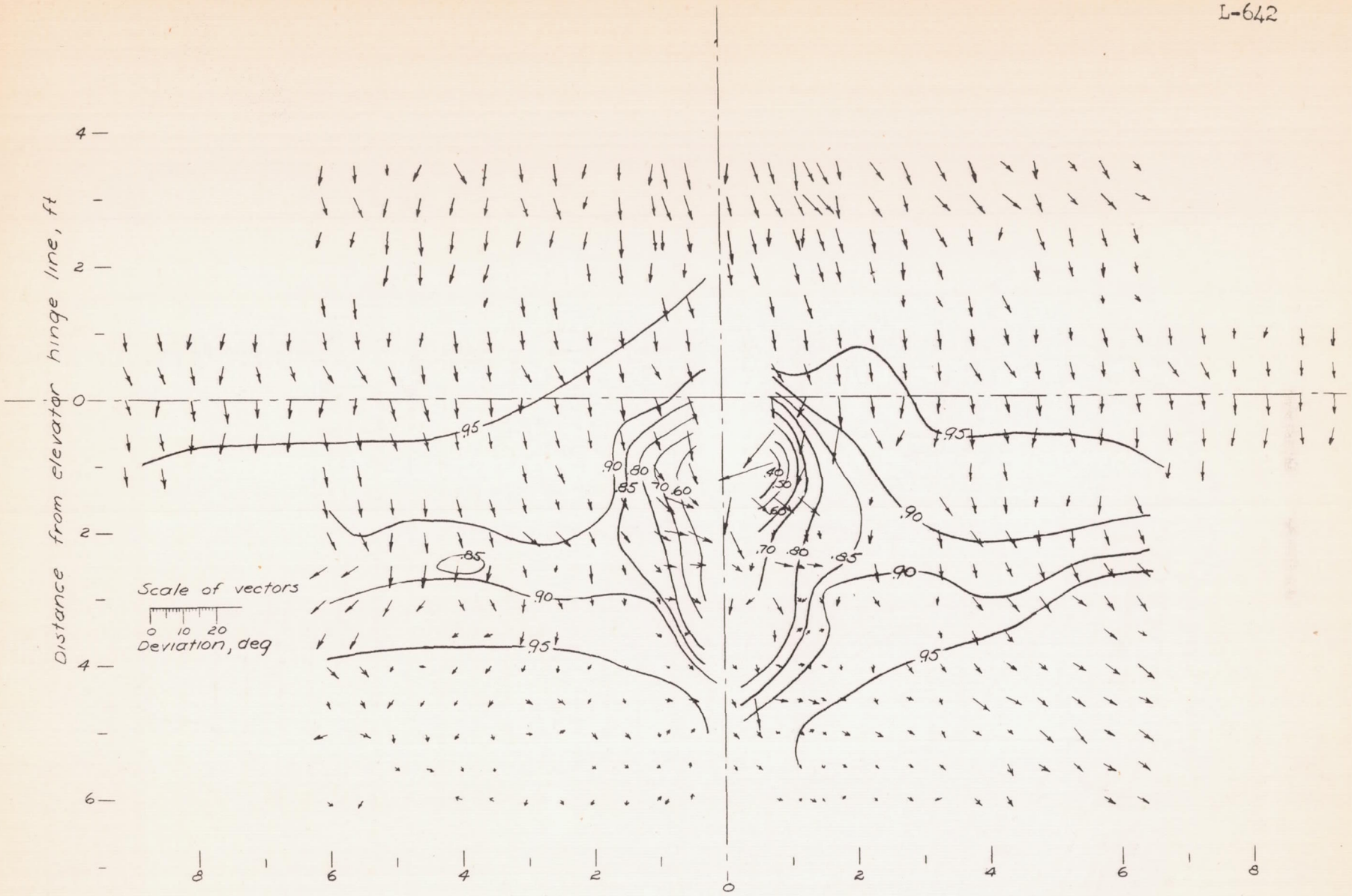

(c) $\alpha = 8.1°$

Figure 77. - Concluded.

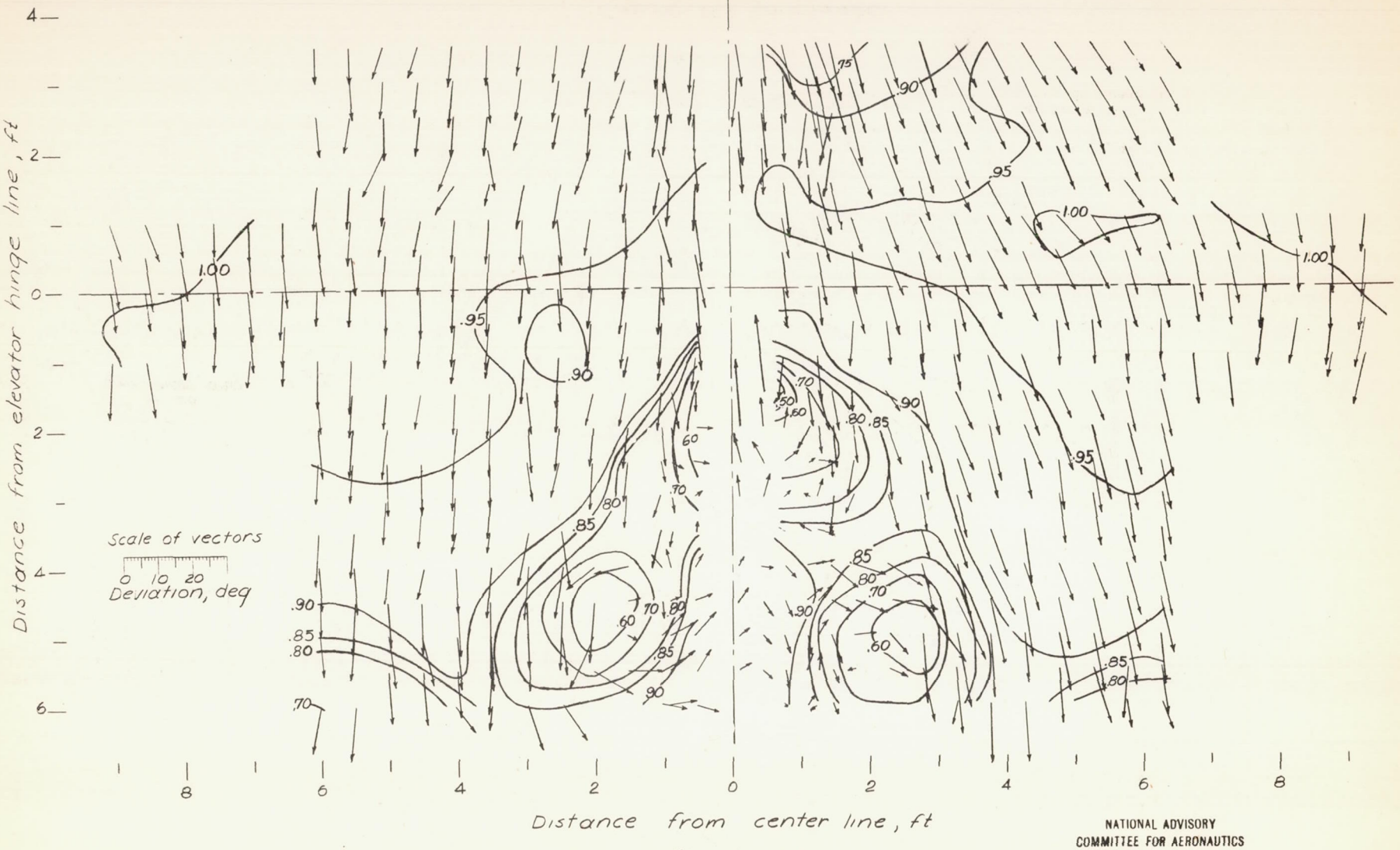

(a) $\alpha = 7.1°$

Figure 78.- Dynamic pressure (q/q_0) contours and inclination of the air stream in the plane of the elevator hinge line. Vectors show angular deviation of air flow from free-stream direction. View looking forward. Propellers removed; flaps deflected 40°; horizontal and vertical tail surfaces removed.

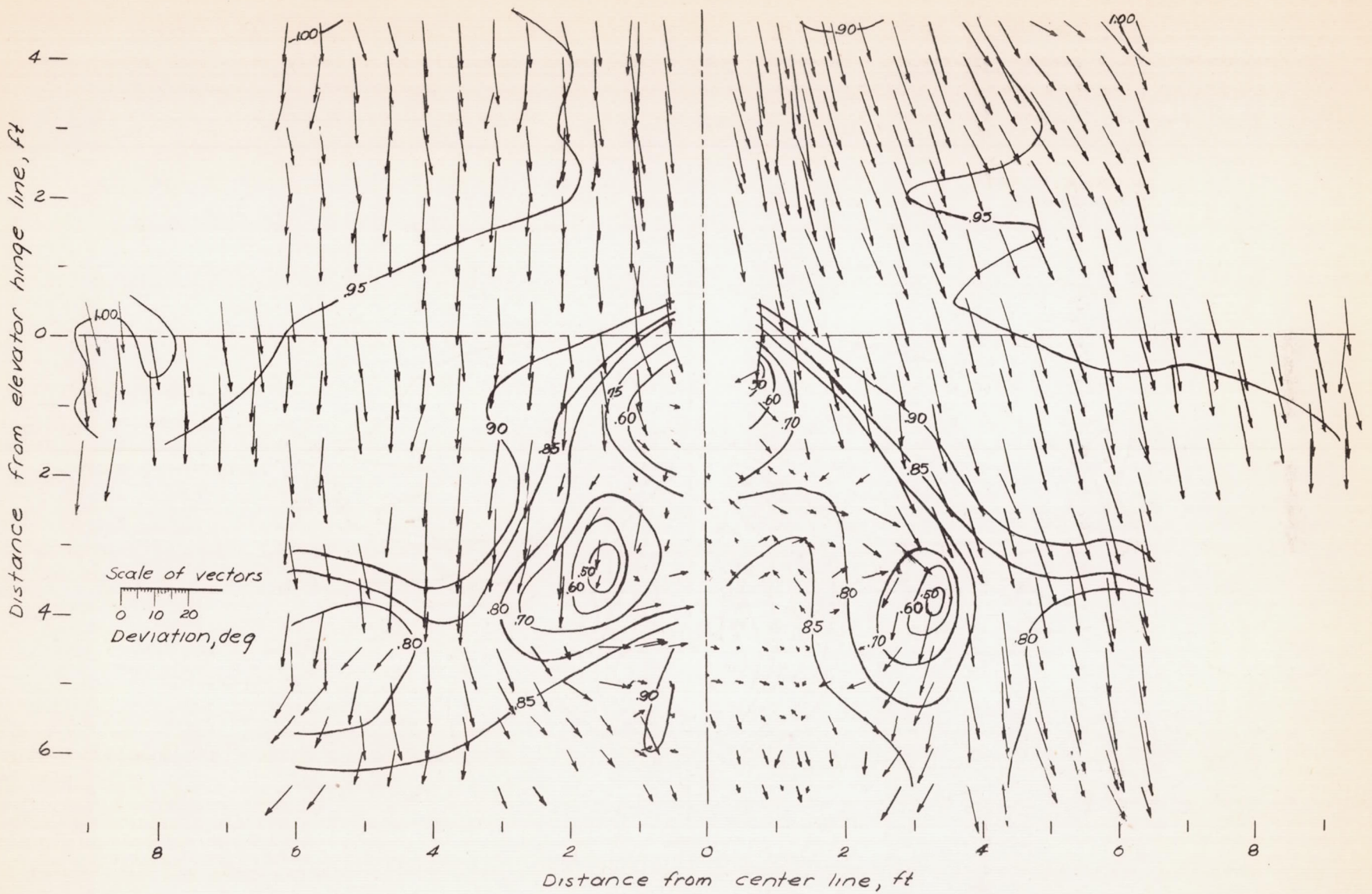

Figure 78.- Concluded

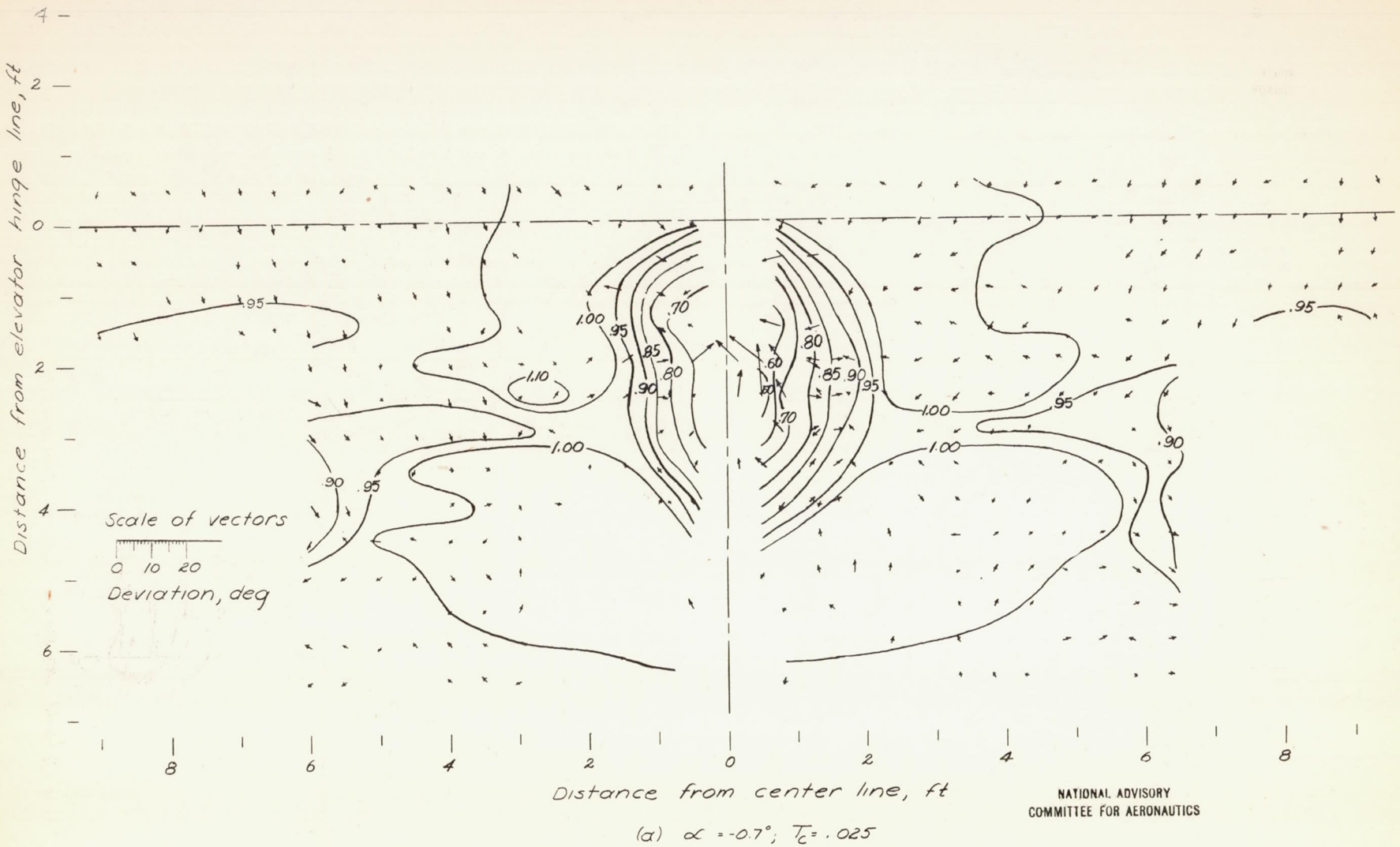

(a) $\alpha = -0.7°$; $T_c = .025$

Figure 79. - Dynamic pressure (q/q_0) contours and inclination of the air stream in the plane of the elevator hinge line. Vectors show angular deviation of air flow from free-stream direction. View looking forward Propellers operating; flaps retracted; vertical and horizontal tail surfaces removed.

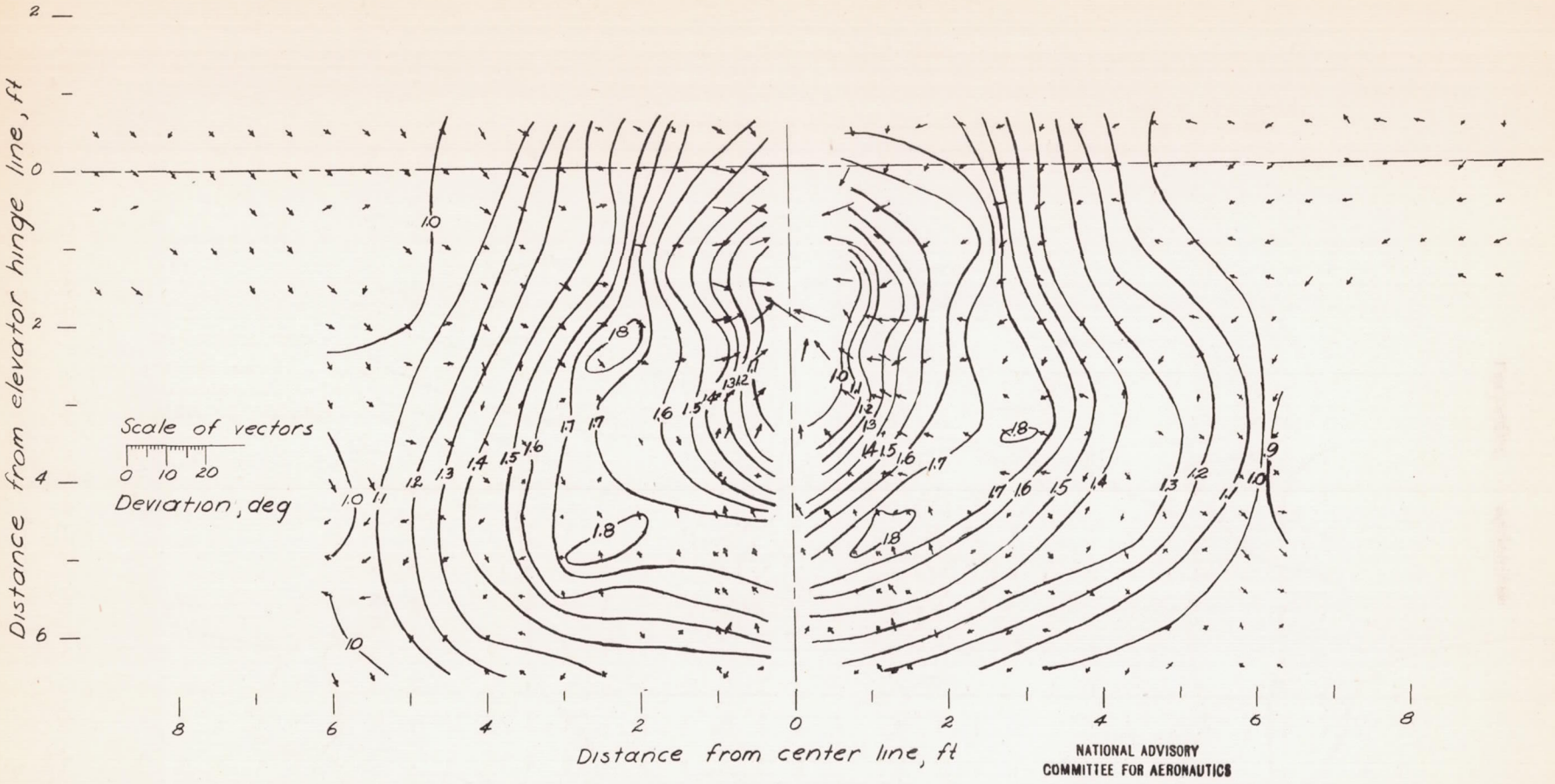

(b) $\alpha = -0.7°$; $T_c = .25$

Figure 79.- Continued.

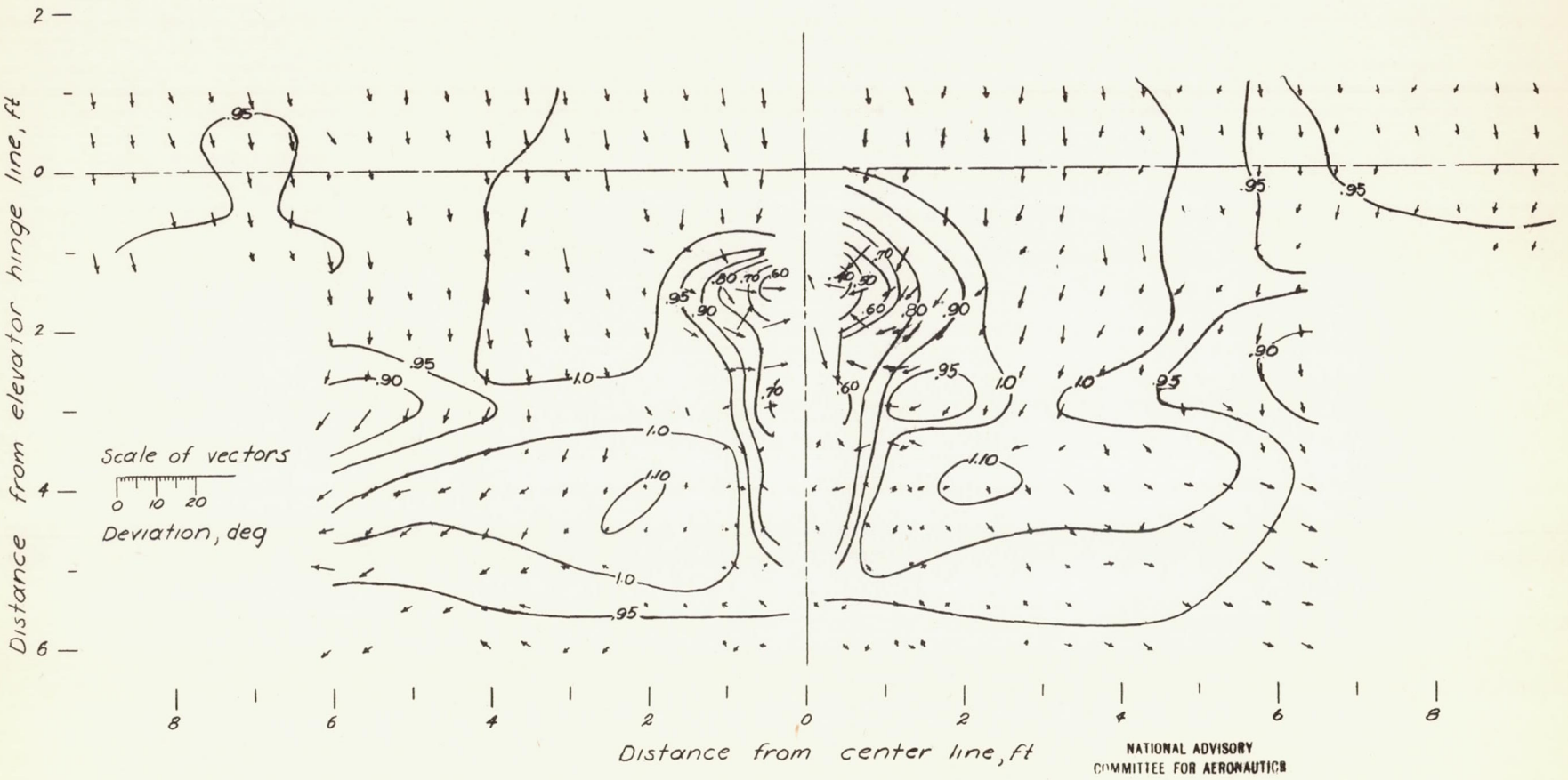

(c) $\alpha = 3.7°$; $\bar{T}_c = .025$

Figure 79.- Continued.

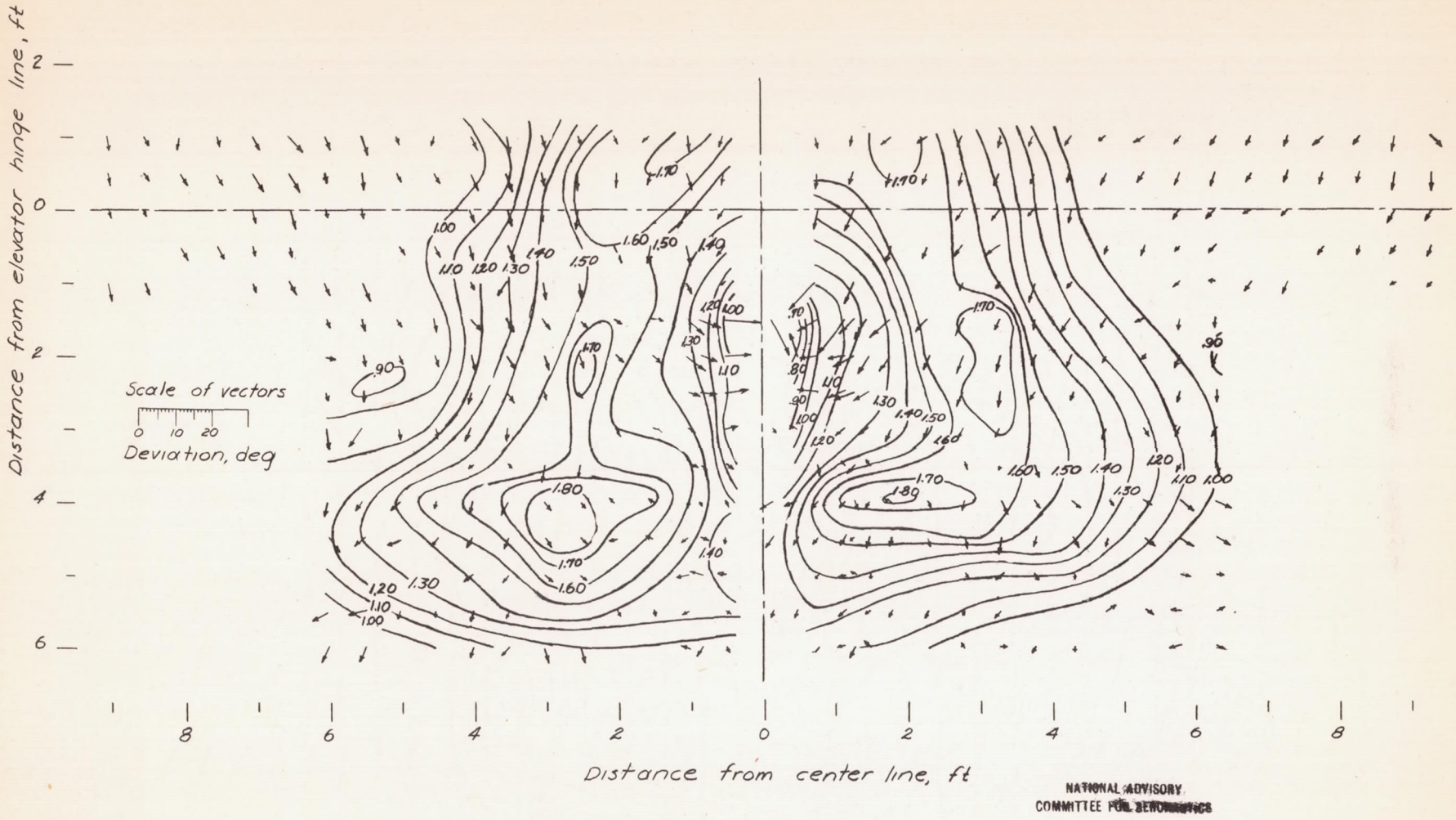

(d) $\alpha = 3.7°$; $T_c = .25$

Figure 79. - Concluded.

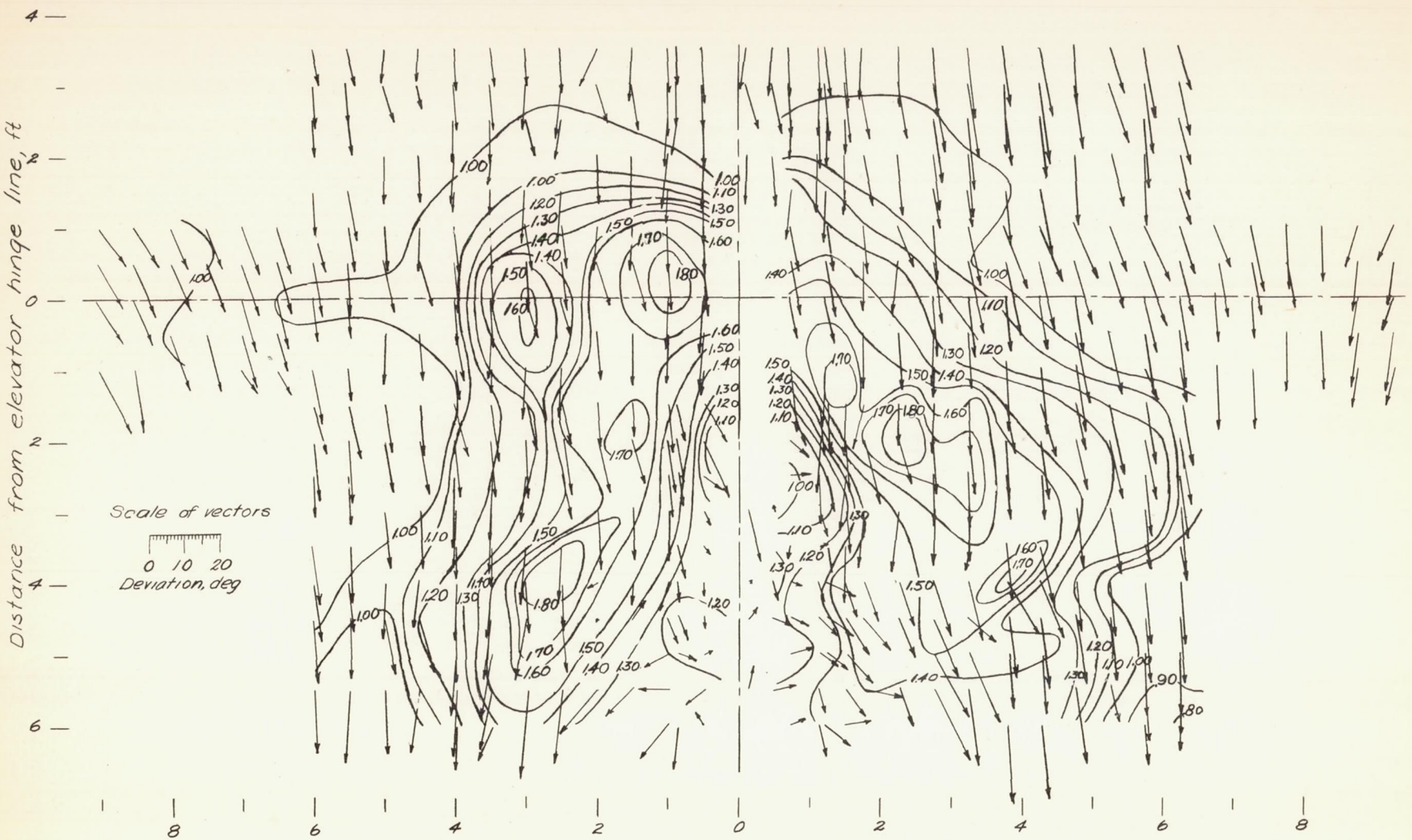

(a) $\alpha = 7.0°$; $T_c = .300$

Figure 80.- Dynamic pressure (q/q_0) contours and inclination of the air stream in the plane of the elevator hinge line. Vectors show angular deviation of air flow from free-stream direction. View looking forward. Propellers operating; flaps deflected 40°; horizontal and vertical tail surfaces removed.

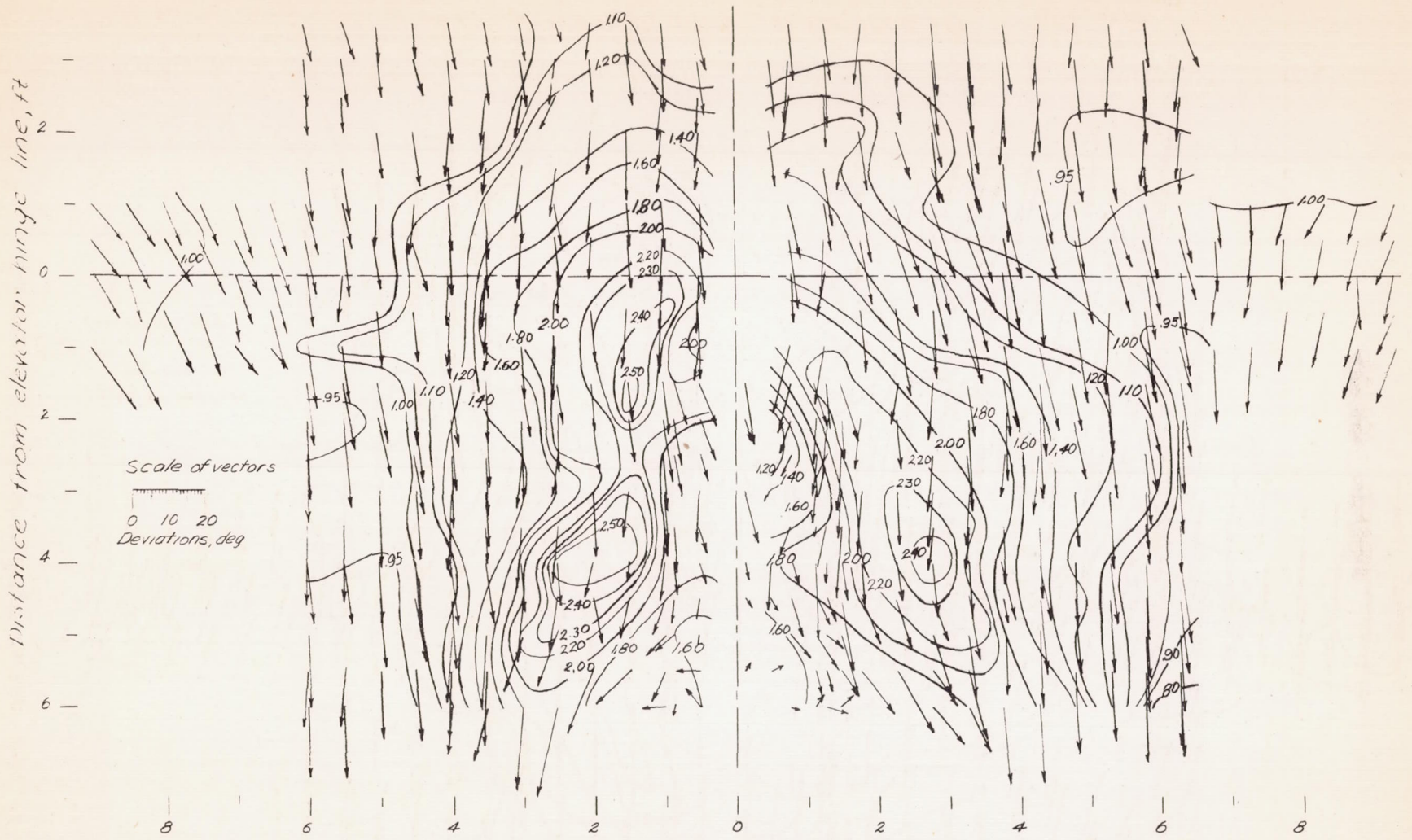

(b) $\alpha = 6.8°$; $T_c = .600$

Figure 80.- Continued.

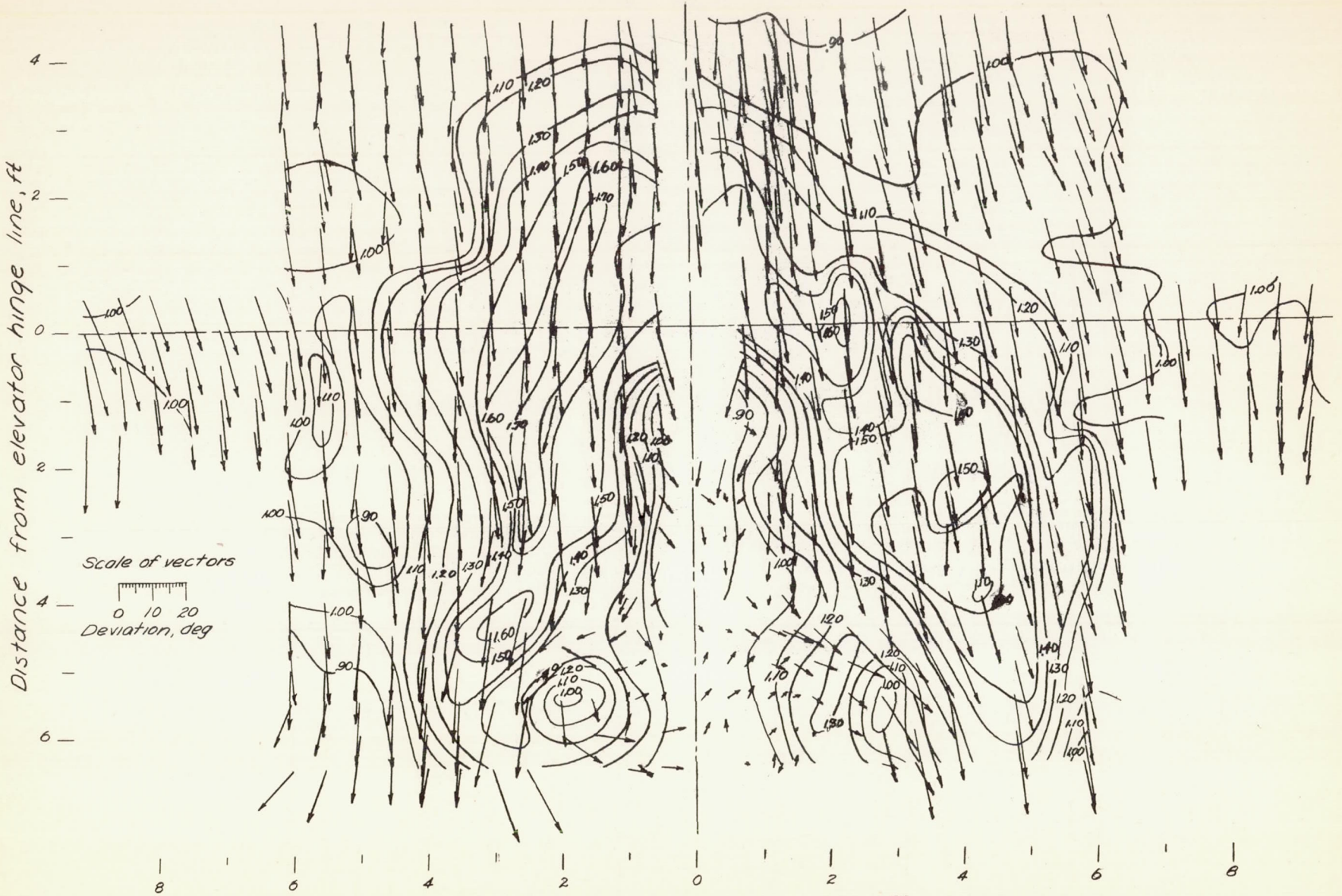

(c) $\alpha = 11.3°$; $T_c = .300$

Figure 80 - Continued.

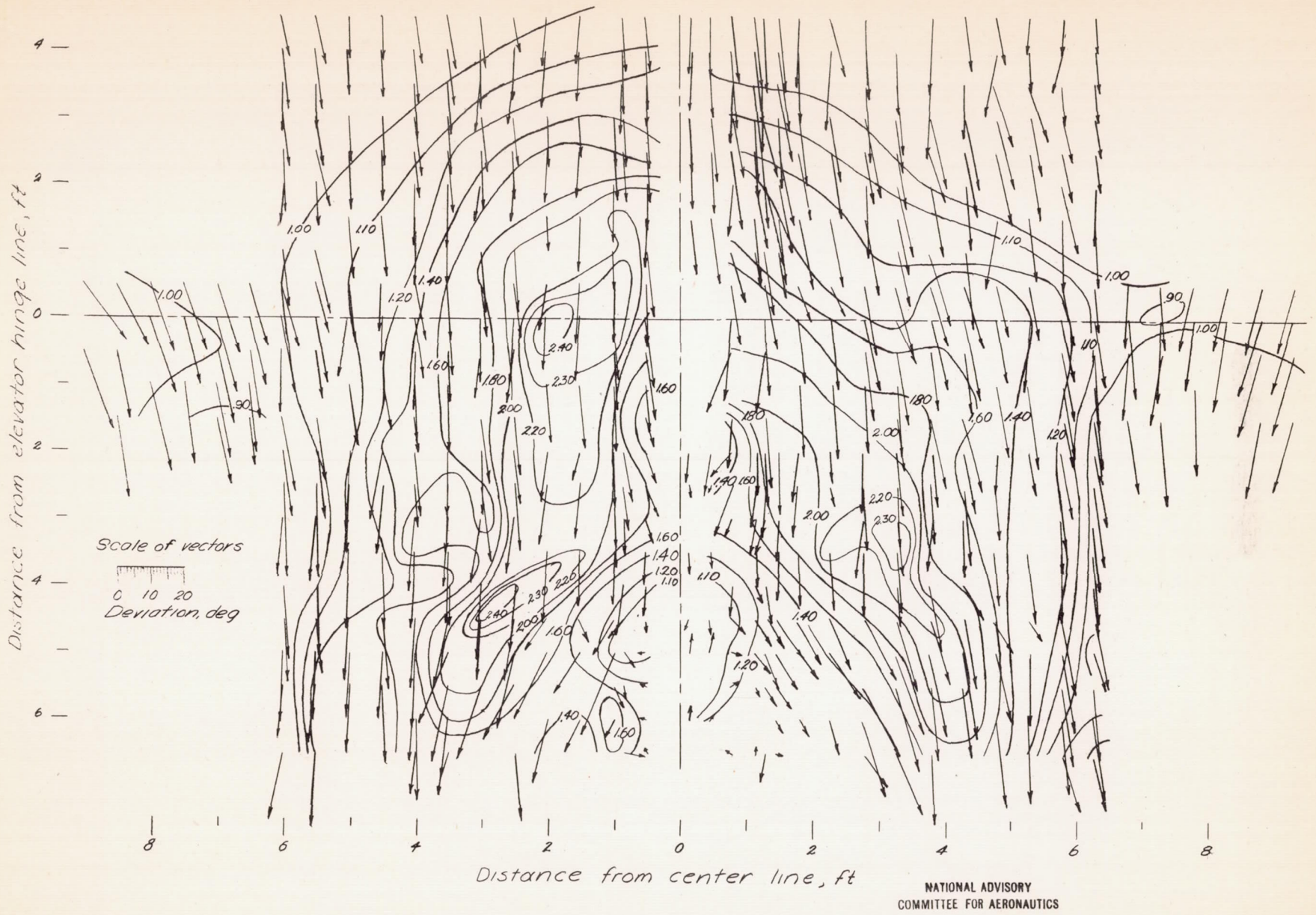

(d) $\alpha = 11.3°$; $T_c = .600$

Figure 80.- Concluded.